UNIVERSITÀ
DEGLI STUDI
DI PADOVA

Head office: Università degli Studi di Padova

Department of Medicine

Ph.D. Course: Traslational Specialistic Medicine "G.B. Morgagni"

Curriculum: Endocrine and Metabolic Sciences

XXXV Cycle

NETosis as mediator of the metabolic effects of high fat diet-modified microbiota

Coordinator: Prof. Annalisa Angelini

Supervisor: Prof. Gian Paolo Fadini

Ph.D. STUDENT: Ludovica Migliozzi

INDEX

ABSTRACT 4

INTRODUCTION 6

Chronic inflammation and metabolic diseases 6

Adipose tissue and liver inflammation 7

The intestinal barrier 7

The intestinal microbiota 10

Dysbiosis in obesity and T2D 12

Neutrophils in health and diseases 14

Neutrophil aging 15

Crosstalk between neutrophils and the microbiota 16

Neutrophils Extracellular Traps and NETosis 17

PAD4 in the onset of NETosis 21

NETs and NETosis in type 2 diabetes and their complications 22

NETs in the pathophysiology of gastrointestinal inflammatory diseases 23

AIM OF THE WORK 25

MATERIALS AND METHODS 26

Mice 26

High-fat diet 26

Genotyping 26

Metabolic tests 26

Whole body composition and metabolic cages 27

Neutrophils isolation 27

In vitro NETs release 27

Live confocal microscopy 28

Bioluminescence imaging assay *in vitro* 28
Western blot of neutrophils 28
Immunofluorescence of neutrophils 29
Glucose uptake 29
Thioglycollate-induced peritonitis 29
Neutrophil migration 30
dsDNA quantification 30
RNA isolation and quantitative Real time PCR 30
Tissue processing 33
Analysis of adipose tissue sections 33
Immunofluorescence of adipose tissue sections 33
Immunofluorescence of liver sections 34
Oil red O staining of liver sections 34
Multiplex bioplex 34
Histology of colonic sections 34
FITC-dextran assay 35
ELISA (plasma LPS) 35
Fecal DNA extraction and Microbiota analysis 35
PCR for 16S 35
Fecal microbiota transplantation (FMT) 36
ELISA (S100A8) on fecal samples 36
Flow cytometry of tissues 36
Organoids and intestinal epithelial cells 36
GSK-484 treatment 37
Statistical analysis 37
RESULTS 38
Hematopoietic-restricted deletion of Padi4 in mice prevented histone citrullination and reduced NETs release 38

Padi4 deletion did not affect neutrophils activation during acute inflammation 43

Padi4 deletion did not affect neutrophil migration 43

HFD induced weight gain and change in body composition..... 44

Padi4KO mice were partly protected against the metabolic derangements induced by HFD 45

HFD reduced glucose uptake in insulin-sensitive tissues 47

Padi4KO mice were partially protected against HFD-induced inflammation in insulin-responsive tissues 48

Padi4 deficiency protected against systemic inflammation induced by HFD..... 54

Effects of the HFD in shaping gut microbiota composition..... 54

Padi4KO mice were protected against HFD-induced metabolic endotoxemia and intestinal hyperpermeability..... 55

Padi4KO mice showed improvements in the gut barrier integrity after HFD..... 56

Padi4KO mice were spared from HFD-induced gut neutrophil recruitment and intestinal inflammation 58

Microbiota depletion with antibiotics reverted HFD-induced dysmetabolism and endotoxemia.. 59

Padi4 deletion prevented the onset of dysmetabolism, endotoxemia and inflammation after transplantation with HFD-modified microbiota..... 61

Treatment with a selective PAD4 inhibitor improved glucose tolerance and intestinal permeability after HFD..... 62

NETting neutrophils and impaired intestinal barrier..... 64

DISCUSSION 66

BIBLIOGRAPHY 72

ABSTRACT

Introduction. Emerging evidence suggest an essential role for neutrophils in the pathogenesis of metabolic diseases. Obesity and type 2 diabetes (T2D) are associated with an alteration in the composition of gut microbiota, termed dysbiosis, and with intestinal barrier dysfunction, which favors the translocation of bacterial lipopolysaccharide (LPS) into the bloodstream, contributing to systemic chronic inflammation and metabolic derangement. Microbiota also plays a crucial role in shaping host immunity, modulating the magnitude of inflammatory responses, and regulating neutrophil production and function. In diabetes, the response of neutrophils to pathogens is abnormal as they are primed to release NETs (neutrophil extracellular traps) composed by sticky chromatin filaments decorated with granular enzymes, and undergo NETosis

Aims. We aimed to investigate whether NETosis abridges the effects of dysbiosis toward systemic dysmetabolism.

Methods and results. Since the Padi4 (peptidyl arginine deiminase) activity is required for the release of NETs, we used a hematopoietic-restricted Padi4 knockout mouse (Padi4KO) to study the role of NETosis in the development of obesity and T2D. Two-photon confocal imaging, kinetic assays, and luminol-based bioluminescence showed that *Padi4* deletion results in less release of NETs in response to PMA or calcium ionophore. Histone citrullination, the key hallmark of NET release, was not present in neutrophils from Padi4KO mice, as assessed by Western blot. After 12 weeks of HFD (60% of calories from fat, 21% carbohydrates and 19% from proteins) Padi4KO and control mice became equally obese, but Padi4KO mice were protected from the development of glucose intolerance and insulin resistance. Furthermore, Padi4KO mice displayed less accumulation of neutrophils and macrophages within the VAT and liver in comparison to their littermates after HFD, as shown by flow cytometry. In line with that, HFD-fed Padi4KO mice showed a seemingly "anergic" cytokine fingerprint and lower levels of plasma dsDNA, compared to control mice, indicating they were protected from the onset of inflammation that accompanies T2D. Through the FITC-dextran gavage assay, we showed that Padi4KO mice were protected from intestinal hyperpermeability induced by HFD and from the surge in plasma concentrations of LPS, a marker of metabolic endotoxemia. Shotgun sequencing of the microbiota showed similar HFD-induced dysbiosis in both control and Padi4KO mice. However, intestinal inflammation (fecal s100a8 levels) and gut neutrophils ($CD45^+CD115^-Ly6G^+SiglecF^-$ cells) abundance were lower in Padi4KO mice. To test whether NETosis is a first-line response to dysbiosis and drives systemic dysmetabolism, we performed fecal microbiota transplantation. Control mice transplanted with gut flora from HFD mice

became glucose intolerant despite being fed a chow diet. Remarkably, Padi4KO mice transplanted with gut flora from HFD mice were protected from the surge of LPS and displayed a less proinflammatory signature in the peripheral circulation. Finally, pharmacological inhibition of PAD4, like hematopoietic *Padi4* deletion, prevented HFD-induced body weight gain, glucose intolerance, and intestinal hyperpermeability.

Conclusions. We show for the first time that NETosis is involved in the pathogenesis of dysmetabolism during the onset of obesity. Our study contributed new insight into the role of neutrophils in translating the deleterious effects of a diet-modified microbiota. Therefore, inhibition of NETosis emerges as a target to counter metabolic diseases like T2D.

INTRODUCTION

Chronic inflammation and metabolic diseases

Diseases linked to modern society and lifestyle changes, such as type 2 diabetes (T2D), obesity and chronic liver disease, are reaching pandemic proportions. A key risk factor for these diseases is a Western diet, typically defined as high in calories and rich in sugars, saturated fats, salt and processed foods. Moreover, this diet is poor in fruits, vegetables, fibers, vitamins and minerals [1]. The World Health Organization (WHO) reported that in 2016 more than 1.9 billion people in the world were overweight. Among them, 650 million were obese.

Obesity is a very complex disease characterized by the contribution of several factors, including genetics, socioeconomic status, and environment, which in turn affect food consumption, nutrient absorption, thermogenesis, and fat storage in various adipose tissues [2]. Obesity is associated with the development of multiple pathological conditions also known as obesity-related complications, including T2D, cardiovascular diseases, some types of cancer, and worsened the outcomes of coronavirus disease 2019 (COVID-19) [3]. Since obesity is the most common cause of insulin resistance in humans, the obesity epidemic is the major cause of the rising global incidence of T2D [2]. Insulin resistance is defined as impaired insulin responsiveness in metabolically active tissues, such as muscles, fat and liver. Major metabolic insulin actions include: blunted hepatic glucose output, increased skeletal muscle glucose uptake and glycogen synthesis, suppression of free fatty acid (FFA) released from adipocytes (lipolysis), and increased lipid accumulation in the liver and adipocytes [5]. To compensate for insulin resistance, after a window of increases insulin secretion, progressive failure of β cells can occur, which are not able to cope with the increased secretory needs [6].

Over the past 20 years, immunometabolism, which studies the interconnections between inflammation and metabolism, has provided new insight in the field of obesity and metabolic disorders [7]. Immunometabolism includes the effects of immune cells on the regulation of systemic metabolism, as well as the role of intrinsic metabolic pathways on the (dys)function of immune cells. Indeed, obesity is canonically associated with a mild, chronic, systemic and local inflammatory signature [7]. In particular, inflammatory markers have been reported in the adipose tissue, the liver, the central nervous system, the gastrointestinal (GI) tract, within pancreatic islets, and skeletal muscle, that have all been associated with insulin resistance [8].

Adipose tissue and liver inflammation

The role of chronic inflammation of the adipose tissue in the pathogenesis of T2D and the related complications is now well established. During the development of obesity, white adipose tissue (WAT) grow mainly through adipocytes size (hypertrophia) and later through adipocytes numbers (hyperplasia) [9]. Thus, adipocytes become dysfunctional and apoptotic. Obesity-induced fat expansion release a plethora of intrinsic signals, such as adipocyte death, hypoxia, and mechanical stress, that trigger an inflammatory response [10].

The high amount of visceral fat contributes to the development of T2D, possibly, by releasing adipokines and pro- inflammatory molecules, which are known to induce resistance to insulin [11]. This low-grade inflammatory state is further amplified by the recruitment of immune cells [12]. Neutrophils are the first to infiltrate into adipose tissue and produce neutrophil elastase, which enhances inflammation [13]. Lymphocytes, mast cells, natural killer (NK) cells accumulate later and produce inflammatory mediators, such as tumor necrosis factor alpha (TNF-α) and Interferon γ (IFN-γ) [14] . At the late stages of obesity, macrophages accumulate and secrete inflammatory cytokines, such as TNF-α, interleukin 6 (IL-6), interleukin 1β (IL-1β), C-C motif chemokine ligand 2 (CCL2), also referred to as monocyte chemoattractant protein 1 (MCP-1). Subcutaneous or visceral VAT, is responsible for the secretion of an array of signalling molecules, termed adipokines. Among these, Leptin, TNF-α and IL-6 are classified as pro-inflammatory adipokines [14]. On the other hand, adiponectin, a secreted protein produced exclusively by adipocytes, has an anti-inflammatory role and it increases insulin sensitivity [15]. Dead adipocytes are surrounded by macrophages that aggregate to form crown-like structures (CLS) [16].

Ectopic lipid accumulation in the liver is a common feature of obesity [12], which could result in a sterile inflammatory response in this tissue, worsening systemic insulin resistance [8]. Moreover, VAT could directly deliver fatty acids and inflammatory mediators to the liver, probably via the portal system [12], thus contributing to hepatic steatosis and insulin resistance.

The intestinal barrier

The contribution of the gut as an important metabolic regulator, beyond its role as a site for nutrients absorption, has recently emerged [17] .

The barrier function protects the intestine wall and regulates the passages of microorganisms, antigens pro-inflammatory molecules and toxins [18]. Three different layers protect the gastrointestinal (GI) tract and mantain gut homeostasis (Figure 1.1).

The first layer of physical defense is the mucus layer, which creates a physical barrier between the lumen and the tissues, but at the same time, allows the passage of small molecules[19]. Mucus is mainly formed by water and glycosylated proteins (mucins) secreted by goblet cells. In addition, it contains antimicrobial peptides (AMPs), secreted by Paneth cells, and immunoglobulin A (IgA), produced by plasma cells and secreted in the lumen [19]. The intestinal mucosa is an active semipermeable barrier that allows the absorption of nutrients and transport of substances and prevents the entry of harmful substances, luminal antigens, and pathogens.

The mucus layer is supported by the underlying monolayer of intestinal epithelial cells (IECs). IECs are columnar-shaped and polarized cells, characterized by an apical and a basolateral domain, facing the lumen of the gut and the intestinal tissue, respectively. The luminal surface is organized in apical microvilli to increase the absorptive area and minimize the volume, and express proteins (receptors, transporters, channels) to communicate with the intestinal microenvironment [20]. IECs are crucial mediators that maintain the host-commensal microbial relationship and immune cell homeostasis in the intestine [21]. IEC are derived from somatic stem cells, residing at the intestinal crypts, and their progenitors differentiate into a variety of cell types including absorptive enterocytes, mucus-secreting goblet cells and Paneth cells (Figure 1.1).

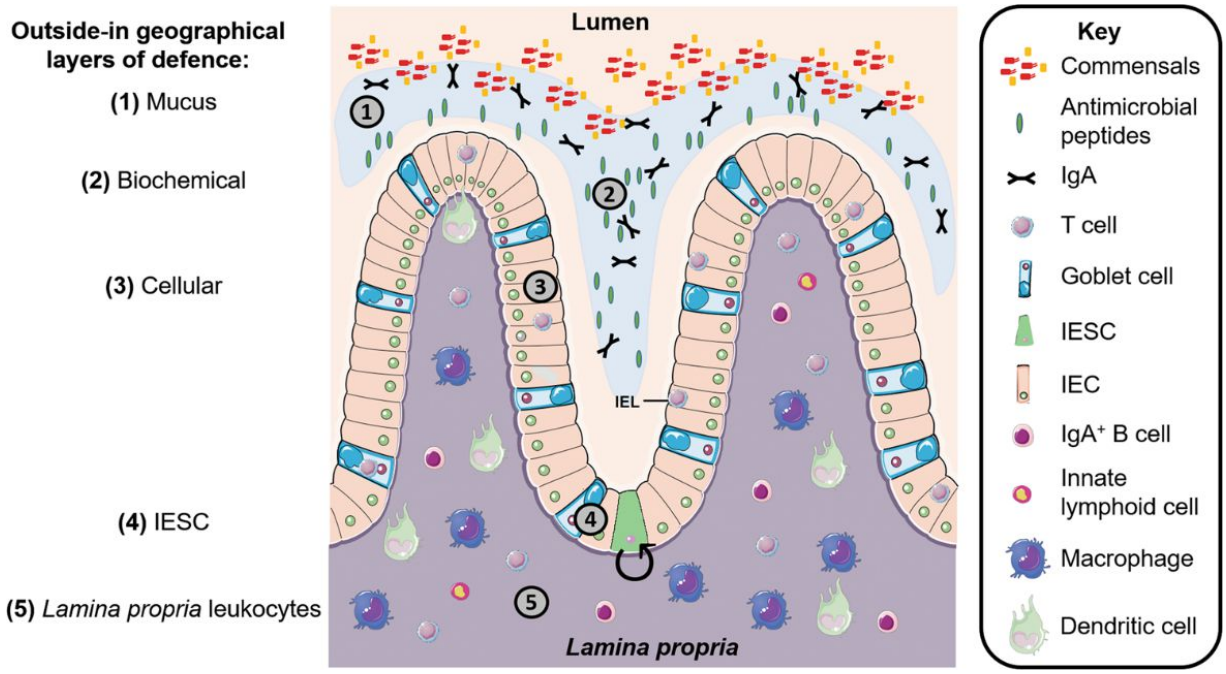

Figure 1.1. Layers of intestinal defense mechanisms: (1) the outer most layer consists of mucus (2) with antimicrobial peptides and immunoglobulin A. (3) Intestinal epithelial cells forming a single-cell layer of protection which is interspersed with intraepithelial lymphocytes. (4) Within intestinal crypts are intestinal epithelial stem cells. (5) Beyond the epithelial layer is the lamina propria, populated with leukocytes [22].

The IECs function as a physical barrier is also facilitated by transmembrane tight junctions (TJ), adherent junctions (AJ) gap junctions and desmosomes [23] (Figure 1.2). Tight junctions are composed of transmembrane proteins such as claudins, occludin, E-Cadherin and junctional adhesion molecules (JAM). Cytosolic plaque constituents, including zonula occludens (ZO) proteins, α-catenin, β-catenin and p120-catenin, enhance the adhesive properties of transmembrane TJ/AJ proteins and couple them to different intracellular structures. ZOs act as scaffold proteins, connecting claudins and occludin to cytoskeletal actin. These proteins work together to maintain the integrity of the epithelial barrier by regulating the paracellular transport of ions, metabolites, and macromolecules [23].

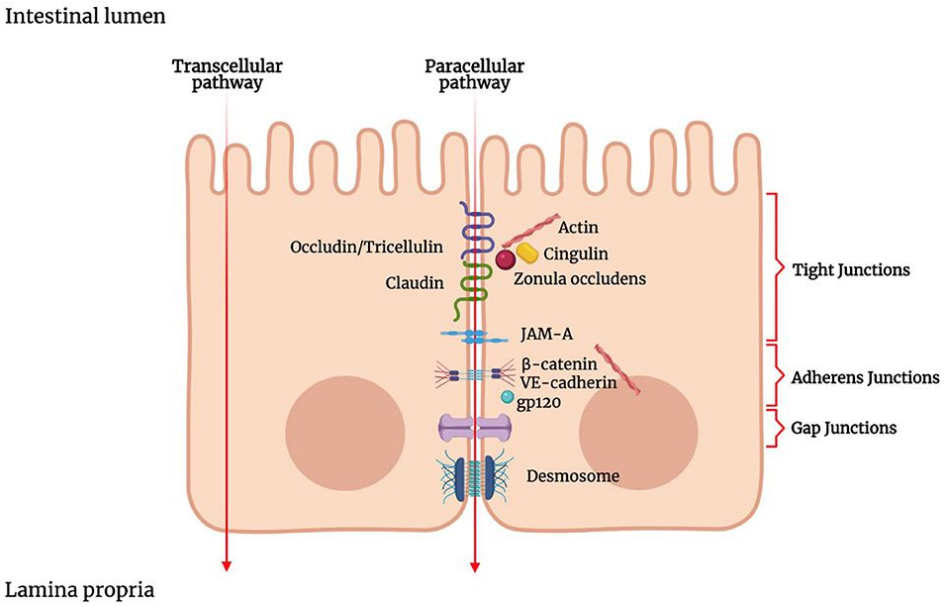

Figure 1.2. Rapresentation of the junctional complex in the intestinal epithelium. Molecules can cross the intestinal epithelial monolayer through the intercellular space (paracellular route), including tight junctions, adherens junctions, gap junctions and desmosomes or through the cells (transcellular route) [24].

The lamina propria is located underneath the intestinal epithelium and consists of innate and adaptive immune cells, such as neutrophils, T-regulatory cells (T-regs), macrophages and mast cells. These cells react against foreign microorganisms and molecules to protect the host, and they act together to clear the inflammation [25]. Most cells of the innate immune system express Pattern recognition receptors (PRR), such as the membrane-bound TLR superfamily and nucleotide-binding oligomerization domain- containing protein 1 (NOD1) and NOD2 [26]. These receptors recognize the pathogen-associated molecular patterns (PAMPS), such as LPS or flagellin, and facilitate the inflammatory response [27].

The intestinal microbiota

The intestinal microbiota is the collective community of microorganisms which colonize the gastrointestinal tract. It plays key roles in the digestion of food, in contributing to the pool of circulating metabolites and in the regulation of the immune system [28]). Microbiota composition and distribution is anatomically defined by barrier specificity and nutrient availability. The dominant phyla in the gut of human and mouse under basal conditions are: Firmicutes (Gram-positive) (60–65%), Bacteroidetes (Gram-negative) (20–25%), Proteobacteria (such as Escherichia and Enterobacteriaceae) (10%), and Actinobacteria (Gram-positive) (3%) [30]. However, at deeper taxonomic classification, such as of genus/species, clear differences are present between mouse and human microbiota, as shown in Figure 1.3.

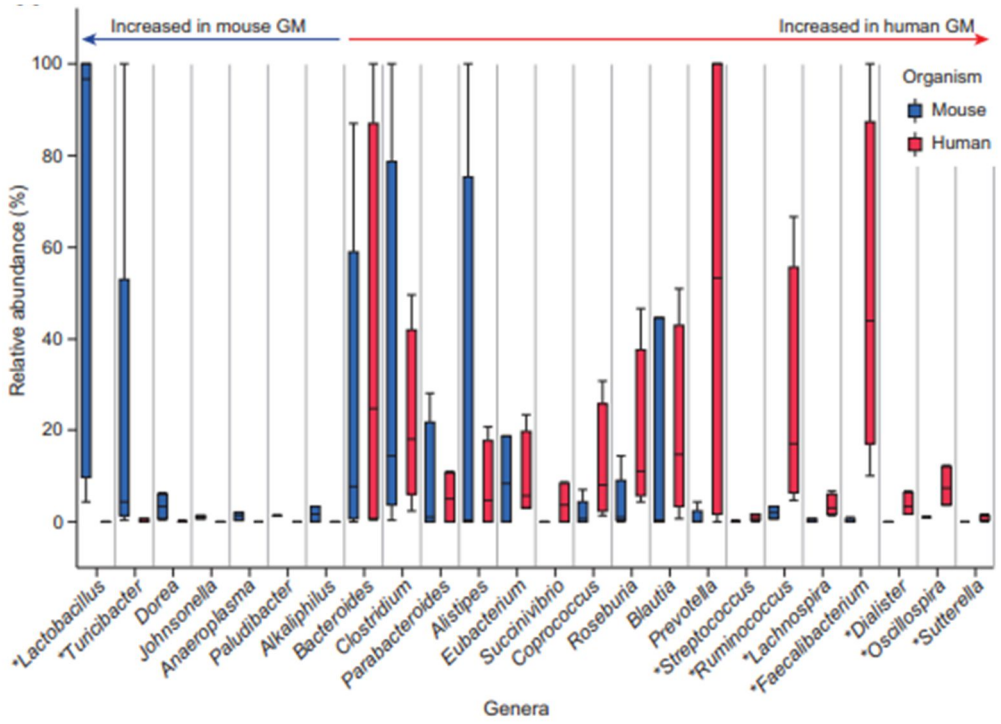

Figure 1.3. Relative abundance of microbial composition at genera level in the healthy gut microbiota of human and mouse [31].

The resident microbial community, referred as commensal, fulfill beneficial functions and protect the host against colonization of pathogens within the intestine [32].

The mantainance of the symbiosis between the host and microbiota is essential for systemic homeostasis. The key function of the immune system as a keeper of this equilibrium is supported by the fact that the highest density of immune cells in the body are resident at sites colonized by commensals, such as the skin or the GI tract [33]. Indeed, a key role of the immune system is to control

our relationship with the microbiota, which in turn promote and regulate both innate and adaptive immunity, thus modulating the magnitude of inflammatory responses [33].The complex regulatory system involves epithelial cells, mucus, IgA, AMPs, innate and adaptive immune cells to control the composition and distribution of the microbiota [34](Figure 1.4). Microbial antigens can induce secretion of AMPs from Paneth cells and epithelial cells. Dendritic cells and macrophages can sense these signals and activate T-cells subsets (such as T-reg and Th17) and B-cells. Th17 cells can produce IL-17 and IL-22, that promote inflammation at the local site and recruitment of neutrophils from the blood. In contrast, T-regs secrete IL-10 and TGF-β, which can inhibit the activity of multiple immune cells and create an anti-inflammatory cytokine milieu [35]. Indeed, both commensals and pathogenic microbes interact with the host immune system through TLRs and NODs receptors [36]

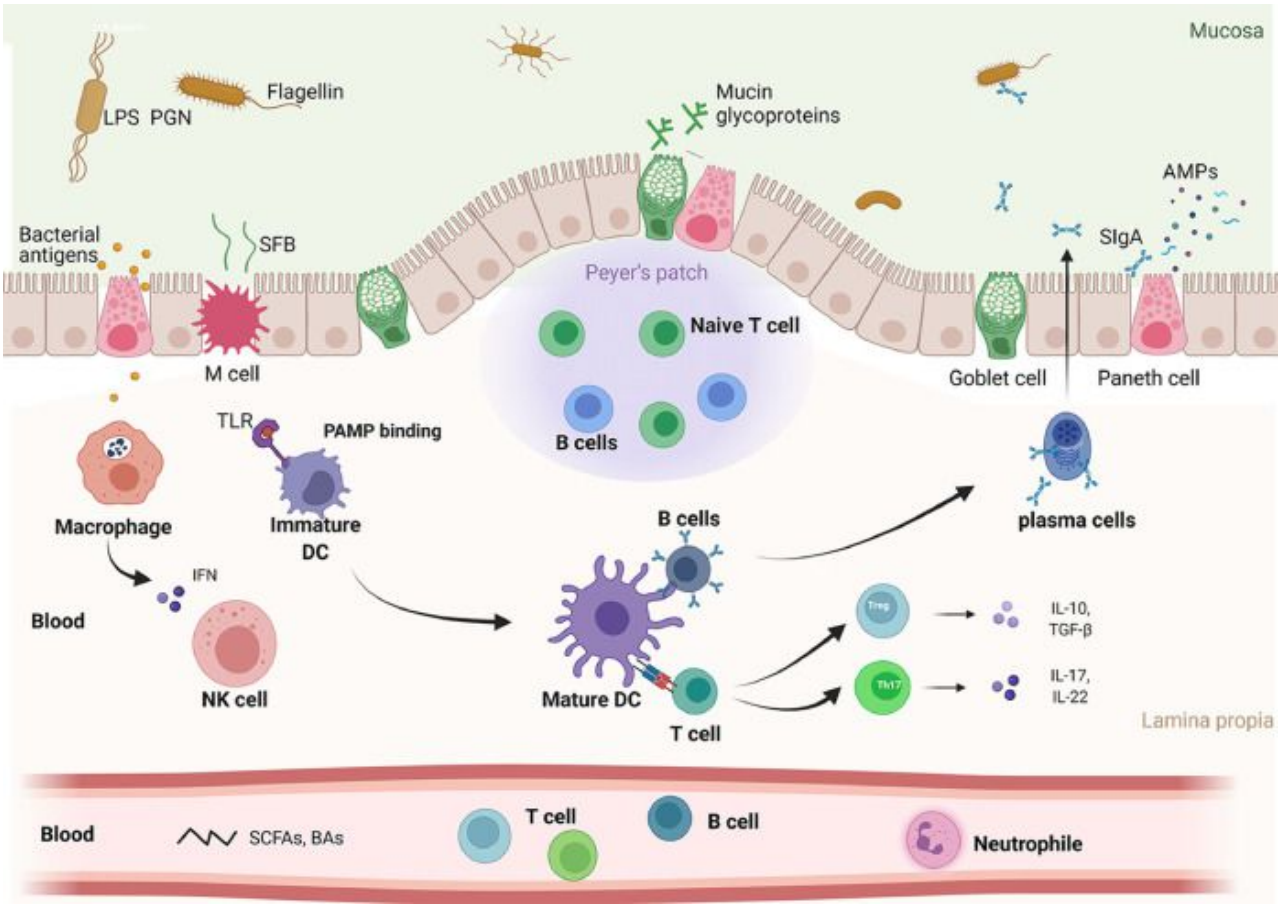

Figure 1.4 Gut microbiome and host immunity. The intestinal microbiota can affect the local activation of both innate and adaptive immunity in the mucusa, lamina propria, Peyer's patches, and mesenteric lymph nodes. The gut microbiota helps to create a thick mucus protective layer composed by mucins glycoproteins released from Goblet cells. [37]

Dysbiosis in obesity and T2D

The composition of the microbial communities in the gastrointestinal tract is shaped by the host metabolic and inflammatory status, by the presence of concurrent infections and by the diet [38]. A major alteration in the microbiota composition is termed dysbiosis which is often associated with inflammatory, autoimmune, and metabolic diseases [35]. Dysbiosis in general is characterized by:

- an abnormal microbiome structure which affects the taxonomical composition and the metagenomic function of the microbial community [39]
- the expansion of the pathobionts, such as the *Enterobacteriaceae,* with the loss of commensals, for example *Bacteroides thetaiotaomicron*, leading to reduced microbial diversity [40]. Pathobionts are bacteria present at low concentrations in healthy conditions, but they proliferate in the presence of infection or inflammation [39]

A westernized lifestyle is known to change drammatically the gut microbiota [1]. The commensal microbiota of obese individuals is significantly altered. The major change found in both human and mouse is the increase of Firmicutes/ Bacteroidetes ratio [41]. Studies in humans linked low bacterial richness with features of metabolic syndrome, such as dyslipidemia and insulin resistance [42]. Changes of the gut microbial composition and a lower microbial diversity in obese subjects have been associated with higher inflammatory tone [43]. In T2D, for example, it has been reported an increased abundance of pro-inflammatory Gram-negative bacteria (e.g., *Escherichia coli*) at the expense of anti-inflammatory bacteria (e.g., *Fecalibacterium prausnitzii*) [43].

Microbiota-metabolites can enter the systemic circulation and produce metabolic effects also on distant tissues. The most widely studied metabolites are short-chain fatty acids (SCFAs): acetate, butyrate and propionate. SCFAs are produced by gut microbiota from anaerobic fermentation of indigestible dietary complex carbohydrates (fibers), such as oats, beans and vegetables [44]. In diabetes, a reduced SCFAs production has been reported, since they are important for intestinal mucosal integrity, glucose and lipid metabolism, and inflammatory responses [45]. For example, butyrate and propionate induce the secretion of gut hormones from the enteroendocrine cells, such as hormone peptide tyrosine (PYY) and glucagon-like peptide 1 (GLP-1) [46]. Trimethylamine-N-oxide (TMAO), produced by intestinal microbiota from choline and carnitine-rich nutrients, such as meat, egg yolks, and high-fat dairy products, has been linked to vascular inflammation and atherosclerosis [47]. Bile acids have recently been proposed to be involved in glucose metabolism. They include small molecules derived from cholesterol, which are synthesised in the liver and excreted in the intestine, where they are transformed by the microbiota. Primary bile acids chenodeoxycholic acid (CDCA) and cholic acid (CA) released in the intestine, activate their receptors Farnesoid- X receptor (FXR)

and Takeda- G- protein- receptor-5 (TGR5), which promote glycogen synthesis and gluconeogenesis [48]. Recent evidences reported that in metabolic syndrome, tryptophan metabolites were unable to activate aryl hydrocarbon receptor, leading to defective mucosal barrier integrity and reduced GLP-1 secretion [49].

The crucial role of the microbiota in regulating metabolism was suggested by the findings that germ-free mice were resistant to diet-induced obesity, while the grafting with microbiota from obese donors resulted in an increase of body fat [50]. There is substantial agreement that the ratio of two main bacterial phyla, Firmicutes and Bacteroidetes, represents the paradigm, and the hallmark, of dysbiosis: while both in lean mice and humans Bacteroidetes are more abundant, in obese individuals and mice, the ratio is inverted with higher abundance of Firmicutes at the expenses of Bacteroidetes. Interestingly, it appears that changes in the microbiota are reversible as the withdrawal of high-fat diet in mice restored a "lean" ratio of Firmicutes/Bacteroidetes [51].

One major consequence of the altered microbiota composition is increased intestinal permeability, leading to bacteria and bacterial products translocation [52]. Decrease intestinal barrier function is also referred as 'leaky gut syndrome' [53]). Lipopolysaccharide (LPS) is a component of the outer membrane of Gram-negative bacteria and it is one of the major bacteria-derived products that crosses the intestinal barrier and that can be measured as a readout for increased intestinal permeability [54]. Metabolic endotoxemia refers to a diet-induced increase in gut-derived plasma LPS level, which may contribute to propagate low-grade systemic and tissue inflammation, contributing to a metabolic dysfunction [55]. Indeed, a continuous infusion of low-dose LPS mimic the low-grade chronic inflammation found in diabetic patients and most of the features of the metabolic diseases, such as visceral fat deposition, glucose intolerance and hepatic insulin resistance [56]. It was demonstrated that antibiotic treatment in mice significantly lowers plasma LPS levels, reduces gut permeability, visceral adipose tissue inflammation, oxidative stress, macrophage infiltration, thus improving metabolic disorder [53]. Other pathologies, including liver diseases, inflammatory bowel conditions show signs of a "leaky" gut phenotype, that can facilitate translocation of bacterial components, such as LPS or peptidoglycan (PNG), form the intestine into the periphery [45]. Release of PAMPs in the systemic circulation causes inflammation in peripheral tissues, especially in the adipose tissue and the liver, and ultimately insulin resistance [57].

One mechanism by which diet-induced obesity is associated with increased intestinal permeability is through altering the distribution and expression of epithelial tight junction proteins, such as ZO-1 and occludin [58]. Moreover, hyperglycemia directly drives intestinal barrier permeability though Glut2-dependent reprogramming of intestinal epithelial cells [59] (Figure 1.5)

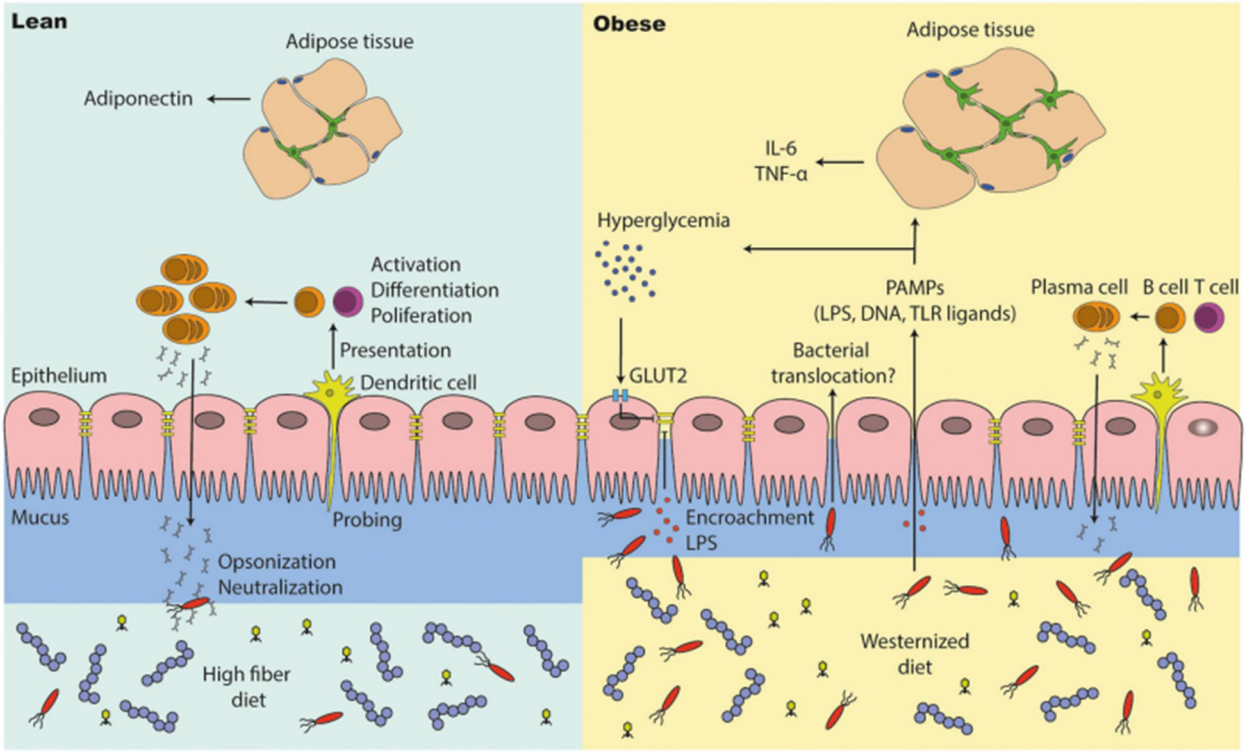

Figure 1.5. Intestinal barrier characteristic in lean and obese people. A high fiber diet supports intestinal barrier function. Dendritic cells, T and B cells work in concert for immune tolerance and inflammatory response. In metabolic syndrome the intestinal barrier is compromised, the mucus layer is thinner and lower levels of IgA favour the penetration of bacteria and PAMPs. [45]

Therefore, the systemic consequences of dysbiosis are possibly due to three main mechanisms:

- the production of pathogen-associated molecular patterns (PAMPs) and metabolites;
- a breach in the interface partitioning the gastrointestinal microbiome from the underlying host tissue;
- the remodeling of the gut microenvironment, consisting of thinning of the mucus layer, the different activation states of the immune system and the rearrangement of the epithelial barrier

Neutrophils in health and diseases

Neutrophils, also known as polymorphonuclear cells (PMNs), are the most abundant white blood cells in humans, accounting for 60%-70% of circulating leukocytes. Neutrophils are the first cells to participate in the innate immunity since they are rapidly recruited at sites of infection.

Neutrophils can be identified by their distinctive lobulated nucleus and the abundance of granules in their cytoplasm. These cells develop from hematopoietic stem cells (HSCs) in the bone marrow (BM) and undergo a series of differentiation stages to become mature neutrophils, including the transition

from granulocyte-macrophage precursors (GMPs) to myeloblasts and then promyelocytes, myelocytes, metamyelocytes, band cells, and finally, mature neutrophils. During terminal differentiation, neutrophils acquire their characteristic granules [60]. Mature neutrophils are released into the circulation to reach the site of infection/inflammation. In the absence of inflammatory stimuli, they either return to the BM where they are phagocytosed by resident macrophages or undergo apoptosis in peripheral tissues within 24-48 hours [60]. Apoptosis of neutrophils is required in order to balance basal neutrophil production and, under inflammatory conditions, it is crucial for the resolution of tissue inflammation. The estimated half-life of neutrophils in the bloodstream is 6-12 hours in mice and 9 hours in humans [61]. At steady state, 1-2 x 10^{11} neutrophils/day are released from the BM [60].

The constant production of neutrophils is called granulopoiesis and it is regulated by the cytokine granulocyte colony-stimulating factor (G-CSF). G-CSF promotes the differentiation of myeloid progenitors toward the granulocytic lineage and it controls the release of neutrophils into blood. In response to systemic infection endothelial cells sense PAMPs and respond by producing vast amounts of G-CSF, leading to granulopoiesis and neutrophils' release in the bloodstream [62].

Neutrophil aging

Neutrophils release–clearance dynamics requires a fine balance between production and elimination.[63]. Aged neutrophils are defined as those that have accumulated while in the circulation and are primed for clearance.[64]

Neutrophils trafficking from the BM through the vascular endothelium to reach extravascular tissues is modulated, among other pathways, by the interaction between CXCL chemokines (C-X-C motif Ligand) and their cellular receptors CXCR (C-X-C motif Receptor) [65]. Several lines of evidence suggest that CXCR4 and CXCR2 antagonistically regulate neutrophil trafficking from the BM. CXCL12/CXCR4 signalling is central to the retention of neutrophils and their mobilization from the BM. CXCL12, also known as stromal cell derived factor-1α (SDF-1α), is constitutively produced by BM stromal cells, including vascular endothelial cells and osteoblast [66]. BM-derived neutrophils aged ex-vivo upregulate the expression of CXCR4, the receptor for CXCL12, that mediates their retention and their homing back to the BM. In contrast, CXCR2 promote release from the BM by binding to CXCL1. CD62L (polymorphonuclear leukocytes L-selectin), which is highly expressed when neutrophils are released from the BM, progressively decreases as they transit in the circulation [63] (Figure 1.6). The process of neutrophils aging *in vivo* displayed circadian oscillations, with a period of active release between zeitgeber times (ZT) 17 and 5 (17 and 5 hr after initiation of light), and a period of clearance between ZT5 and 13 [64]. The circadian oscillations could be explained by changes

in the expression of adhesive and chemotactic molecules (P- and E-selectins, ICAM-1, VCAM-1, CXCL12, and CCL2) both at the RNA and protein level [63]. Aged neutrophils, characterized by a $CD62L^{low}$ $CXCR4^{high}$ phenotype, display pro-inflammatory properties in the circulation [67], while nascent neutrophils exhibit limited proinflammatory activities [63]. A recent work reported that neutrophils lose their granule content whilst ageing in the circulation, rendering them less toxic and reducing the magnitude of inflammation. [68]

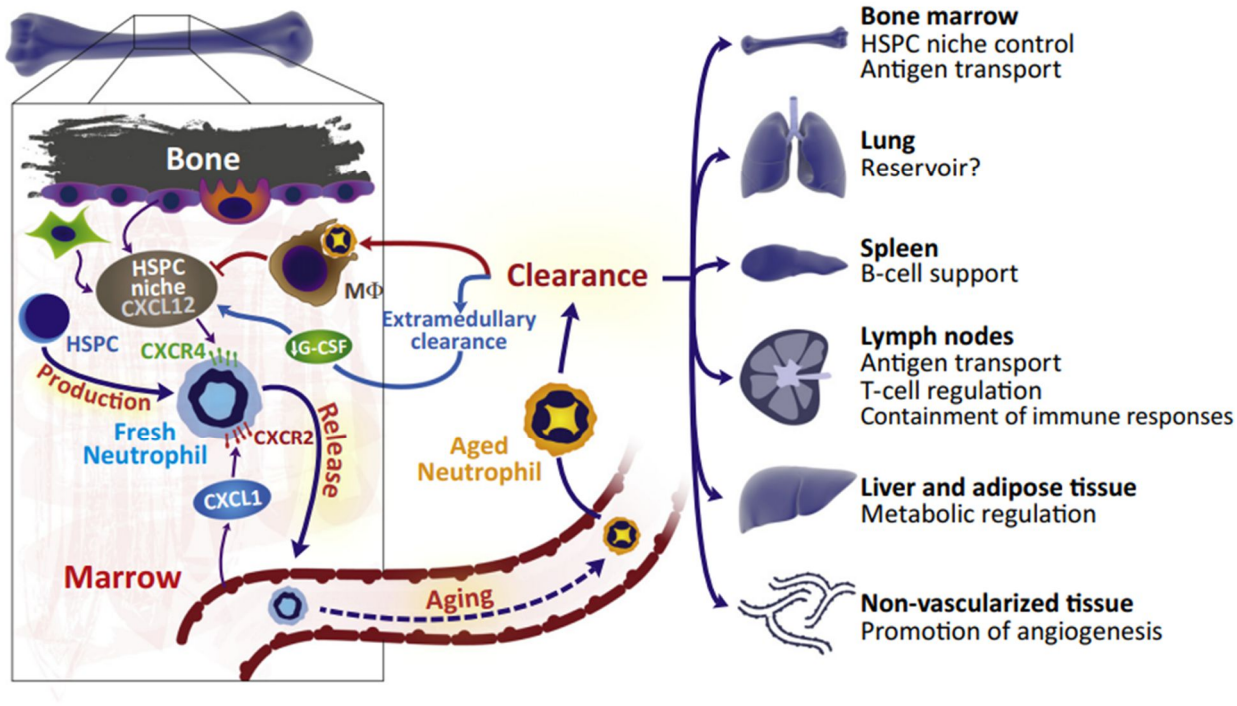

Figure 1.6. Neutrophils ageing. Neutrophils are produced in the BM and released in the circulation where they undergo aging before being cleared into tissues. The release in the blood is regulated by CXCL12-CXCR4 retentive signals and CXCL1-CXCR2 mobilizing signals. The consequences of clearance are niche inhibition and release of HSCs and progenitor cells (HSPCs).[63]

Crosstalk between neutrophils and the microbiota

The gut microbiota plays a fundamental role in the regulation of neutrophil production and function, even if the mechanisms are not completely understood [69]. Neutrophils can sense microbiotal components and metabolites, such as LPS, PNG, SCFAs and tryptophan metabolites, with their own pattern recognition receptors, including most TLRs (except for TLR3), NODs, and inflammasome [70]. In the intestine, TLR and NODs induce innate lymphoid cells to produce interleukin-17 (IL-17) via the Toll like receptor/ myeloid differentiation factor signalling (TLR4/Myd88) pathway, resulting in neutrophils differentiation through G-CSF production. In the blood, microbiota-derived signals are

sensed by neutrophils with TLRs and regulate their aging through Myd88 pathway. [67]. Antibiotic treatment in mice dramatically reduced the number of aged neutrophils, but treatment with LPS partly restored the aging phenotype [67]. Microbial products can also be sensed by stromal cells in the BM, which in turn support lineage differentiation by producing citokynes [69] (Figure 1.7).

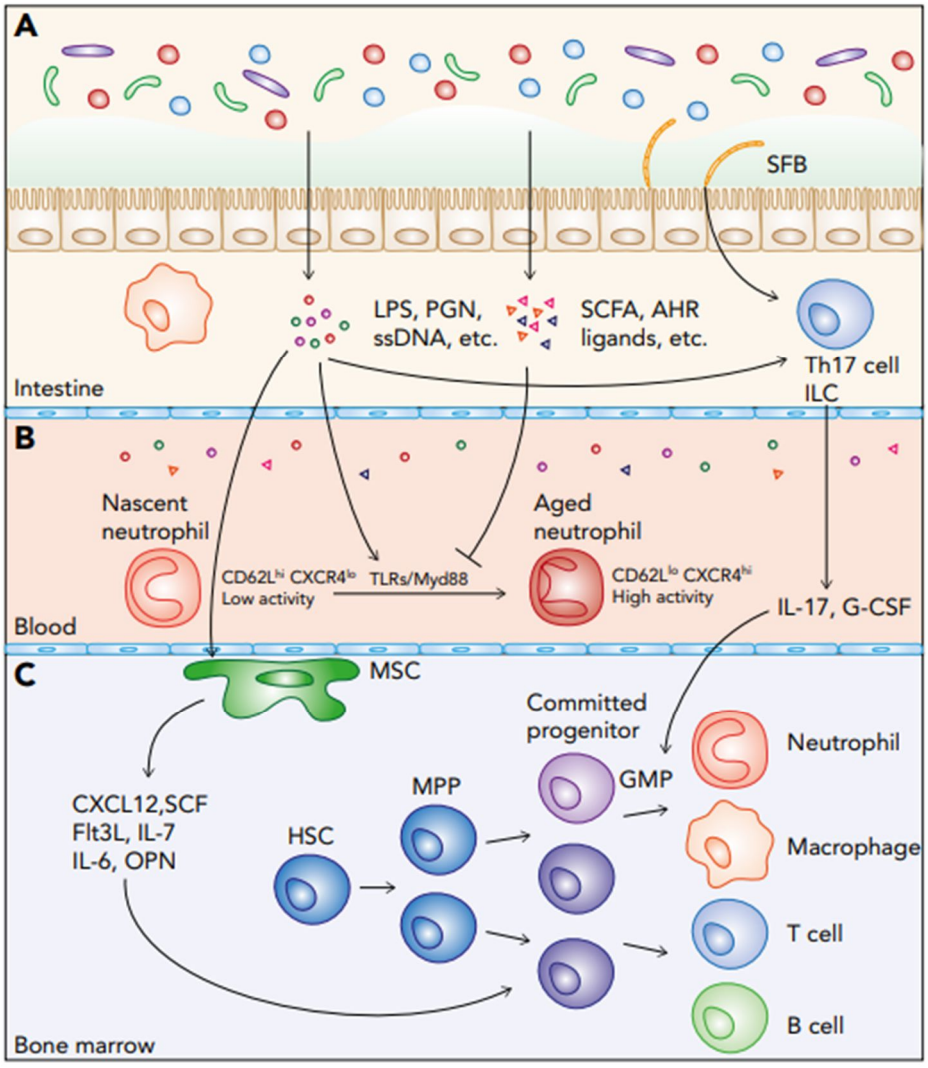

Figure 1.6. Schematic rapresentation of neutrophils regulation by microbiota in the intestine (A), in the blood (B) and in the BM (C). [69]

Neutrophils Extracellular Traps and NETosis

Elimination of pathogens by neutrophils was known to be mediated by superoxide production and degranulation [71]. Phagocytosis is a major mechanism to remove pathogens and cell debris. It is an active, receptor-mediated process during which a particle is internalized by the cell membrane into a vacuole, called the phagosome. Granules are reservoir of proteins that can degrade microbes by fusing with phagosome or with the plasma membrane. This fusion permits assembly of the nicotinamide adenine dinucleotide phosphate (NADPH) oxidase complex and allows reactive oxygen species

(ROS) production both inside the phagolysosome and outside of the cell, thus activating the oxidative burst, leading to oxidative damage to microorganisms in the phagosome [72]. Moreover, the microbicidal activity is also performed through the release of the content of their cytoplasmatic granules (degranulation) into the extracellular space [71]

However, activated neutrophils can release a mesh of nuclear chromatin, associated with nuclear histones, antimicrobial proteins and some cytoplasmic proteins forming an extracellular network, called neutrophil extracellular traps (NETs), that kill bacteria and degrade virulence factors [73] . NETs contain proteins from azurophilic (primary) granules, such as neutrophil elastase (NE), cathepsin G, and myeloperoxidase (MPO). Proteins from secondary and tertiary granules, such as lactoferrin and gelatinase, are also present. However, the major structural component of the NETs is the nuclear DNA [73] . The antimicrobial effect is mainly attributed to DNA, this is why DNase production is a strategy developed by microorganisms to escape clearance by host's neutrophils [73] . Histones and enzymes are attracted by the negatively charged DNA, that forms the sticky backbone of NETs. These filaments organize in networks that physically entrap bacteria, but also allow the local concentration of bactericidal components. Fuchs et al. demonstrated that neutrophils-releasing NETs could undergo a novel form of cell death, that has been termed NETosis [74]. The cellular events that led to NETs release can be described as a coordinated multi-step process (Figure 1.7):

- disassembly of the actin and intermediate filament cytoskeletons, remodelling of the microtubule, ER vesciculation and shedding of plasma membrane microvescicles containing granules and cytosolic components [75]
- histone citrullination, chromatin decondensation, migration of elastase and other granule enzymes into the nucleus [76]
- disintegration of the nuclear membranes, plasma membrane rupture and release of DNA, histones and granule proteins into the extracellular space [76]

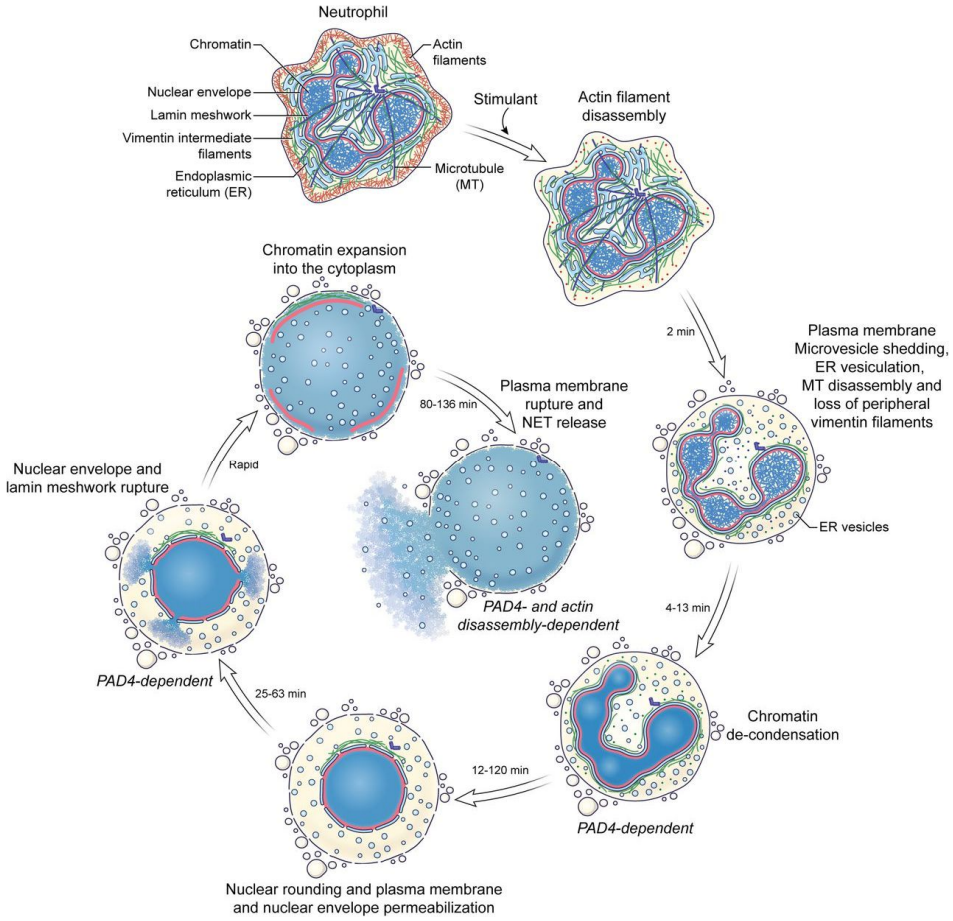

Figure 1.7. Cellular events mediating NETs release. [75]

It has been demonstrated that NETosis is different from apoptosis and necrosis: in contrast to apoptosis or necroptosis, there is no involvement of caspases and plasma membrane integrity is maintained until the last steps of the process, but it features the disintegration of the nuclear envelope [77]. When the plasma membrane finally ruptures, the microbicidal extracellular traps are released [78]. However, the intracellular signalling pathways are not well known. A potential role is attributed to p38 MAPK and to the upstream regulator MAPKK (such as MKK3) and MAPKKK (such as MEKK3), which are activated both by osmotic changes and glucose toxicity [79]. NETs formation is induced by pro-inflammatory stimuli, such as LPS, IL-8 and TNF-α, but also by several microorganisms and pathogens [78]. The molecular events that lead to NETs formation have been divided into two major pathways that have been termed NADPH oxidase (NOX)-dependent and -independent NETosis [60] (Figure 1.8)

• NOX-dependent NETosis (Figure 1.8) is induced by antibodies, microbes, cholesterol and *in vitro* by phorbol 12-myristate 13-acetate (PMA). These stimuli trigger c-Raf, MEK, Akt, ERK that in turn activate protein kinase C (PKC). PKC is responsible for membrane translocation and assembly of the

NADPH oxidase complex. Hydrogen peroxide triggers dissociation of the azurophilic granules, where NE MPO are stored. NE translocates into the nucleus, where it digests nucleosomal histones and promotes extensive chromatin decondensation. MPO has a synergistic activity with NE [80]. Chromatin decondensation is also mediated by citrullination of histone H3 and H4 by Peptidyl arginine deiminases-4 (PAD4) [81]. It has been demonstrated that patients with chronic granulomatous disease (CGD), who carry mutations in NADPH oxidase components and are susceptible to infections, show a severe deficiency in NET release [82].

• NOX-independent NETosis can be induced by calcium ionophore such as A23187, produced during the growth of *Streptomyces chartreusensis*, and the potassium ionophore nigericin, derived from the bacteria *Streptomyces hygroscopicus* [60]. A23187 causes a massive influx of calcium and nigericin stimulates potassium effluxes in cells which also results in the influx of calcium [83] . The calcium-activated potassium channel of small conductance (SK3 channel), induces mitochondrial ROS production and rapid citrullination of histone H3. This alternative pathway shows greatly reduced activation of ERK and Akt, while p38 is similar to the NOX-dependent NETosis [84].

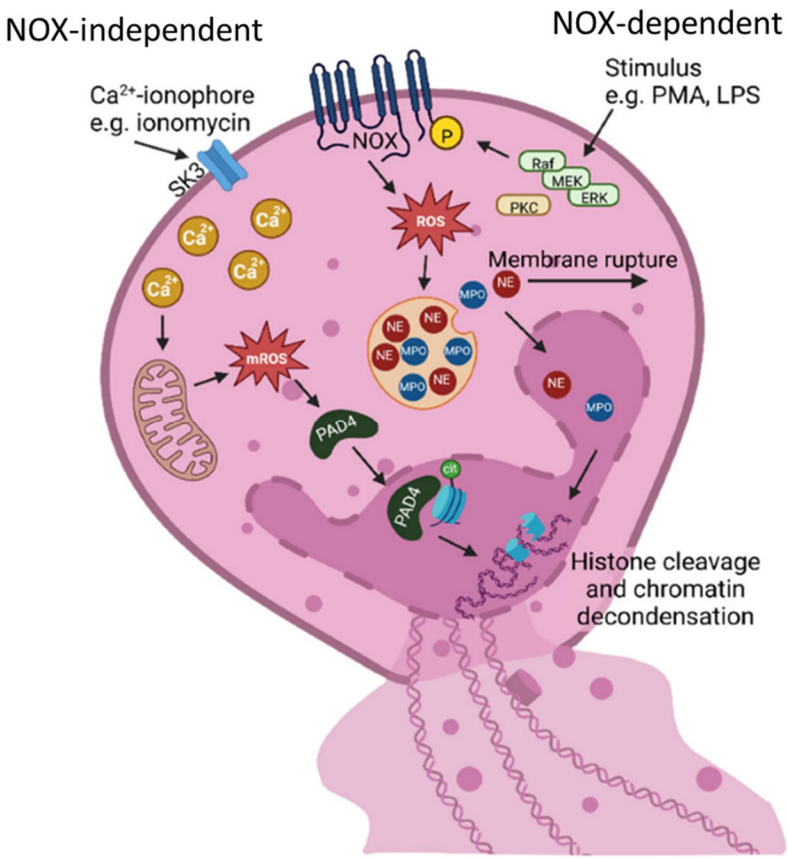

Figure 1.8. Representation of the two main pathways of NET formation. NOX-independent triggered by calcium ionophores and NOX-dependent by PMA and LPS. [85].

While the extrusion of nuclear material is believed to inevitably lead to cell death, Jorch et al distinguished two types of NETosis, termed suicidal and vital NETosis [86,87]. Suicidal NETosis occurs hours after stimulation with PMA and the release of NETs requires the disruption of the plasma membrane, resulting in the death of neutrophils [74]. On the other hand, during vital NETosis plasma membrane integrity is maintained. It takes place within minutes after the stimulation of neutrophils with bacteria or microbial-specific molecular patterns. NETs are released via nuclear-envelope blebbing and vesicular export [87], therefore neutrophils seem to maintain functional properties such as chemotaxis and phagocytosis [88]. It could be argued that a cell cannot function and live without an intact nucleus. Hovewer, red blood cells are metabolically active and survive for 120 days in circulation despite not possessing a nucleus. Therefore, since the half-life of neutrophil is only 24 to 48 hours, the concept of anuclear neutrophil survival is not impossible [88].

PAD4 in the onset of NETosis

Peptidyl arginine deiminases (PADs) is a family of calcium dependent enzymes that convert a positively charged arginine side chains into polar but uncharged citrulline side chains by deimination. This post-translational modification reduces the electrostatic bond between histones and DNA, allowing chromatin decondensation (Figure 1.9). Importantly, the citrullination of histone H3 has been reported to counteract transcription by preventing the methylation of arginine [89]. In each of the mammalian vertebrate genomes, five highly conserved PADs exist, including PAD1, 2, 3, 4 and 6, which differ in tissue distribution, gene features and preferred substrates. PAD4 is the most extensively studied, and it is detected in white blood cells, including granulocytes and monocytes under normal physiological conditions. The gene *Padi4* is localized in the nucleus and contains a nuclear localization signal sequence at its N-terminus (NLS). Human PAD4 can bind five calcium ions. Several flexible parts of PAD4 form stable secondary structures after the binding of calcium and substrate, indicating that calcium stabilizes the conformation of PAD4 and may facilitate the formation of the active site clef [89]. PADs and its citrullinated products have been associated with many human diseases, such as rheumatoid arthritis (RA), multiple sclerosis (MS) and cancer [89]. PAD4 is an important factor for NET-mediated innate immune functions and against infection from both Gram positive and negative bacteria[90]. Furthermore, NETs released within the vasculature could be a part of the thrombus scaffold promoting coagulation causing platelet adhesion, activation, and aggregation[91]. Recent findings demonstrated that Padi4 knockout mice are protected from deep vein thrombosis [92]. The same group showed that Padi4 knockout mice are protected in part from the

consequences of sepsis, underlining the subtle balance between antimicrobial host defence and the pathological consequences of NET release [93].

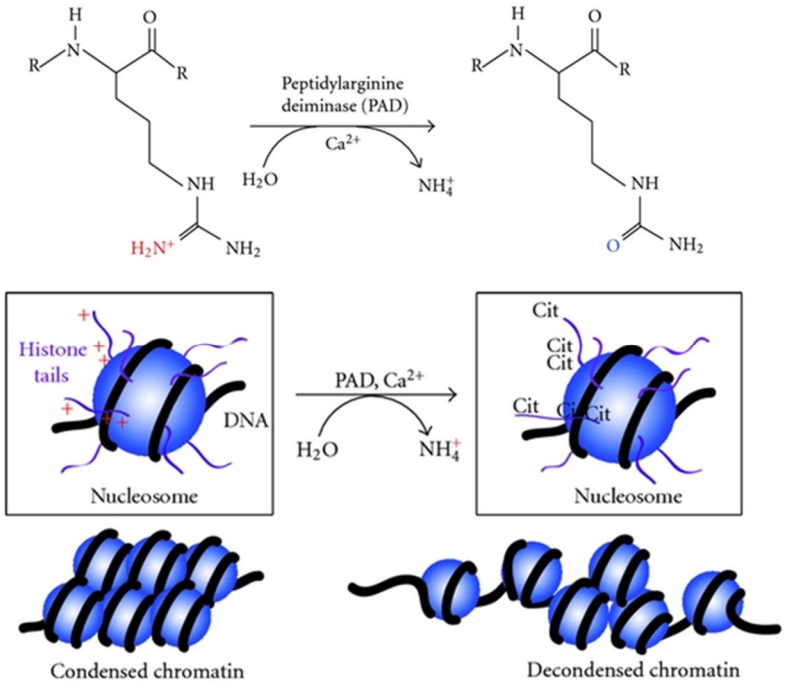

Figure 1.9 Histone citrullination and chromatin decondensation mediated by PAD4. [94]

NETs and NETosis in type 2 diabetes and their complications

NETs are an important component of the antimicrobial response of neutrophils. However, the detrimental effects of an exaggerated release of NETs are associated with occlusion, tissue damage or amplification of the immune response [95]. Such damages derive from NETs components, production of ROS and release of cytotoxic granule proteins. Extracellular histones can induce cytotoxicity [96] and circulating cell-free double strand DNA released with NETs is recognized as a "danger-associated molecular pattern" (DAMP), that can promote an exaggerated activation of innate immunity, leading to tissue damage [97] . More recently, NETs were found in tracheal aspirate and lung tissues of patients with severe COVID-19 [98]. NETosis play a crucial role in cardiovascular diseases, cystic fibrosis, thrombosis, periodontitis, autoimmunity and diabetes [76]. NETs deposited on the vasculature can promote thrombosis by formation of fibrin and platelet aggregation [91]. Autoantibodies present in patients with autoimmune diseases can recognize NETs antigens and induce NETs formation [99].

Schaper and colleagues defined diabetes as a "disease of impaired damage control" [100], and in line with this concept recent studies tried to understand the effects of diabetes and hyperglycaemia on NETosis. Studies *in vitro* demonstrated that high glucose is able to stimulate neutrophils to release nuclear material, histones and DNA [101]. This result was confirmed also by analysing sera of type 2 diabetic patients (T2D) and matched-control individuals: in T2D patients there was a significant increase in the levels of mono and oligonucleosomes, cell-free double-strand DNA and neutrophil NE compared to age- and sex matched controls, even though the count of neutrophils in peripheral blood was similar [101]. Moreover, circulating NET markers were found to positively correlate with the percentage of glycated haemoglobin A1c (HbA1c), a marker of glucose control [102]. Furthermore, deregulation of NETosis promotes chronic diabetic complications. Excess NETosis contribute to delayed wound healing in diabetic mice [103] and skin wounding was associated with a striking increase in NETting neutrophils infiltrating the tissue (Roth Flach & Czech, 2015). However, genetic deletion or pharmacological inhibition of PAD4 rescued wound healing in diabetic mice [104].

Neutrophils appeared to be involved in the pathogenesis of T2D, since they migrate in the visceral fat of obese mice 3 days after high-fat diet [13]. Neutrophils secreted NE have been suggested to develop IR, by inhibiting hepatic insulin signaling and sustaining liver and adipose tissue inflammation. [105]. However, it is not clear whether the sources of NE are NETs. The contribution of NETosis in the context of obesity and T2D is still under investigations. It was reported that HFD-induced obese mice, treated with the PAD4 pharmacological inhibitor Cl-Amidine, didn't show any significant benefits in terms of weight gain or metabolic performance. The paper, however, has some limitation regarding a rather modest obese and dismetabolic phenotype that didn't rule out completely a potential role of NETosis in the onset of obesity and metabolic dysfunction[106]

NETs in the pathophysiology of gastrointestinal inflammatory diseases

Recently, NETs were suggested to be involved in various intestinal diseases, such as inflammatory bowel disease (IBD), colorectal cancer (CRC) and intestinal ischemia/reperfusion injury [107]**.** Recent evidence underlies a connection between neutrophil infiltration within the gut and epithelial barrier impairments. Infiltrating neutrophils utilize several immune mechanisms, including phagocytosis, reactive oxygen species production, degranulation and the release of NETs. Several studies reported a role of NET formation in intestinal diseases [107]. For example, NETs are important in preventing systemic bacterial dissemination [108]. Gut microbiota translocation and the release of intestine-derived inflammatory factors in the systemic circulation are drivers of sepsis and organ injuries, and abundant neutrophils are activated to release NETs in the gut in lipopolysaccharide- (LPS-) induced sepsis.

NET formation during IBD could exacerbate mucosal inflammation and contributes to intestinal Ischemia/reperfusion injury [109]. In addition, NET is enhanced in the inflamed intestinal mucosa of mice with experimental colitis [110].

AIM OF THE WORK

In obesity and type 2 diabetes, the response of neutrophils is deregulated as they are primed to release NETs and undergo NETosis. Since PAD4 activity is required for NETs release, we aimed to study the effects of *Padi4* deletion in the onset of dysmetabolism and chronic inflammation in a mouse model of diet-induced obesity. Since alterations in gut composition, accompanied with enhanced intestinal permeability and metabolic endotoxemia have been suggested as key players of metabolic disorders, we will explore if the onset of dysbiosis could represent a trigger for neutrophils to undergo NETosis. Our hypothesis is that NETs might abridge the effects of an obesogenic gut flora toward systemic metabolism.

MATERIALS AND METHODS

Mice

All of the procedures were approved by the local ethics committee and the Italian Ministry of Health. National and international guidelines for the use and care of laboratory animals were followed. Mice were housed in the animal facility of the Venetian Institute of Molecular Medicine (VIMM), where they were kept in constant 12-h dark–light cycles and gave access to food and water ad-libitum and they were backcrossed on the C57BL/6J background. Hemizygous B6(Cg)- Padi4tm1.2Kmow mice were bought from the Jackson Laboratory (Bar Harbor, Maine, United States) and were crossed to obtain homozygously *Padi4* floxed (*Padi4fl/fl,* Floxed) mice. These mice were then crossed with B6(Cg)-*Commd10Tg(Vav1-icre)A2Kio*/J from the Jackson Laboratory for the generation of Vav1-Cre+ mice bearing *Padi4* hemizygous floxed alleles. *Padi4* floxed homozygous were finally crossed with Vav1-Cre+ *Padi4* floxed hemizygous to obtain Vav1-Cre+ *Padi4fl/fl* (Padi4KO) mice.

High-fat diet

For the high-fat diet protocol, male and female mice at 8 weeks of age were assigned to a standard diet (STD, 68% of calories from carbohydrates, 23.5% from proteins, 8.5% from fat 4RF21; Mucedola, Milan, Italy) or an high-fat diet (HFD, 60% of calories from fat, 21% from carbohydrates, 19% from proteins, EF acc. D12492 (I) mod.; Ssniff, Soest, Germany) for 12 weeks. Mice were individually weighted once a week for the entire duration of the experiments.

Genotyping

Genomic DNA (gDNA) from ears' fragments was extracted by digesting sample for 1 hour at 56°C in 50 μL of lysis buffer (proteinase K 20 ng/mL in Tris HCl 1M pH 7.5). The primer sequences for PCR genotyping were the following: (forward) TGACCAATGGATGCAGGACG and (reverse) CTCTGTCCCTCGGGGAGTC. Samples were amplified using the C1000™ Thermal Cycler (Bio-Rad Laboratories, Milano, Italy).

Metabolic tests

Mice were fasted for 5 hours before the ipGTT (intraperitoneal Glucose Tolerance Test), ipITT (intraperitoneal Insulin Tolerance Test) or ipPTT (intraperitoneal Pyruvate Tolernce Test) was performed. Basal glucose levels were measured and 1 g/kg of d-glucose (ipGTT), 0.75 U/kg human

recombinant insulin (ipITT) or 1g/kg sodium pyruvate (ipPTT) was injected. Glycemia was measured at 30, 60, and 120 min after injection by assessing a drop of blood taken from the tail of each animal (tail vein puncture). Peripheral blood triglycerides and cholesterol were measured using Allegro ® analyzer (Nova Biomedical, Waltham, MA, USA). HOMA-IR was calculated as follows: $\text{HOMA-IR}=\frac{\left(\text{glucose}\left(\frac{\text{mmol}}{\text{L}}\right)\times\text{insulin}\left(\frac{\text{mU}}{\text{L}}\right)\right)}{22.5}$.

Whole body composition and metabolic cages

Body composition was determined with EchoMRI™ 100 (EchoMRI™ LLC, Texas, USA) and lean mass was used to calculate metabolic parameters: VO2, VCO2. Animals were singularly housed in TSE PhenoMaster cages (TSE Systems GmbH, Germany) for 4 days at 23°C with a 12h light/dark cycle. Mice were allowed to adapt to new environments for 24 hours before measurement. VO2, VCO2, food intake and water consumption were recorded for 3 consecutive days. Respiratory Exchange Ratio (RER) was calculated as VCO2/VO2 [26]. Energy Expenditure was calculated using the formula [26]: Energy Expenditure = 3.941·VO2 + 1.106·VCO2 1000 Kcal·h -1 ·Kg

Neutrophils isolation

Neutrophils were isolated by flushing femurs and tibie of 2- to 6- month-old mice and purified with the Neutrophil Isolation Kit (MACS Miltenyi Biotec). Purified neutrophils were cultured in RPMI with L-Glutamine (Glu) (Gibco).

***In vitro* NETs release**

Isolated neutrophils were stained with 1 μg/ml Hoechst 33342, seeded in a 96 well plate at a density of 100.000 cells/mL and stimulated with medium, 100 nM phorbol 12-myristate 13-acetate (PMA), 5 μM ionomycin for 3 hours. Sytox green (125nM) was added to the medium. Release of dsDNA in the extracellular space was monitored by quantifying Sytox green fluorescence on a plate reader (Perkin Elmer Kaleido 2.0), relative to the Hoechst 33342 signal. Fluorescence was recorded every minute for 180 minutes using the following filters: (Sytox green Exc. 503 nm, Em. 523 nm; Hoechst 33342 Exc. 350 nm, Em. 450 nm).

Live confocal microscopy

Isolated neutrophils were stimulated with 100 nM PMA for two hours. Cells were stained with 1 µg/ml Hoechst 33342 and, just before imaging, 100 nM Sytox green (Life Technologies) was added to the medium to allow visualization of NETs. A modular multiphoton microscope (Bergamo II, Thorlabs) equipped with 8 kHz resonant scanner, extended-field-of-view collection optics, 4 independent detection channels in the backward direction and laser-scanned Dodt contrast in the forward direction was used. The microscope was coupled to two synchronized pulsed laser beams generated by a Ti:Sapphire pump laser (Chameleon Ultra 2, Coherent) and an optical parametric oscillator (Camelion Compact OPO). Photon microscopy at 800 nm excitation was used to visualize Sytox Green and Hoechst 33342. Experiments were performed with an 60x objective (Olympus LUMFLN60XW, N.A. 1.1, 1.5 WD) and cells were imaged from 0 to 120 minutes. In separate experiments, the Nikon ECLIPSE Ti2 microscope, which delivers a 25 mm field of view (FOV), equipped with a Nikon 20x air objective was used. The fully motorized system allows fast recording of 3 different wells for up to 2 hours and the stage is at controlled temperature (37°C). 3 different information were obtained: in epifluorescence intact nuclei in blue (Hoechst 33342, excitation LED 395 nm; emission DAPI filters) and the formation of NETs in green (Sytox green, excitation LED 525 nm; emission FITC filters); bright illumination detected cell morphology in grey scale.

Bioluminescence imaging assay *in vitro*

Neutrophils were separated from bone marrow of the mice according to the density-gradient centrifugation-based protocol previously described by others [111]. Purified neutrophils were seeded (100'000 cells/mL) in black coated 96 well plates. We performed assays in RPMI with L-Glutammine and Penicillin-Streptomycin supplemented with luminol (200µM). We imaged the plate at the indicated time points in the absence or presence of PMA (300nM).

Western blot of neutrophils

2-4 x 10^6 purified neutrophils (pre-tretead with 10µM GSK-484 inhibitor for 40 minutes) stimulated with 5 µM calcium ionophore (A23187) for 1h or 300 nM PMA for 3h, were lysed using RIPA buffer prepared as follows: 150 mM NaCl pH 7.5, 50 mM Tris HCl, 1% Sodium Deoxycholate, 0.1% SDS, 1 mM EDTA, 1% TritonX-100, 1:100 Phosphatase inhibitors cocktail II and III (Sigma-Aldrich) and 1:50 Complete Protease inhibitor (Roche). Protein concentration was determined using the BCA protein assay (Pierce)

Proteins were subjected to 12% SDS/polyacrylamide gel and transferred to PDVF membrane. Membranes were blocked with 5% milk or 2% BSA in TBS (1M Tris HCl pH 7.4, 5M NaCl, 0.1% Tween 20) and then incubated with primary antibodies anti-PAD4 (1:2000, abcam, ab214810), anti-Histone H3 (citrulline R2-R8-R17) (1:1000, abcam, ab5103) and against β-actin (1:5000, abcam, ab6276) as loading control. Immunolabeled proteins were detected by using appropriate HRP-conjugated secondary antibodies (Jackson ImmunoResearch), and immunoreactive bands were revealed using enhanced chemiluminescence (ECL) detection (Pierce).

Immunofluorescence of neutrophils

Isolated neutrophils were seeded in culture slides (Becton Dickinson) and stimulated with 100 nM phorbol 12-myristate 13-acetate (PMA) for 3 hours or 5 μM calcium ionophore (A23187) for 1 hour. Next, cells were fixed in 4% paraformaldehyde and washed with PBS. After 30 minutes blocking and permeabilization (PBS/BSA 1%, goat serum 10%, Triton 0,4%), the sections were stained with the primary antibodies s100a9 (1:100, abcam ab105472) and anti-Histone H3 (citrulline R2-R8-R17) (1:75, abcam, ab5103) followed by Goat Anti-Rabbit Alexa Fluor® 488 (Jackson ImmunoResearch, Cat. No. 111-545-046, 1:200) and Cy3 (Chemicon-international, 1:200) conjugated secondary antibodies. Hoechst 33342 was used for cell nuclei staining. Zeiss LSM900 was used to acquire confocal images.

Glucose uptake

Mice were injected intraperitoneally with a 37:1 ratio of D-glucose (1 g/kg) and 2-Deoxy-D-Glucose (2DG, 0.027 g/kg, Merck). After one hour, mice were humanely sacrificed, and tissues were frozen in liquid nitrogen. Glucose uptake was measured using 2DG Uptake Measurement Kit (CosmoBio Co., LTD, Tokyo, Japan) as previously described [112].

Thioglycollate-induced peritonitis

Mice were injected intraperitoneally with 1 mL of 4% sterile thioglycollate. 5 hours later, mice were killed and 10 mL of cold PBS was injected slowly into peritoneal cavity using a 26G1/2 needle. Mice were briefly agitated to wash peritoneal cavity. Then, an 18G1/2 needle connected with a 10 mL syringe was inserted to retrieve the maximal amount of PBS. The cells were centrifugated and the pellets resuspended in MACS buffer for the neutrophils' separation, according to the Neutrophil Isolation Kit (MACS Miltenyi Biotec) protocol. Neutrophils's purity was checked with flow

cytometric analysis by incubating them with the following antibodies: 1 µL Alexa Fluor-488 α-mouse CD115 (Invitrogen) and 1 µL PE - α-mouse Ly-6G/ Gr-1 Ab (eBionsciences). Then, neutrophils were resuspended in 1 mL of QIazol Reagent for RNA extraction (Quick-Startprotocol).

Neutrophil migration

After neutrophils immunomagnetic separation (MACS Miltenyi Biotec protocol), neutrophils' purity was checked with flow cytometry. Cells were resuspended at 10^6 cells/mL in RPMI 0.1% Bovine Serum Albumin (BSA) with L-Glutamine (Glu) and Penicillin-Streptomycin (P/S) medium without FBS and incubated at 37°C for 30 min. 600µL of RPMI 0.1% BSA Glu and P/S medium was added on the bottom of a 24 well plate, with or without 100 ng/mL mouse recombinant SDF-1 (R&D). 200 µL of cells were loaded into 3 µm-pore Transwell (BD Falcon). The plate was incubated at 37°C for 1 hour. 500 µL of cells from each well were harvested and cells counted with flow cytometry.

dsDNA quantification

Plasma dsDNA was quantified with Qubit fluorometer 2.0 (Thermo Fisher Scientific).

RNA isolation and quantitative Real time PCR

RNA was isolated according to the manufacturer's instructions using QIazol® Lysis Reagent (79306; QIAGEN Sciences) and quantified with a Nanodrop 2000 spectrophotometer (Thermo Fisher Scientific, Waltham, MA, USA) or with a Qubit fluorometer 2.0 (Thermo Fisher Scientific). cDNA was synthesised with the SensiFast cDNA Synthesis Kit (BIO65054; Bioline, London, United Kingdom). Quantitative real-time PCR was performed using the SensiFAST™ SYBR® Lo-ROX Kit (Bioline, London, UK) via a QuantStudio 5 Real-Time PCR System (Thermo Fisher Scientific, MA, USA) using the primer list in table 1. Results are shown as fold change relative to the controls after normalization for ubiquitin C transcript levels.

Gene	Symbol	Sequence
Peptidyl arginine deiminase, type IV	Padi4	Fw: TGACCAATGGATGCAGGACG
		Rv: CTCTGTCCCTCGGGGAGTC
Interleukin 1 β	IL-1 β	Fw: AGCTTCCTTGTGCAAGTGTCT
		Rv: GACAGCCCAGGTCAAAGGTT
Interleukin 6	IL-6	Fw: AGTCTCCTCTCCGGACTTGT
		Rv: TCCTCTCTGCAAGAGACTTCC
Tumor necrosis factor	TNF-α	Fw: AAAAGCAAGCAGCCAACCA
		Rv: CGGATCATGCTTTCTGTGCTC
Myeloperoxidase	MPO	Fw: TCCCACTCAGCAAGGTCTT
		Rv: TAAGAGCAGGCAAATCCAG
Neutrophil elastase	Elane	Fw: GTTGGGCACAAACAGAAC
		Rv: GCAAACTCAGCCACAGG
Adiponectin	AdipoQ	Fw: GACGACACCAAAAGGGCTCA
		Rv: GAGTGCCATCTCTGCCATCA
Leptin	Lep	Fw: TCACACACGCAGTCGGTATC
		Rv: CACATTTTGGGAAGGCAGGC
Monocyte chemoattractant protein 1	MCP-1	Fw: GTGCTGAAGACCTTAGGGCA
		Rv: AGCTGTAGTTTTTGTCACCAAGC
Oncostatin-M	OSM	Fw: AGCCCTATATCCGCCTCCAA
		Rv: GTGTGTCCTCACTGGGGAAG
Phosphoenolpyruvate carboxykinase	PEPCK	Fw: ATGAAAGGCCGCACCATGTA
		Rv: GCACAGATATGCCCATCCGA

C-X-C motif chemokine receptor 2	CxCr2	Fw: CTTCCAGTTCAACCAGCCCT
		Rv: ATCTTTGAGGTAACTTTAATCCTGC
Cytochrome b-245 light chain	Cyba	Fw: TGGACGTTTCACACAGTGGT
		Rv: TGGACCCCTTTTTCCTCTTT
Neutrophil cytosol factor 1	Ncf1	Fw: ATACCTGGTGCCCAAAGATG
		Rv: CTGTTCCCGAACTCTTCTCG
C-X-C motif chemokine 12	CxCl12	Fw: CGGGTCAATGCACACTTGTC
		Rv: GAGCCAACGTCAAGCATCTG
Polyubiquitin-C	Ubc	Fw: GCCCAGTGTTACCACCAAGA
		Rv: CCCATCACACCCAAGAACA
Glucagon-like peptide 1	GLP-1	Fw: TCTGACGAGATGAGCACCA
		Rv: TGACTGGCACGAGATGTTG
Interleukin-17	IL-17	Fw: AAGGCAGCAGCGATCATCC
		Rv: GGAACGGTTGAGGTAGTCTGAG
Interleukin-22	IL-22	Fw: CATGCAGGAGGTGGTGCCTT
		Rv: CAGACGCAAGCATTTCTCAG
Arginase	Arg	Fw: ACAAGACAGGGCTCCTTTCAG
		Rv: GGCTTATGGTTACCCTCCCG
Regenerating islet-derived protein 3 gamma	Reg3g	Fw: CGCTGAAGCTTCCTTCCTGT
		Rv: GGGTTCATAGCCCAGTGTCG
Zonula Occludens-1	ZO-1	Fw: CCACCTCTGTCCAGCTCTTC
		Rv: CACCGGAGTGATGGTTTTCT
Thermogenin	Ucp-1	Fw: CCGAAACTGTACAGCGGTCT
		Rv: CCGAGAGAGGCAGGTGTTTC

Mannose receptor C-type 1	Mrc-1	Fw: CCTTGCCTGATGCCAGGTTA
		Rv: TTGCACTTTGAGGGAAGCGA
Vascular endothelial growth factor	Vegf	Fw: GAGCAGGCTGCTGTAACGAT
		Rv: GACCCTTTCCCTTTCCTCGAA
Glucose 6-phosphatase	G6pase	Fw: AGGAAGGATGGAGGAAGGAA
		Rv: TGGAACCAGATGGGAAAGAG
Calprotectin	S100a8	Fw: TCACCATGCCCTCTACAAGA
		Rv: CCAATTCTCTGAACAAGTTTTCG

Table 1. Primer list for qPCR.

Tissue processing

Tissues were snap-frozen in liquid nitrogen and kept at -80°C. Portions of intestine were placed in Killik cryostat medium (Bio-Optica, Milan, Italy), immersed in cold 2-methylbutane (Sigma-Aldrich), and kept at −80°C. 10/15-µm-thick sections were obtained with a Leica CM 1950 cryostat (Leica Biosystems S.r.l., Milan, Italy), placed on Superfrost Plus slides (J1800AMNZ; Gerhard Menzel GmbH, Braunschweig, Germany) and stored at -20°C. Portions of adipose tissues were placed on Ethanol 100% and embedded on paraffin.

Analysis of adipose tissue sections

Paraffin-embedded VAT were cut into 4µm sections and stained with H&E. Images were acquired with the Leica DM6B microscope. Individual adipocytes were detected in a semiautomated manner using the SMASH segmentation program and manually curated with ImageJ software. Dimension was determined using a pixel-to-micron conversion factor.

Immunofluorescence of adipose tissue sections

Paraffin-embedded VAT sections were deparaffinized with xylene and hydrate with ethanol. A citrate-based antigen-retrieval protocol was applied. The tissues were then blocked with PBS/BSA 1%, goat serum 10% and stained with anti-Histone H3 (citrulline R2-R8-R17) (1:75, abcam, ab5103) or anti-Elastase (1:200, abcam ab68672) overnight at 4°C. Next, the slides were incubated with the

secondary antibody goat anti-rabbit Cy3 (Chemicon-international, 1:200) and Alexa Fluor® 488 conjugated WGA (Wheat Germ Agglutinin). Cell nuclei were stained by incubating sections in Hoechst 33342. Leica DM6B microscope was used to acquire the images.

Immunofluorescence of liver sections

Snap-frozen liver specimens were sectioned at 10/15-µm. The tissues were blocked with PBS/BSA 1%, goat serum 10% and stained with anti-Histone H3 (citrulline R2-R8-R17) (1:75, abcam, ab5103) or anti-Elastase (1:200, abcam ab68672) overnight at 4°C. Next, the slides were incubated with the secondary antibody goat anti-rabbit Cy3 (Chemicon-international, 1:200) and Alexa Fluor® 488 conjugated WGA. Cell nuclei were stained by incubating sections in Hoechst 33342. Leica DM6B microscope was used to acquire the images.

Oil red O staining of liver sections

Snap-frozen liver specimens were sectioned at 10/15-µm and stained with Oil red O. The quantification of lipid droplets was expressed as percentage of the lipid cells (red) relative to the area with ImageJ software.

Multiplex bioplex

Peripheral blood citokynes were quantified using a multiplex immunoassay (Mouse Diabetes 8-Plex, Bio-Rad Laboratories, USA). GSEA software was used to analyse the array (Broad Institute, USA).

Histology of colonic sections

Frozen colon sections were stained with H&E and images were acquired with the Leica DM6B microscope.

lmmunofluorescence of colonic sections

Cryosections of the intestine were fixed in 4% paraformaldehyde and blocked (PBS/BSA 1%, goat serum 10%) for 30 minutes. Sections were immunostained using anti ZO-1 Polyclonal Antibody (1:100, Invitrogen, Cat. 40-2200) or anti-Histone H3 (citrulline R2-R8-R17) (1:75, abcam, ab5103), followed by Cy3-conjugated affinity purified secondary antibody (1:100, Chemicon®-international,

Cat. No. AP192C). Cell nuclei were stained by incubating sections in Hoechst 33342. Leica DM6B microscope was used to acquire the images.

FITC-dextran assay

Mice were fasted for 4 hours and orally gavage with 44mg/100g body weight 4kDa fluorescein isothothiocyanate-labelled dextran (FITC-4D, Sigma-Aldrich). After 3 hours, blood was collected and serum was separated. The concentration of FITC-dextran was determined by fluorescence spectroscopy (excitation of 485 nm and emission of 528 nm) relative to a linear standard curve made using diluted FITC.

ELISA (plasma LPS)

LPS level was assessed by enzyme-linked immunosorbent assay (ELISA) according to the manufacturer's instructions (CUSABIO, Cat. No. CSB-E13066m)

Fecal DNA extraction and Microbiota analysis

Fecal specimens were collected from each cage (one mouse/cage) in sterile vials and rapidly stored at -80°C. Bacterial DNA extraction was performed QiAmp® Fast DNA Stool Mini Kit (QIAGEN) according to the manufacturer's instructions. DNA concentration was determined by absorbance at 260 nm using NanoDrop (Thermo Fisher Scientific, Waltham, MA, USA), or Qubit (Thermo Fisher Scientific) for sequencing purposes.

PCR for 16S

Fecal bacterial DNA was extracted using Stool DNA isolation kit (NORGEN BIOTECH) according to the manufacturer's instructions**.** 40 mg of fecal pellets were used for each extraction. DNA concentration was determined by absorbance at 260 nm using NanoDrop (Thermo Fisher Scientific, Waltham, MA, USA). Quantitative real-time PCR was performed using the SensiFAST™ SYBR® Lo-ROX Kit (Bioline, London, UK) via a QuantStudio 5 Real-Time PCR System (Thermo Fisher Scientific, MA, USA) using the following primers: 16S R 1392r ACGGGCGGTGTGTAC, 16S F 1055f ATGGCTGTCGTCAGCT

Fecal microbiota transplantation (FMT)

Fecal pellets were collected from each cage and kept at -80°C. Before the gavage, pellets were homogenized in sterile water and filtered. For FMT, 2 months-old mice were placed in empty autoclaved cages (1-2 mice/cage) and divided into the following groups: Floxed FMT from STD fed mice, Padi4KO FMT from STD fed mice, Floxed FMT from HFD fed mice and Padi4KO FMT from HFD fed mice. All mice were provided the following antibiotics, in drinking water, for 3 weeks: neomycin (100 µg/ml), streptomycin (50 µg/ml), penicillin (100 U/ml), vancomycin (50 µg/ml), metronidazole (100 µg/ml), bacitracin (1 µg/ml), ciprofloxacin (125 µg/ml), ceftazidime(100µg/ml), and gentamycin (170µg/ml). FMT was performed by oral gavage for 3 consecutive days after antibiotic treatment. At the end of 3 weeks of flora reconstitution, ipGTT and ELISA for LPS were performed, as previously described.

ELISA (S100A8) on fecal samples

Frozen fecal pellets were reconstituted in PBS containing 0.1% Tween 20 and vortexed with TissueLyser for 20 minutes. Fecal homogenates were then centrifuged for 10 min at 10000 g at 4°C, supernatants were quantified using the BCA protein assay (Pierce) and stored at -20°C. s100a8 level was determined by enzyme-linked immunosorbent assay (ELISA) according to the manufacturer's instructions (DuoSet mouse Heterodimer S100A8/S100A9, R&D Systems). Concentrations were determined by comparison with standard curves.

Flow cytometry of tissues

Mice were previously perfused and tissue samples were placed on ice-cold PBS. Liver, VAT and colon were processed according to the protocol previously described by others [113]. Tissue suspensions were incubated with the following antibodies: 2µL PerCP- Vio 700 TM α-mouse CD45.2 Ab (MACS Miltenyi Biotec), 0.5µL PE-Cy™ 7 rat α -mouse CD11b Ab (BD Pharmingen), 0.5µL PE - α-mouse Ly-6G/ Gr-1 Ab (eBionsciences), 1µL Brilliant Violet 421™(BV421) α -mouse syglecF (BioLegend), 1µL APC α -mouse F4/80 (BioLegend)

Organoids and intestinal epithelial cells

Colonic crypts were isolated from the mice, seeded in Matrigel® (Corning), and cultured in the presence of N2 andB27 supplements (Invitrogen), mouse EGF (Invitrogen, 50ng/ml), Y-27632 (Sigma, 10uM), N-Acetylcysteine (Sigma, 1mM), Wnt3a, Noggin and R-Spondin. After expansion

by several passaging steps, organoids were seeded in 24 well plates for co-colture with neutrophils stimulated to undergo NETosis with 5 μM A23187. FITC-D4 was added in the culture medium for real-time barrier function assessment.

GSK-484 treatment

Male mice at 8 weeks of age were fed with HFD and treated by intraperitoneal injection with either PAD4 inhibitor GSK-484 (Cayman Chemicals) at 8mg/kg or vehicle (0.9% NaCl) every 2 days for 10 weeks. GSK-484 was dissolved in pure ethanol at a concentration of 25 mg/mL to generate a stock solution and further diluted in 0.9% NaCl shortly before injection.

Statistical analysis

All analysis was performed using GraphPad Prism software. Variables were compared between 2 or more groups by Student t-test or ANOVA, respectively, with the Bonferroni post-hoc correction for multiple comparisons. Results were considered significant at $p<0.05$.

RESULTS

Hematopoietic-restricted deletion of Padi4 in mice prevented histone citrullination and reduced NETs release

For the generation of our mouse model, we used the Cre/Lox system. Padi4$^{fl/fl}$ mice (from now on Floxed) were crossed with mice expressing the Cre Recombinase under Vav1 promoter. Vav 1 is a hematopoietic-specific guanine nucleotide exchange (GEF)[114], which drives the expression of Cre only in hematopoietic cells and their progenitors (Figure 2.1)

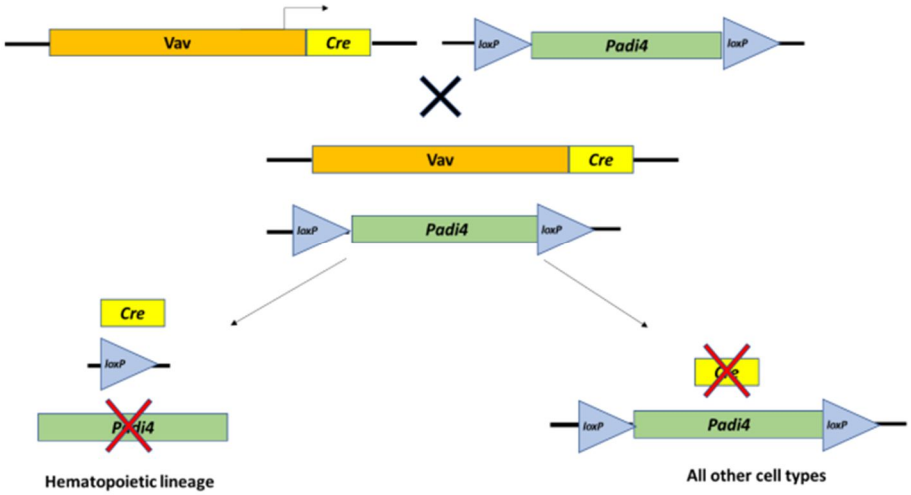

Figure 2.1. Schematic representation of generation of Vav1-Cre+ Padi4fl/fl mice (Padi4KO) as described in Material and Methods.

We confirmed the deletion of PAD4 by showing the complete absence of PAD4 in purified neutrophils from Padi4KO mice. In total BM from Floxed mice, a faint PAD4 band was still present, probably due to residual expression in other cells (Figure 2.2).

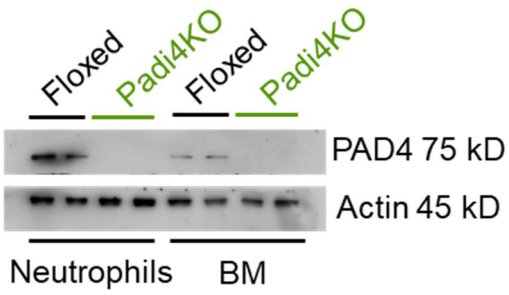

Figure 2.2. PAD4 protein expression. Western blot analysis of PAD4 expression in purified neutrophils and BM. Biological duplicates are shown. Actin was used as a loading control.

We next assessed the relative gene expression of *Padi4* by quantitative PCR (qPCR). As shown in Figure 2.3, neutrophils isolated from the BM of Padi4KO mice had a ~10^3-fold reduction of *Padi4* expression compared to neutrophils from Floxed mice. Skeletal muscle, liver and spleen from Floxed mice showed a negligible expression of *Padi4* compared to neutrophils.

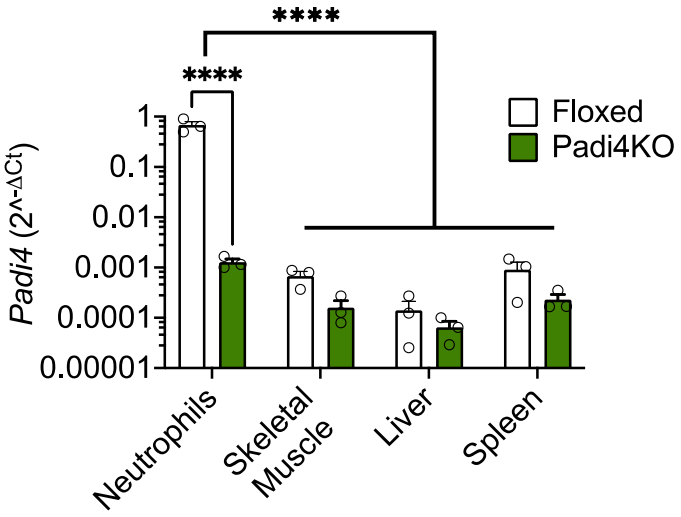

*Figure 2.3. Padi4 gene expression in different tissues. qPCR for Padi4 in skeletal muscle, liver, spleen and purified neutrophils from Floxed and Padi4KO- mice. Following 2way ANOVA and Bonferroni correction for multiple comparison. n=3 ****p<0.0001.*

The detection of citrullinated histone H3 (H3cit) represents a key hallmark of NETosis [115]. After stimulation with 5µM calcium ionophore A23187, H3cit was present only in neutrophils from Floxed mice. According to previous reports [83], PMA did not induce histone citrullination (Figure 2.4 A). These results were also confirmed by immunofluorescence staining for H3cit on isolated neutrophils *in vitro*. A23187 induced an efficient release of nuclear material, in neutrophils from Floxed mice, which was greatly reduced in Padi4KO neutrophils (Figure 2.4 B).

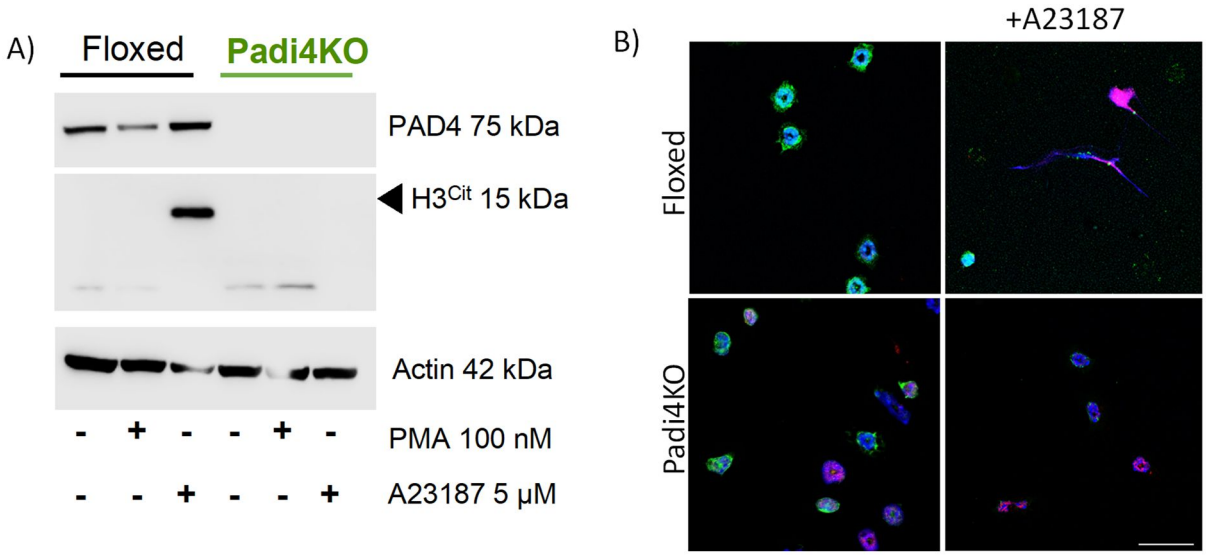

Figure 2.4. A) Western blot for PAD4 and H3cit in purified neutrophils from Floxed and Padi4KO mice after stimulation with 100nM PMA or 5µM A23187. B) Confocal images of unstimulated and A23187-stimulated neutrophils from Floxed and Padi4KO mice. Hoechst 33342 (blue), S100A8 (green) and H3cit (red). Scale bar 20 µm

The active release of dsDNA in the extracellular space can be monitored in vitro by measuring the signal of the cell-impermeable dye Sytox green, which becomes fluorescent when bound to dsDNA. In parallel, fluorescence of the cell-permeable dye Hoechst 33342 is proportional to DNA concentration and therefore decreases with dilution of DNA upon chromatic decondensation and nuclear expansion [116]. Padi4KO neutrophils showed defective NETosis as assessed in vitro by measuring the Sytox green/Hoechst 33342 signal ratio using a plate reader, after stimulation with 100 nM PMA or 5 µM ionomycin (Figure 2.5). In accordance with what was previously described by others (Douda et al., 2015), we found that ionomycin resulted in an earlier and stronger induction of NETosis compared to PMA (Figure 2.5).

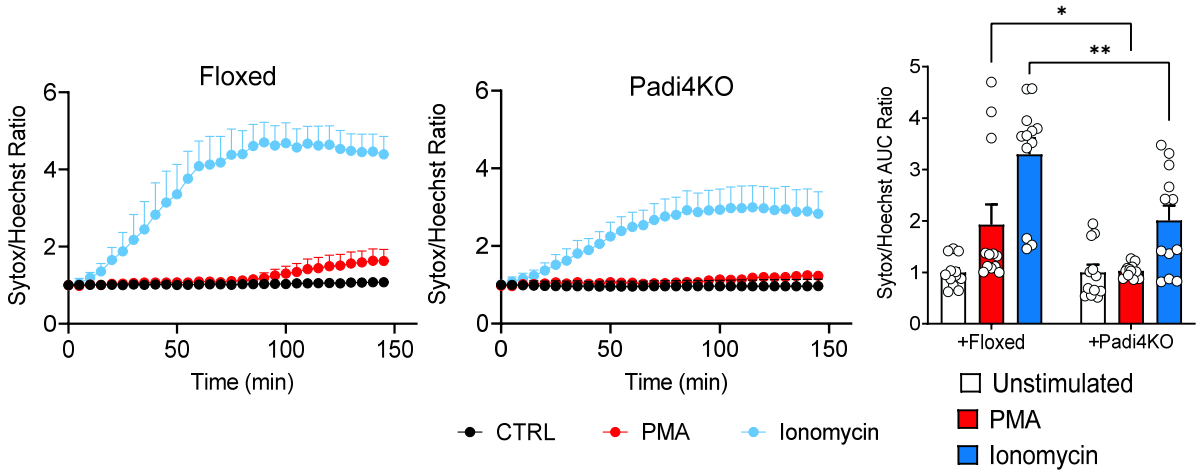

*Figure 2.5. Representative curves of the kinetics of Sytox/Hoechst Ratio from unstimualted neutrophils and after PMA and ionomycin stimulation. Area Under the Curve (AUC) for neutrophils from Floxed and Padi4 KO mice. n>6 **p<0.01 2-way Anova with Bonferroni correction*

Next, we used a luminol-based assay to assess the presence of MPO and indirectly quantify NET release. Luminol (5-amino-2,3-dihydro-1,4-phthalazine-dione) is redox-sensitive compound that emits luminescence (λ max = 425 nm) when exposed to an oxidizing agent. In particular, MPO can use the superoxide anion or other ROS as substrates for peroxidase-catalyzed oxidation of luminol (Gross et al., 2009). We stimulated neutrophils from Floxed and Padi4KO mice with PMA in the presence of luminol and measured luminescence over time. PMA induced a time-dependent increase in bioluminescence with a peak between 30 and 60 minutes, while no significant changes were observed in unstimulated neutrophils. Interestingly, luminescence from PMA-treated neutrophils of Floxed mice was significantly higher than Padi4KO mice (Figure 2.6).

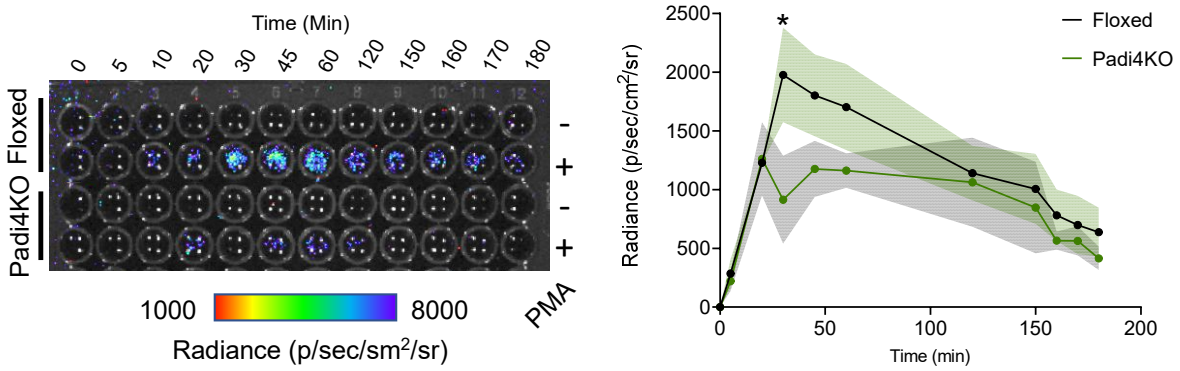

*Figure 2.6. Luminol-dependent bioluminescence. Representative time-course of unstimulated and PMA-stimulated neutrophils from Floxed and Padi4KO mice. n>6. *, p<0.05 2-way Anova with Bonferroni correction*

In order to have a deeper insight into the multi-step process of NETosis, we performed live two-photon confocal microscopy of NETting neutrophils, which allows a direct visualization of dsDNA release and nuclear dynamics in a single-cell fashion. The full-length video can be viewed at https://youtu.be/cy-i09uz15A. Nuclei were stained in blue with the cell-permeant Hoechst 33342 dye; mitochondria were stained in red with tetramethylrhodamine methyl ester (TMRM), which labels only energized mitochondria; the release of extracellular double strand DNA will be evaluated with the cell-impermeant Sytox green in the medium. Nuclear decondensation is observed after mitochondrial de-energization, and takes up to 1 h after PMA stimulation, during which the nucleus progressively enlarges before chromatin is extruded in the extracellular space. Then, NET release occurs very rapidly within seconds to minutes, as evidenced by the bright Sytox green extracellular fluorescence (Figure 2.7A). The image collected after 2 hours showed that PMA-induced NETosis was markedly increased in neutrophils of Floxed mice compared to Padi4KO. In unstimulated conditions (baseline), the green signal was almost absent in both Floxed and Padi4KO cells (Figure 2.7B).

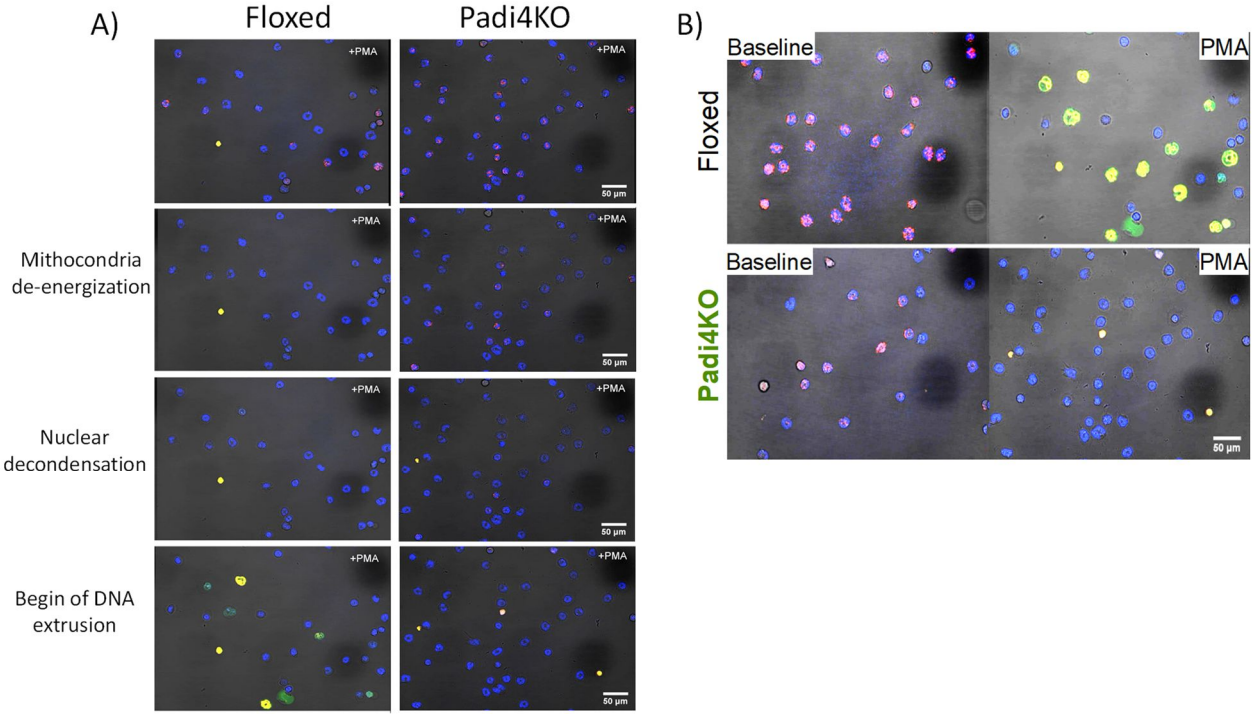

Figure 2.7 Two-photon confocal microscopy of NETting neutrophils. A) Snapshots are taken from the dynamic recording of neutrophils stimulated for 2 hours with 100 nM PMA. B) Images collected after 2 hours of baseline and PMA-stimulated neutrophils isolated from the BM of Floxed and Padi4KO. Hoechst 33342 (blue), Sytox green (green), TMRM (red). Scale bar 50 µm

Padi4 deletion did not affect neutrophils activation during acute inflammation

It has been previously shown that neutrophils exhibit gene expression profile changes as they transit from BM through the circulation and reach sites of inflammation/infection [117]. Therefore, we analysed gene expression of neutrophils isolated from the peritoneal exudate (PE) in a model of thioglycolate–induced peritonitis. Five hours after thioglycolate injection, neutrophils were isolated from the PE and checked for purity with flow cytometric (Figure 2.8 A). We used the BM as a sterile compartment and a source of naïve neutrophils to compare gene expression profiles. All genes in our panel show similar trends for both genotypes: *IL-1β* and *IL-6* expression were higher in PE, while the others decreased in PE neutrophils compared to BM neutrophils. Collectively, *Padi4* deletion did not affect gene expression of neutrophils after acute inflammatory activation (Figure 2.8 B).

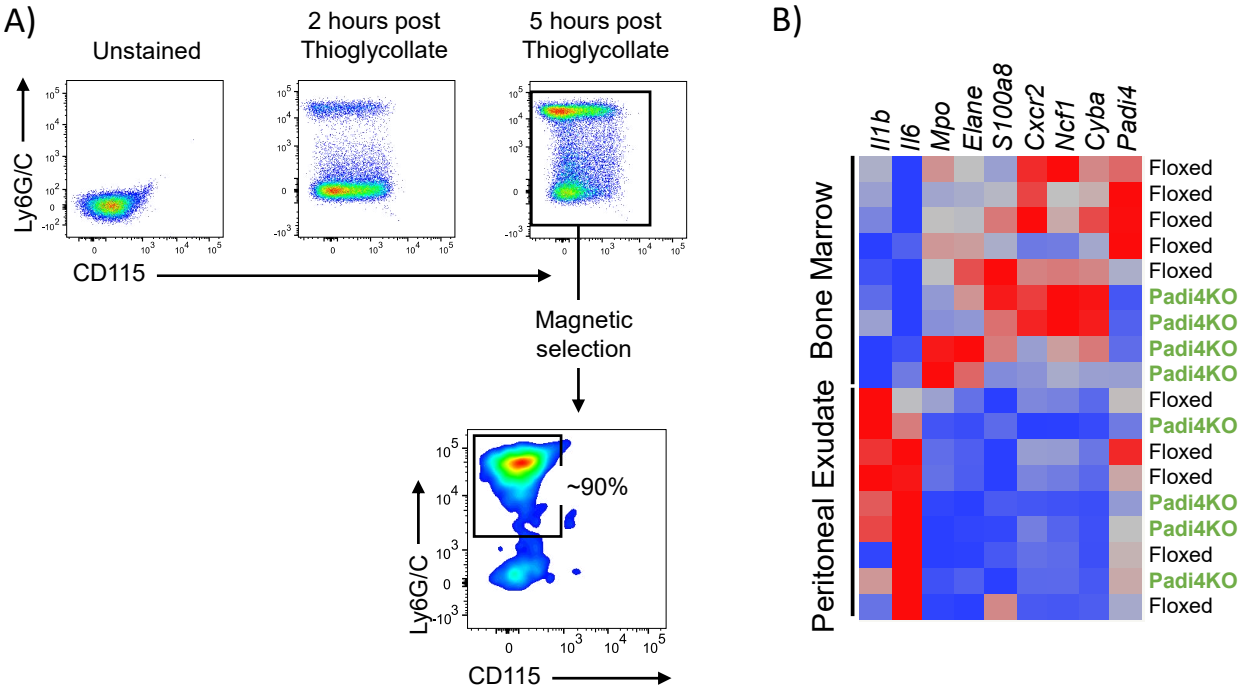

Figure 2.8. A) Gating strategy for neutrophils purity after immunomagnetic separation as described in Materials and methods. B) Heatmap representation of gene expression of neutrophils during inflammation in vivo. qPCR of neutrophils isolated from the bone marrow (BM) and peritoneal exudate (PE) after thyoglicollate-induced peritonitis. n≥4

Padi4 deletion did not affect neutrophil migration

PAD4 is involved in chromatin decondensation and remodelling, that could have an impact in the migration of neutrophils trough the endothelial junctions to enter the tissues. Indeed, migration requires remodelling of the nucleus and its content[118]. We analysed neutrophil migration with a standard trans-well assay toward a gradient of SDF-1α (CXCL12), a cytokine that regulates the

migration and homing of HSC, but also of leukocytes in general, through the binding with its receptor CXCR4 [66]. Neutrophils were isolated from the BM of Floxed and Padi4KO mice and allowed to migrate through a 4 μm pore membrane toward a 100 nM gradient of SDF-1α before being quantified with flow cytometry. Migration was quantified as fold of induction of SDF-1α-stimulated neutrophils vs basal migration (Figure 2.9). Neutrophils isolated from Padi4KO mice displayed a slightly, but not significantly reduced migration compared Floxed mice.

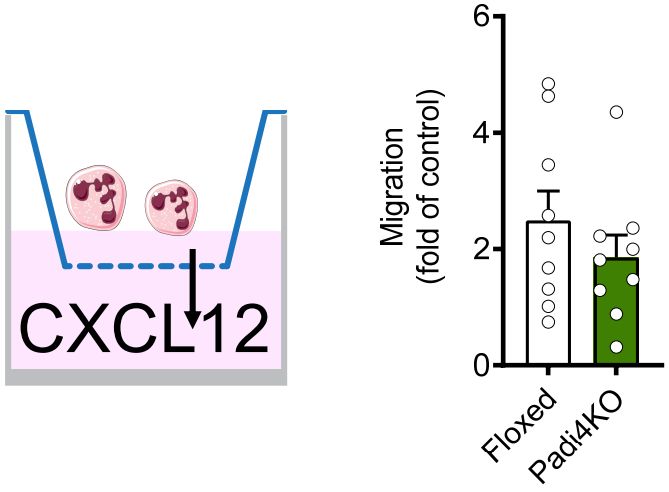

Figure 2.9. In vitro neutrophil migration assay. Neutrophils' migration in response to 100 nM gradient of SDF-1α represented as a fold of induction compare to basal migration. Following Student's t-test p=0.06 n =4.

HFD induced weight gain and change in body composition

To analyse the role of NETosis in the development of obesity and dysmetabolism we fed Floxed and Padi4KO mice with either a Standard Diet (STD) or a High Fat Diet (HFD: 60% of calories from fat, 21% from carbohydrates, 19% from proteins). After 12 weeks of HFD, both groups became obese (Figure 2.10 A). Body composition revealed that fat mass significantly increased in both genotypes after HFD, but this was accompanied by a slight increase of lean mass only in Floxed mice. Overall, HFD induced a remarkable decrease in lean mass/body weight ratio in both Floxed and Padi4KO mice (Figure 2.10 B). Other metabolic parameters, such as Total Cholesterol, Tryglicerides and LDL/HDL cholesterol, showed no meaningful differences between the two genotypes (Figure 2.11).

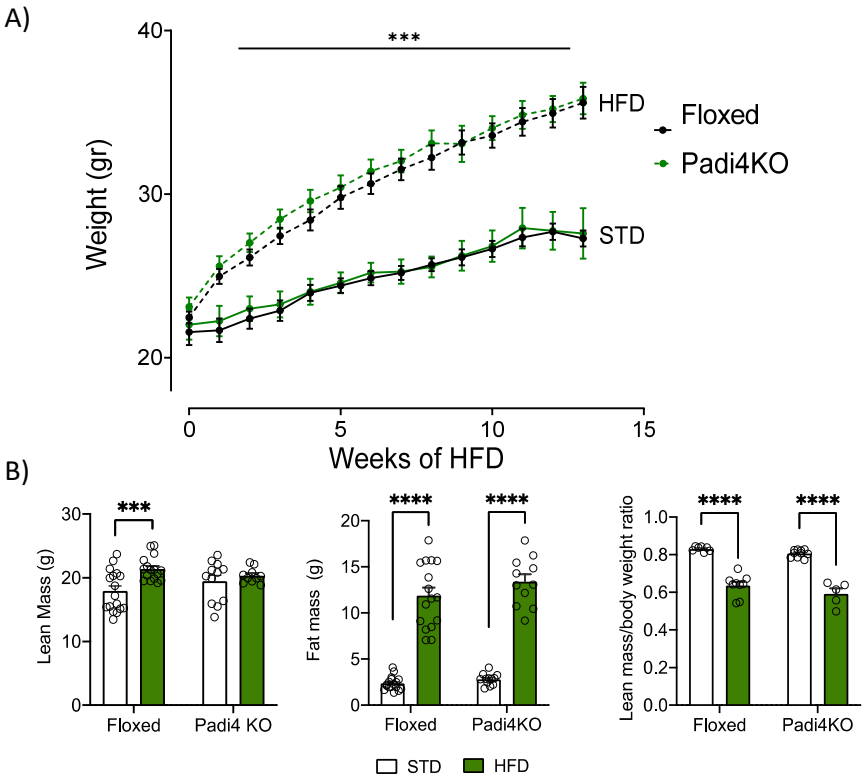

*Figure 2.10. A) Relative weight and B) Body composition of Floxed and Padi4KO mice after STD and HFD. n=15-20 for each group. ****p<0.0001, ***p<0.001. 2-way Anova with Bonferroni correction*

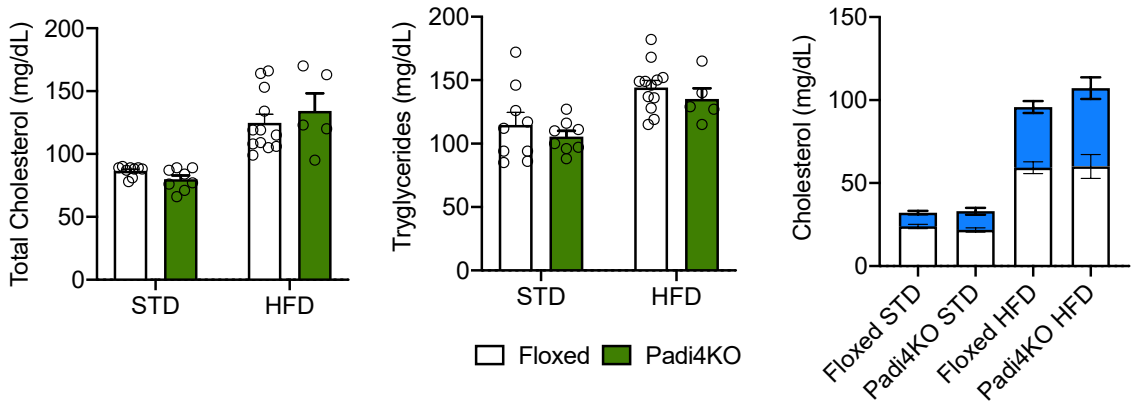

Figure 2.11. Plasma concentration of total cholesterol, tryglicerides and Cholesterol in Floxed and Padi4KO mice on STD and HFD. n=15-20.

Padi4KO mice were partly protected against the metabolic derangements induced by HFD

Since obesity is the major risk factor of metabolic diseases, we investigated the effects of HFD on metabolic performances of the mice. Padi4 KO mice were less glucose intolerant and less insulin resistant than Floxed mice after HFD, as shown by intraperitoneal Glucose Tolerance Test (ipGTT) (figure 2.12 A) and intraperitoneal Insulin Tolerance Test (figure 2.12 B). Accordingly, insulin

resistance in Floxed mice was accompanied by an increase of insulin concentrations in the peripheral circulation (figure 2.12 C) and with an increase of Homeostatic Model Assessment of Insulin Resistance (HOMA-IR), a static surrogate index of insulin resistance (Figure 2.12 D)

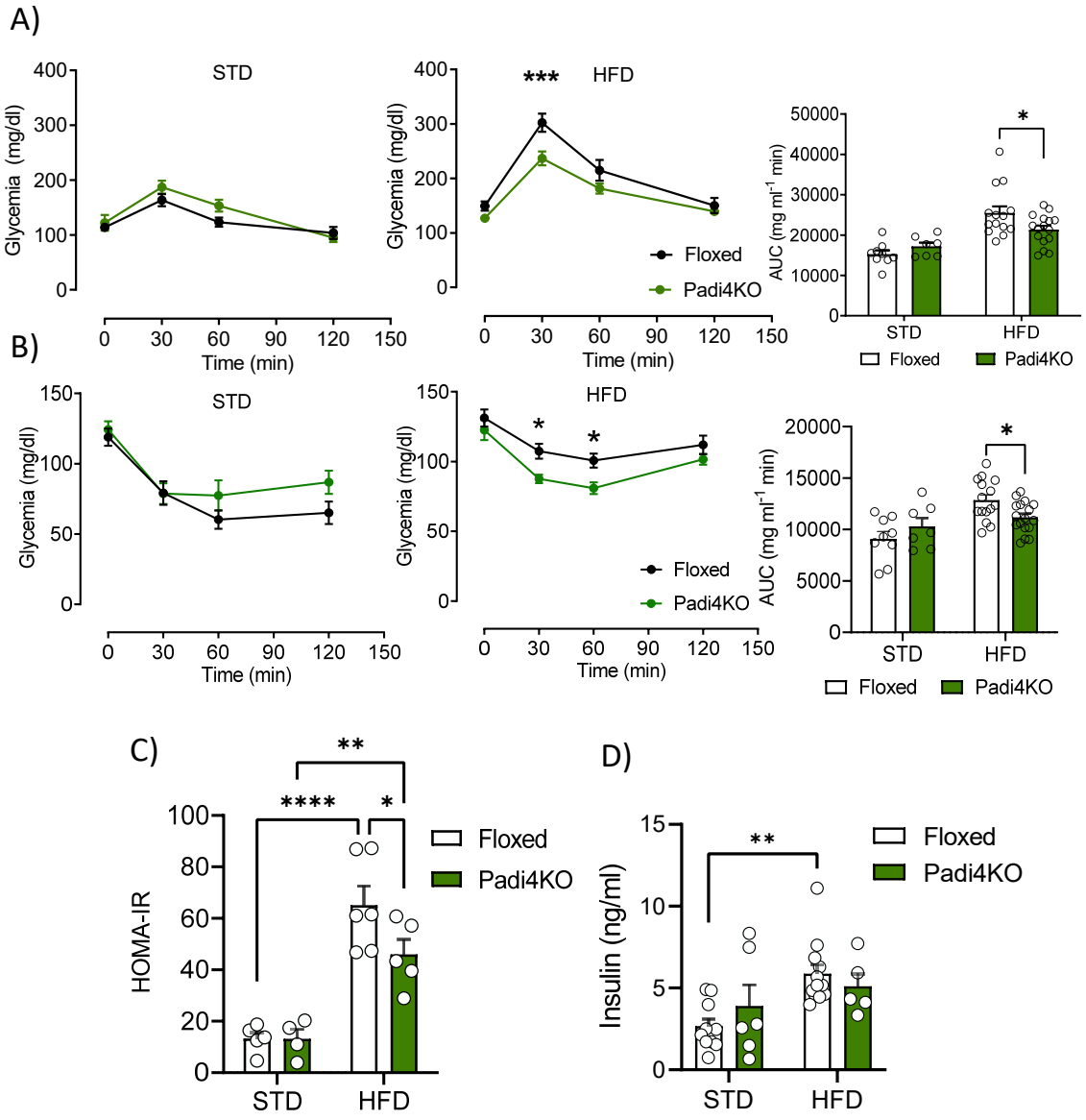

*Figure 2.12. A) ipGTT and B) ipITT of Floxed and Padi4KO mice after STD and HFD. C) Insulin quantification in plasma samples and D) HOMA-IR. n=6-15 ****p<0.0001, ***<p0.001, **p<0.01, *p<0.05 2-way Anova with Bonferroni correction*

By using metabolic cages, we found that the respiratory exchange ratio (RER) showed a similar circadian variation in lean Floxed and Padi4KO mice. As expected, HFD reduced RER and the loss of the circadian profile in both groups (Figure 2.13 A), indicating a shift of substrate utilization from carbohydrates to fatty acids [119]. We also examined changes in feeding behaviors. Figure 2.13 B

showed that the cumulative food intake was higher in both Floxed and Padi4KO after HFD in comparison to their lean counterparts.

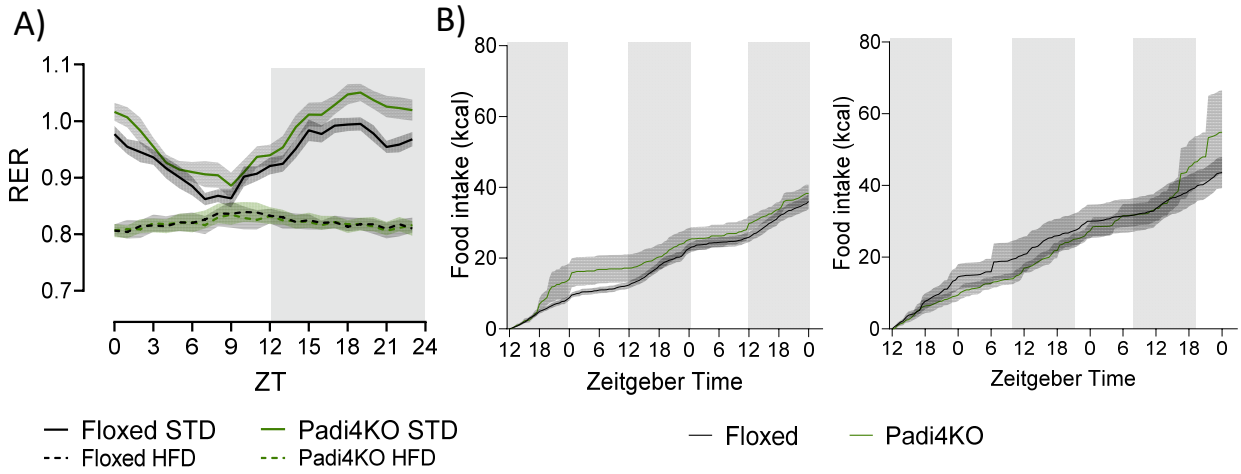

Figure 2.13. A) RER over Zeitgeber Time (ZT) and B) food intake of Floxed and Padi4KO mice after STD and HFD. n=6-15.

HFD reduced glucose uptake in insulin-sensitive tissues

In obesity and T2D, insulin resistance contributes to decreased glucose uptake in the skeletal muscle, liver and adipose tissue. When we assessed 2-deoxyglucose (2DG) uptake in fast-twitch muscle tibilias anterior (TA), we found a significative effect of the genotype. Furthermore, glucose uptake was significatively reduced by HFD in VAT of Floxed mice, while Padi4KO mice seemed to be spared from this effect. No differences in glucose uptake in the liver was observed due to diet or genotype (Figure 2.14).

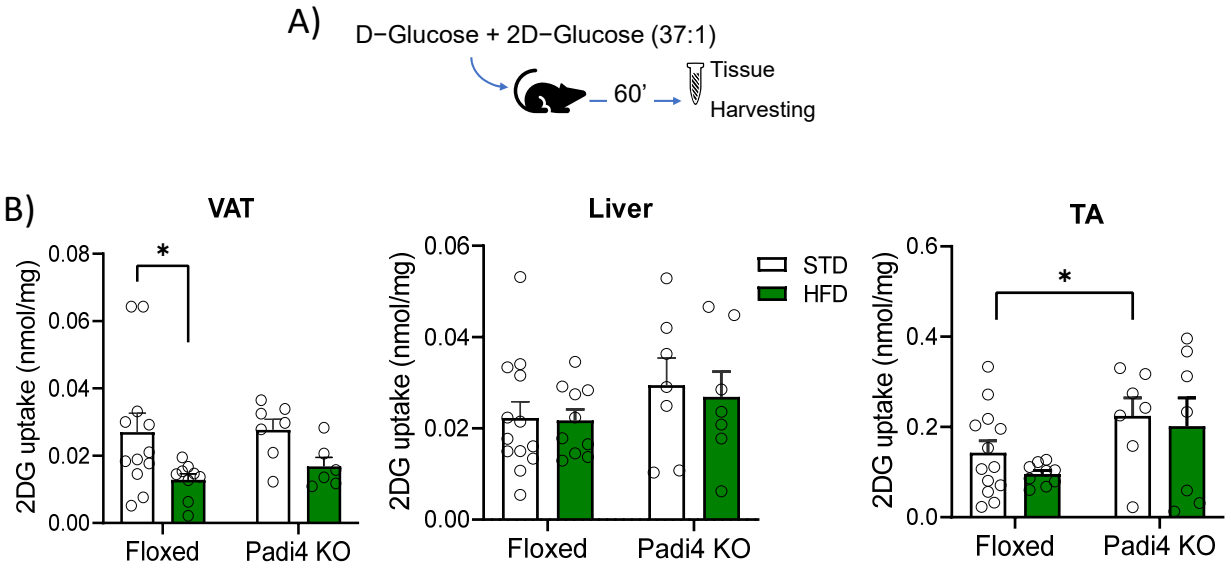

*Figure 2.14. A) Schematic representation of 2DG experiment. Tissues were collected 1 hour after injection of 37:1 ratio of D-glucose (1 g/kg) and 2-Deoxy-D-Glucose. B) 2DG uptake in TA, liver and VAT in Floxed and Padi4KO mice after STD and HFD. n=6-15 *p<0.05 2-way Anova with Bonferroni correction*

Padi4KO mice were partially protected against HFD-induced inflammation in insulin-responsive tissues

During the development of obesity, adipose tissue expansion contributes to chronic inflammation [12]. Adipocytes from the VAT of HFD-fed mice were remarkably larger than those from STD-fed mice, as evidenced by H&E staining (Figure 2.15 A) and the median cross-sectional area (Figure 2.15 B). However, Floxed mice displayed slightly smaller adipocytes in compared to Padi4KO mice after HFD, that was also evident by the distribution of adipocyte areas (Figure 2.15 C). Crown-like structures (CLS), which represent infiltrating macrophages around dying adipocytes, were observed in both Floxed and Padi4KO after HFD, without significant differences (Figure 2.15 D).

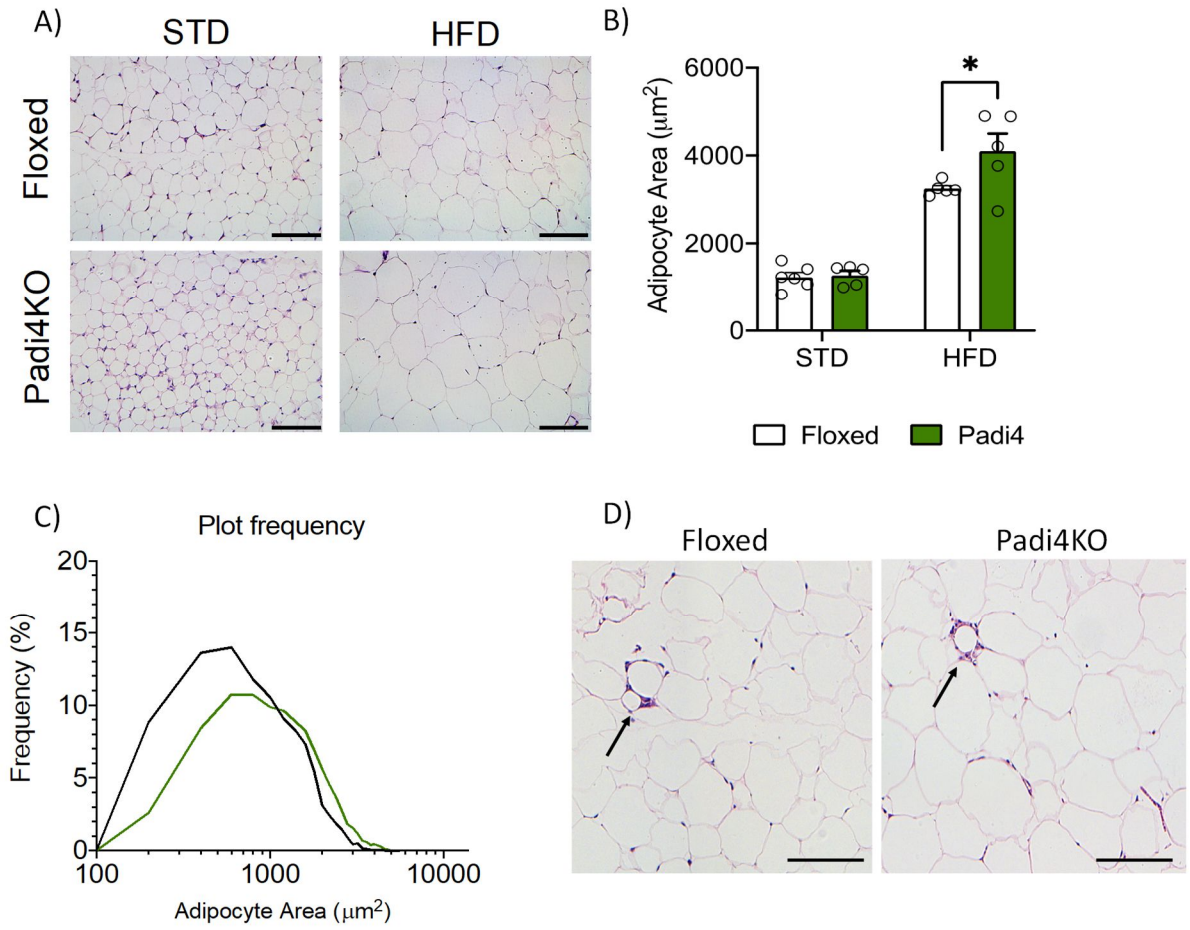

*Figure 2.15. A) and D) Rapresentative images of the H&E stained-VAT sections. The arrows indicate crown-like structures. B) Adipocyte cross-sectional area and C) Adipose distribution of adipocytes area (on a log scale) from Floxed and Padi4KO mice after STD and HFD. n>5 *p<0.05 2-way Anova with Bonferroni correction. Scale bar 120µm.*

Adipose tissues of obese mice and humans are infiltrated by inflammatory cells that contribute to insulin resistance while propagating inflammation (Shoelson et al., 2006). We sought to analyze gene expression profile of the VAT, hypothesizing that improved metabolic performances in Padi4KO mice were associated with reduced inflammatory signature in this tissue. IL-6 and monocyte chemoattractant protein 1 (MCP-1 also known as CCL2) were markedly upregulated in the VAT of Floxed mice, but to a lesser extent in Padi4KO mice after HFD, supporting the concept that HFD elicited an inflammatory milieu within the VAT. On the contrary, adiponectin, which exerts beneficial antidiabetic effects by improving insulin sensitivity in HFD-fed mice [120], was downregulated in Floxed mice, while it was not affected by HFD in Padi4KO mice. The other genes that we analysed showed no meaningful differences (Figure 2.16).

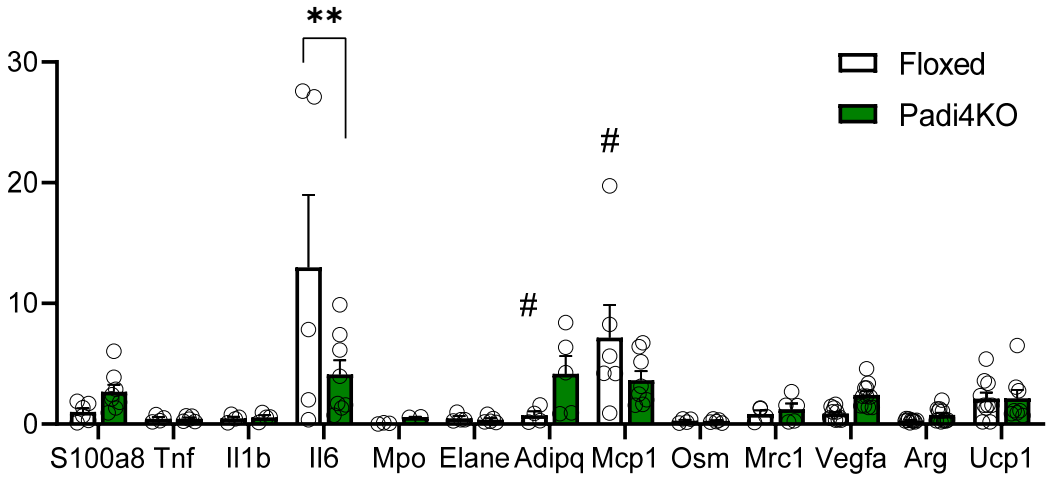

*Figure 2.16. qPCR analysis of VAT gene expression. Expression levels is represented as HFD to STD. **p<0.01, Floxed vs Padi4KO after HFD, #p<0.05 for STD vs HFD. n=6-10 2-two-way Anova with Bonferroni correction*

Activated macrophages are the main source of MCP1 and IL-6 during VAT inflammation [121]. Accordingly, we observed a higher accumulation of macrophages, defined as $CD45^{+}CD11b^{+}F4/80^{+}$ (Figure 2.17 A), and of neutrophils, $CD45^{+}CD11b^{+}Ly6G^{+}$(Figure 2.16 A), in Floxed than in Padi4KO after HFD (Figure 2.17 B).

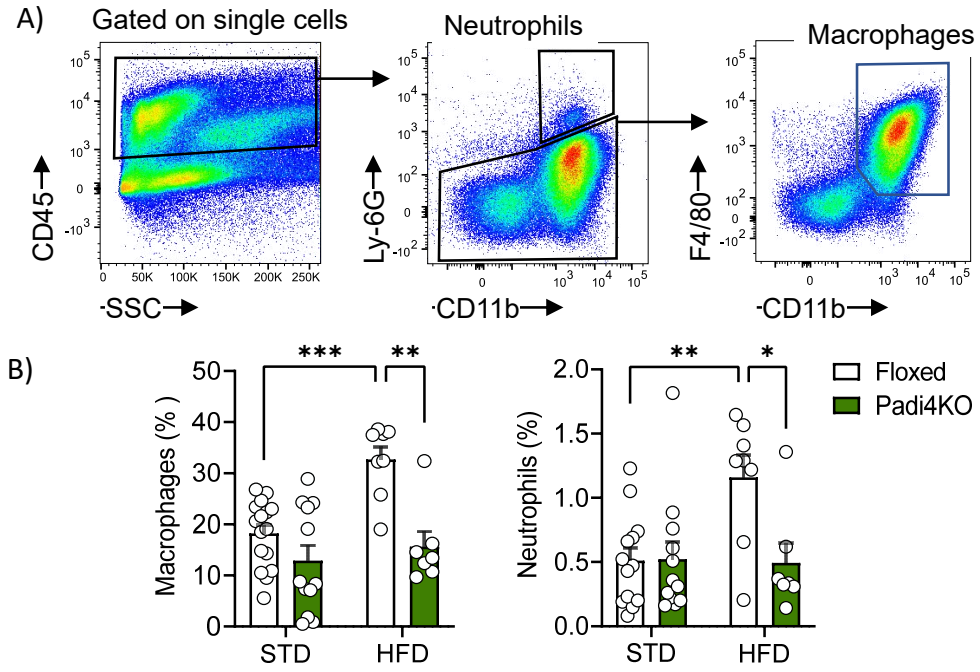

*Figure 2.17. A) Gating strategy for neutrophils $CD45^{+}CD11b^{+}Ly6G^{+}$ and macrophages $CD45^{+}CD11b^{+}F4/80^{+}$ after flow cytometric analyses. B) Quantification of macrophages and neutrophils within the VAT. n=6-15 ***p<0.001, **p<0.01, p*<0.05 2-way Anova with Bonferroni correction.*

Lipid accumulation in the liver, known as liver steatosis, is a common feature of obesity and T2D [12]. HFD induced a significant higher degree of liver fat accumulation compared with mice on STD, as shown by the lipid droplets revealed by the H&E staining (Figure 2.18 A). Oil red-O staining allowed to quantify triglycerides accumulation in the liver (Figure 2.18 B), showing that Padi4KO mice were partially protected from ectopic fat accumulation compared to Floxed mice (Figure 2.18 C).

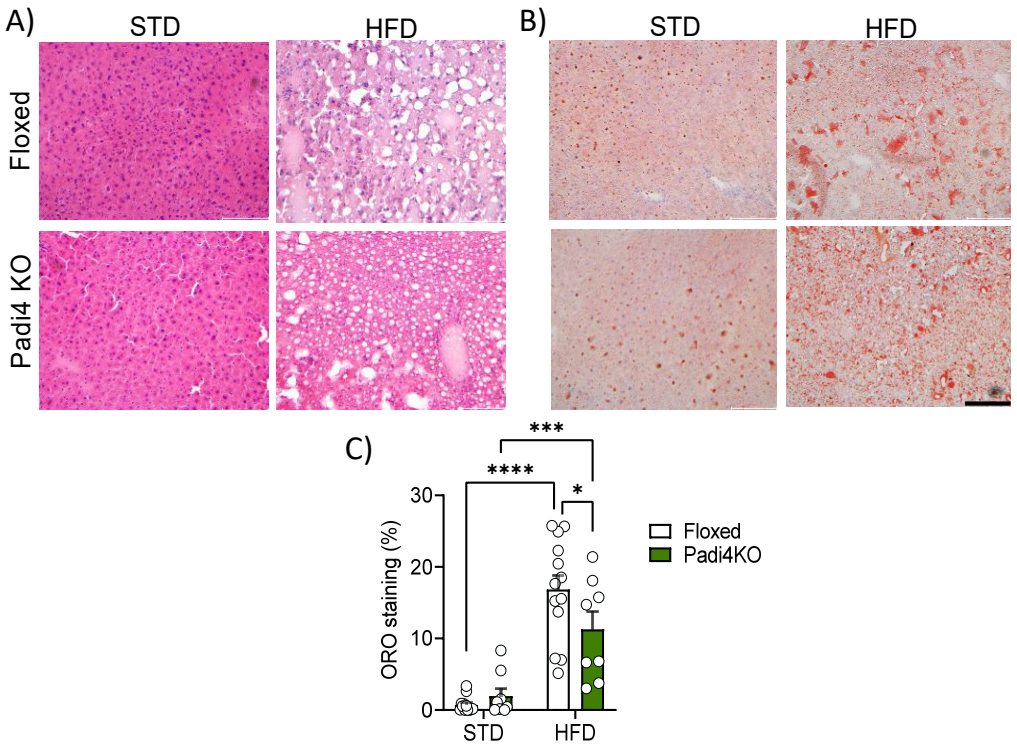

*Figure 2.18. Representative images of the H&E (A) and ORO (B)-stained liver section. C) Quantification of lipid droplets (%ORO staining) for Floxed and Padi4KO mice after HFD and STD. n=6-10 ****p<0.0001, **p<0.001 2-way Anova with Bonferroni correction. Scale bar 120 µm.*

Next, we examined the expression of several genes associated with hepatic inflammation. Interestingly, Padi4KO mice were protected from HFD-induced upregulation of IL-1β and Elastase in the liver. However, the expression of other genes was similar between Floxed and Padi4KO mice, as evidenced by figure 2.19 A. The expression of PEPCK, an important gene involved in gluconeogenesis, was higher in both genotype after HFD. This result was also supported by Pyruvate tolerance test (ipPTT) (Figure 2.19 B), confirming that HFD increased the conversion of pyruvate to glucose in both Floxed and Padi4KO mice.

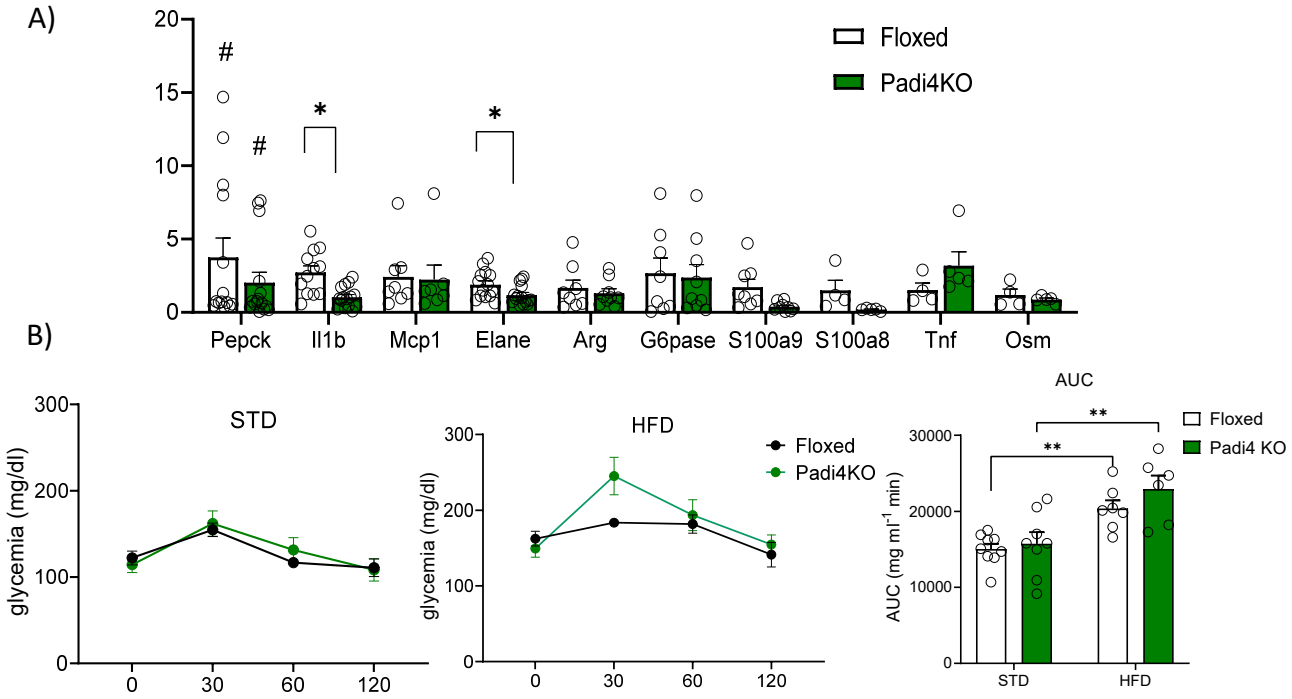

*Figure 2.19. A) qPCR of liver gene expression. Expression levels is represented as HFD vs STD normalized to STD. *p<0,05 for Floxed vs Padi4KO after HFD, #p<0.05 for STD vs HFD. B) ipPTT for Floxed and Padi4KO after STD and HFD. **p<0.01. n=6-15, 2-way Anova with Bonferroni correction.*

In line with these results, flow cytometry revealed a marked accumulation of both neutrophils and macrophages in Floxed mice after HFD, while Padi4KO were protected (Figure 2.20).

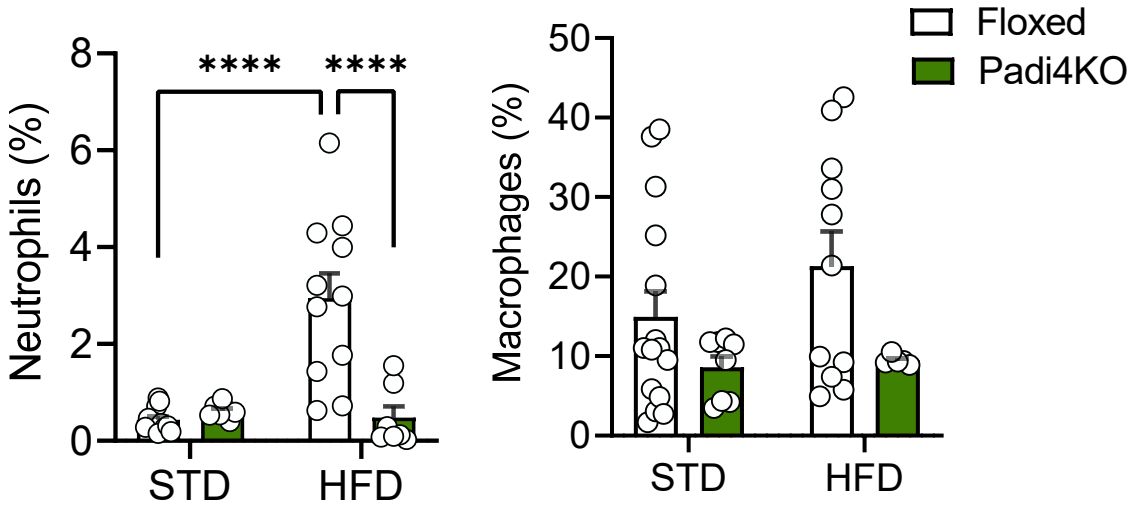

*Figure 2.20. Quantification of neutrophils and marcophages within the liver after flow cytometric analysis.n>10 ****p<0.0001 ***p<0.001 2-way Anova with Bonferroni correction.*

Next, we sought to assess the presence of putative NETting neutrophils within the liver and the adipose tissue. We used immunofluorescence to detect the presence of neutrophils in these tissues. Previous reports have shown that the expression of neutrophil elastase remained higher up to 12 weeks of HFD [105], even though neutrophils are the first immune cells to respond to inflammation and infiltrate tissues. Neutrophil elastase (NE)+ cells, were singularly scattered throughout the tissue in the liver and accumulated in close proximity of the crown-like structures in the adipose tissue without the stringy extracellular structures associated with NETs formation (Figure 2.21).

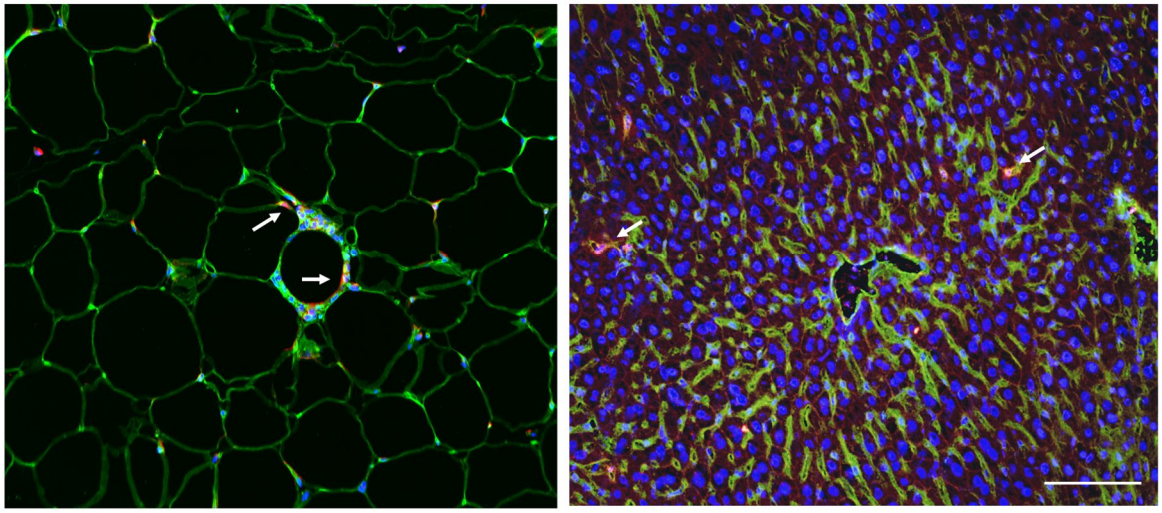

Figure 2.21. Immunofluorescence staining of VAT and liver sections taken from Floxed mice after HFD. The arrows indicate neutrophils elastase (NE)+ cells. Hoechst 33342 (blue), WGA (green), Elastase (red). Scale bar 100 µm.

However, we were not able to detect H3Cit+ cells within the adipose tissue or the liver (Figure 2.22). In the contest of T2D and obesity, the persistent, yet sterile and low-grade inflammatory state might not be sufficient to evoke a massive release of NETs as seen at sites of acute infection.

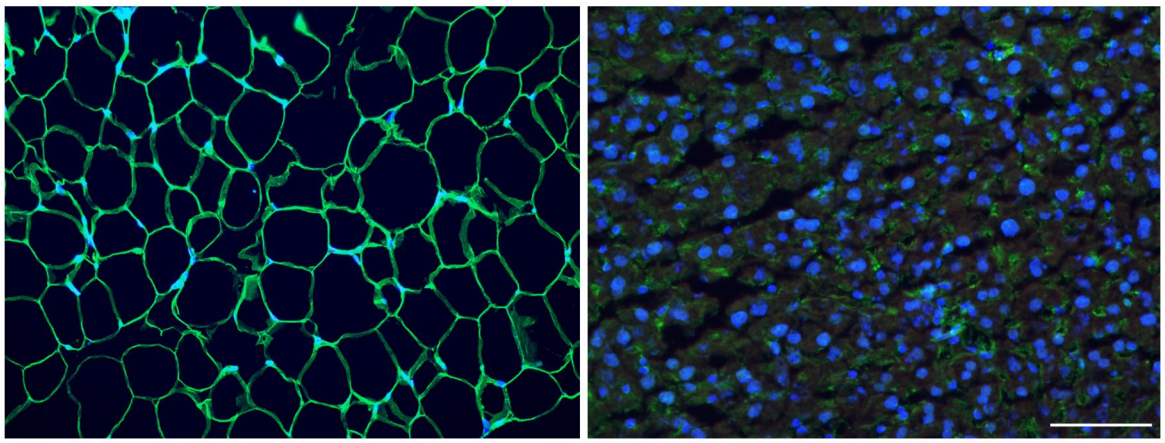

Figure 2.22. Immunofluorescence staining of VAT and liver sections taken from Floxed mice after HFD. Hoechst 33342 (blue), WGA (green), H3-cit (red). Scale bar 100µm.

Padi4 deficiency protected against systemic inflammation induced by HFD

Since we were not able to detect H3cit+ cells or NETs in the adipose tissue and the liver, we shifted our investigations to the peripheral circulation. Indeed, previous findings in patients correlate T2D diabetes with higher plasma levels of mono and oligonucleosomes, cell-free double-strand DNA and neutrophil elastase as surrogate markers for NETosis[101]. Therefore, we quantified the release of double strand DNA (dsDNA) in the peripheral circulation. dsDNA was markedly increased only in the plasma of Floxed mice after HFD, but not in Padi4KO, suggesting that they might be protected from the enhanced NET release induced by HFD (Figure 2.23 A). To gain insight into the inflammatory profile of the mice, we examined the levels of different circulating cytokines. Unbiased analyses clustered separately Floxed and Padi4KO mice after HFD, with the latter displaying a lower expression of several pro-inflammatory cytokines in comparison to their littermates after HFD (Figure 2.23 B).

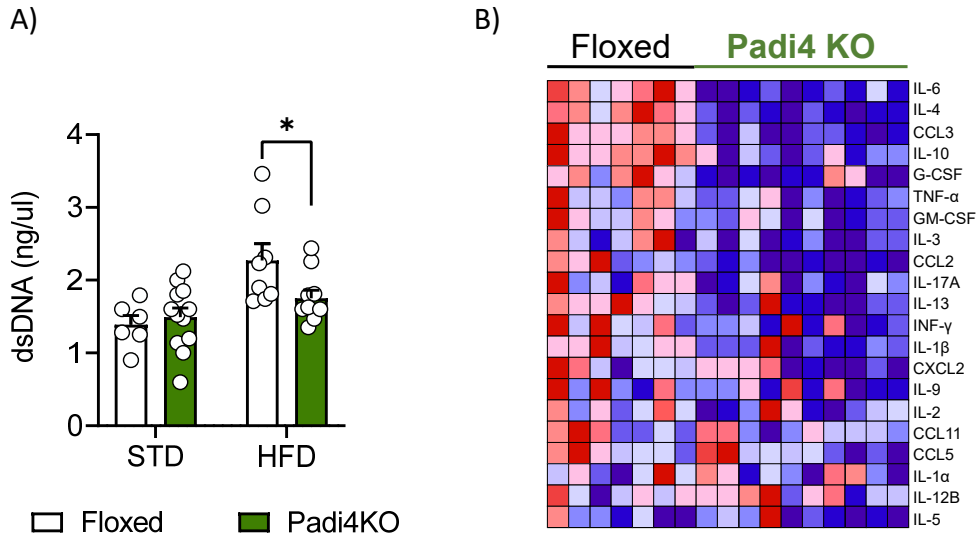

*Figure 2.23. A) Plasma dsDNA quantified with Qubit fluorometer B) Heatmap analysis of peripheral blood cytokines. Expression level of each cytokine is represented as HFD normalized to STD. n=6-12 *p<0.05 2-way Anova with Bonferroni correction*

Effects of the HFD in shaping gut microbiota composition

The consumption of a diet rich in fat is considered as a major environmental risk factor that prompt remodeling of the microbiota composition [1]. Therefore, we assessed whether deletion of *Padi4* could impinge upon the response toward dysbiosis, as the crosstalk between microbiota and neutrophils has been recently investigated [69]. We performed a metagenomic sequencing with a shotgun approach and found that the microbial community markedly changed after HFD in both Floxed and Padi4 KO

(Figure 2.24 A). HFD represented a stronger driver in shaping the gut microbiota than the genotype, as demonstrated by the greater separation among STD and HFD clusters after Principal Component Analysis (PCoA) (Figure 2.24 B). We also analysed the relative abundance of the major phyla (Figure 2.24 C). Interestingly, the Firmicutes/Bacteroidetes ratio, a benchmark for the onset of dysbiosis, increased in both groups after HFD, but to a lesser extent in the microbiome from Padi4KO mice (Figure 2.24 D).

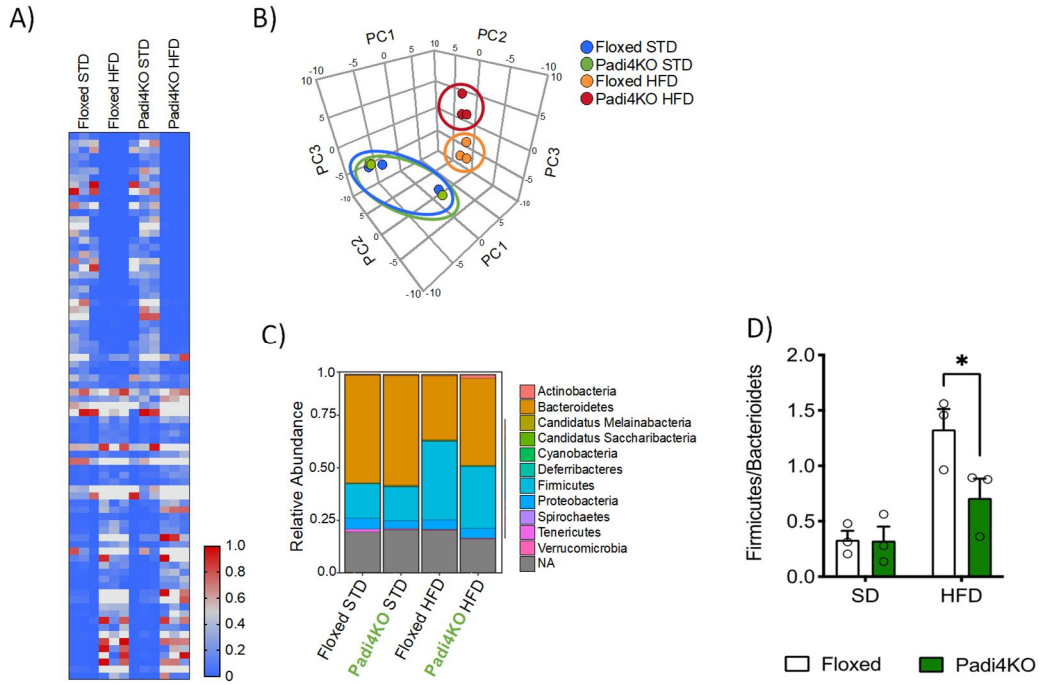

*Figure 2.24. A) Heat map representation of microbiota composition of fecal DNA obtained from Floxed STD, Padi4KO STD, Floxed HFD and Padi4KO HFD. B) Principal component analysis (PCoA), C) column diagram of microbial composition at phylum level. C) Firmicutes/Bacteriodetes ratio. n=3 for each group. *, p<0.05 2-way Anova with Bonferroni correction.*

Padi4KO mice were protected against HFD-induced metabolic endotoxemia and intestinal hyperpermeability

Dysbiosis triggers a breakdown of the epithelial barrier function leading to enhanced intestinal permeability and LPS translocation to the peripheral circulation [52]. We investigated the effect of HFD and gut dysbiosis on intestinal barrier dysfunction and metabolic endotoxemia. Intestinal permeability was assessed by measuring the concentration of 4 kDA FITC dextran in the serum of the mice 3 hours after an oral gavage (Figure 2.25 A). Figure 2.25 B shows that HFD induced a significant increase of FITC dextran only in Floxed mice. Likewise, ELISA quantification of serum lypopolysaccharide

(LPS) revealed a similar pattern (Figure 2.25 C), showing that Padi4KO mice were completely protected from metabolic endotoxemia.

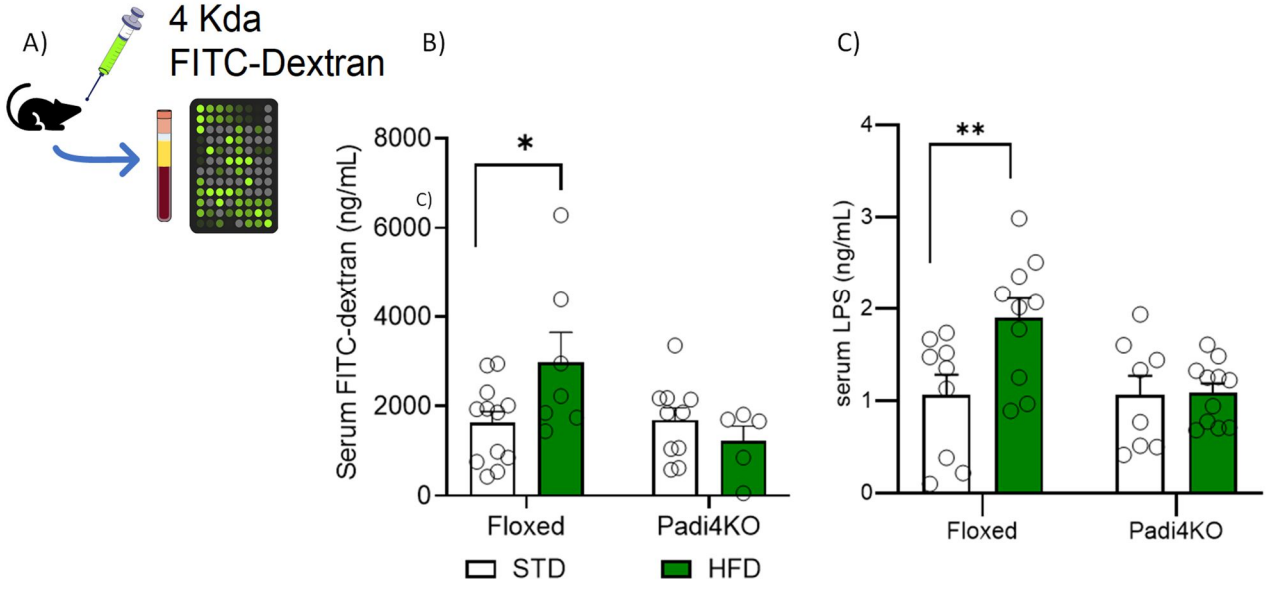

*Figure 2.25. A) Schematic representation of FITC-Dextran assay. 3 hours after oral gavage, B) serum FITC dextran concentration was quantified. C) ELISA of serum LPS, in Floxed and Padi4KO mice after STD and HFD. n=10, **p<0.01, *p<0.05, 2-way ANOVA with Bonferroni correction.*

Padi4KO mice showed improvements in the gut barrier integrity after HFD

Previous findings reported that obesity in mice drives intestinal permeability through alteration of tight junction protein expression [59]. Immunofluorescence staining of colonic sections showed that ZO-1 intensity decreased after HFD in Floxed mice, whilePadi4KO were not affected (Figure 2.26). Unexpectedly, the latter displayed a lower intensity of ZO-1 at baseline, pointing into question the possibility that *Padi4* deletion might influence the expression of other genes/proteins. Histological assessment of colonic sections at the end of 12 weeks revealed signs of structural alteration in Floxed and Padi4KO mice, such as irregular surface and morphology, and submucosal oedema (Figure 2.27 A). However, we were unable to find H3cit+ cells within the intestine of Floxed mice after HFD (Figure 2.27 B)

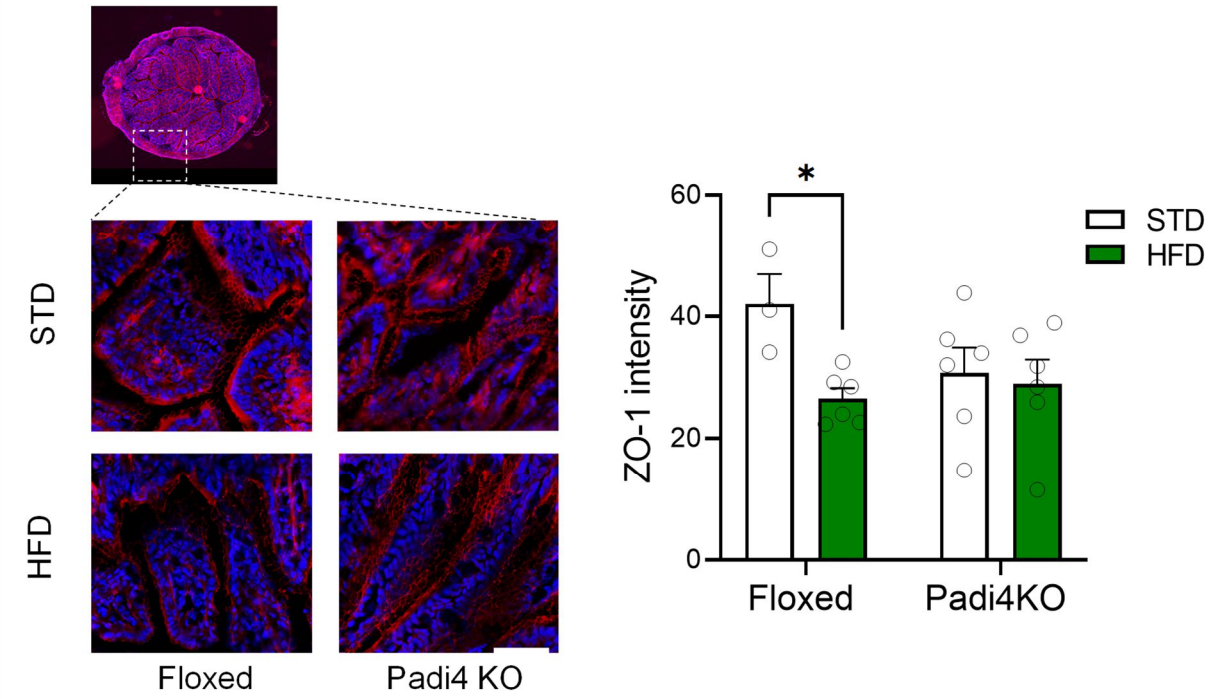

*Figure 2.26. Rapresentative images of immunofluorescence and quantification of ZO-1 intensity of colonic sections taken from Floxed and Padi4KO after STD and HFD. n=3-6 *p<0.05 after 2-way Anova with Bonferroni correction. Scale bar 100µm.*

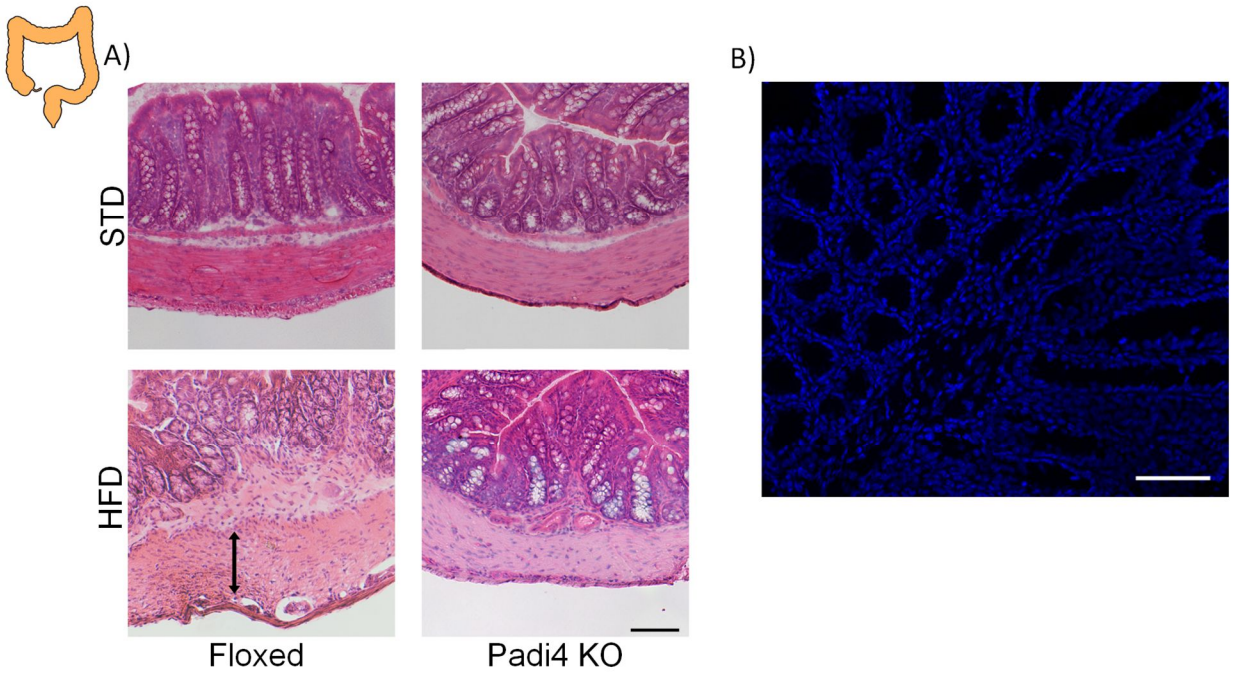

Figure 2.27. A) Rapresentative H&E stained-colonic sections of Floxed and Padi4KO mice after STD and HFD, the arrows indicate submucosal edema. B) Immunofluorescence staining of colonic sections taken from Floxed mice after HFD. Hoechst 33342 (blue), H3-cit (red). Scale bar 100 µm.

Padi4KO mice were spared from HFD-induced gut neutrophil recruitment and intestinal inflammation

The findings on the protection from endotoxemia, prompted further investigation about the inflammatory signature in the gut. We measured fecal Calprotectin (S100A8/A9), a sensitive biomarker of intestinal inflammation, which showed that Padi4KO mice were protected from the increase of S100A8/A9 in comparison to Floxed mice after HFD (Figure 2.28 A). Moreover, flow cytometric analysis of the colonic tissue revealed a significant increase of neutrophils ($CD45^+CD11b^+Ly6G^+$cells, Figure 2.28 B) infiltration within the gut only in Floxed mice after HFD (Figure 2.28 C).

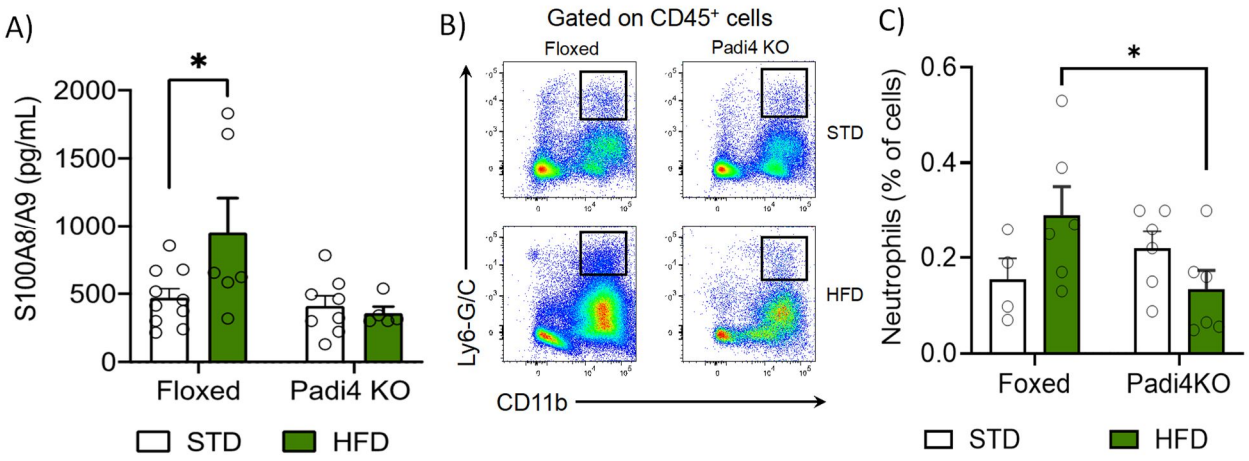

*Figure 2.28. A) ELISA quantification of fecal S100A8/A9. B) Gating strategy and (C) quantification of neutrophils within the colon. Neutrophils were defined as $CD45^+CD11b^+{}^-Ly6G^+$ cells. n>6 *p<0.05, 2-way ANOVA with Bonferroni correction*

We then assessed gene expression of both ileum and colon. s100a8 significantly increased only in the colon of Floxed mice after HFD (Figure 2.29 A), matching the higher level of fecal s100a8 (Figure 2.28 A). Padi4KO mice after HFD displayed a significant upregulation of C-type regenerating islet derived-3g lectin (*Reg3g*) in the ileum (Figure 2.29 B), which is a gut hormone exerting protective effects on host physiology and glucose levels [122]. Interestingly, the incretin hormone Glucagon-like peptide-1 (GLP-1) were reduced by HFD in Floxed mice both at transcriptional level in the ileum (Figure 2.29 C) and as cytokine in the peripheral circulation (Figure 2.29 D), suggesting that in Padi4KO mice the function of intestinal L cells is preserved.

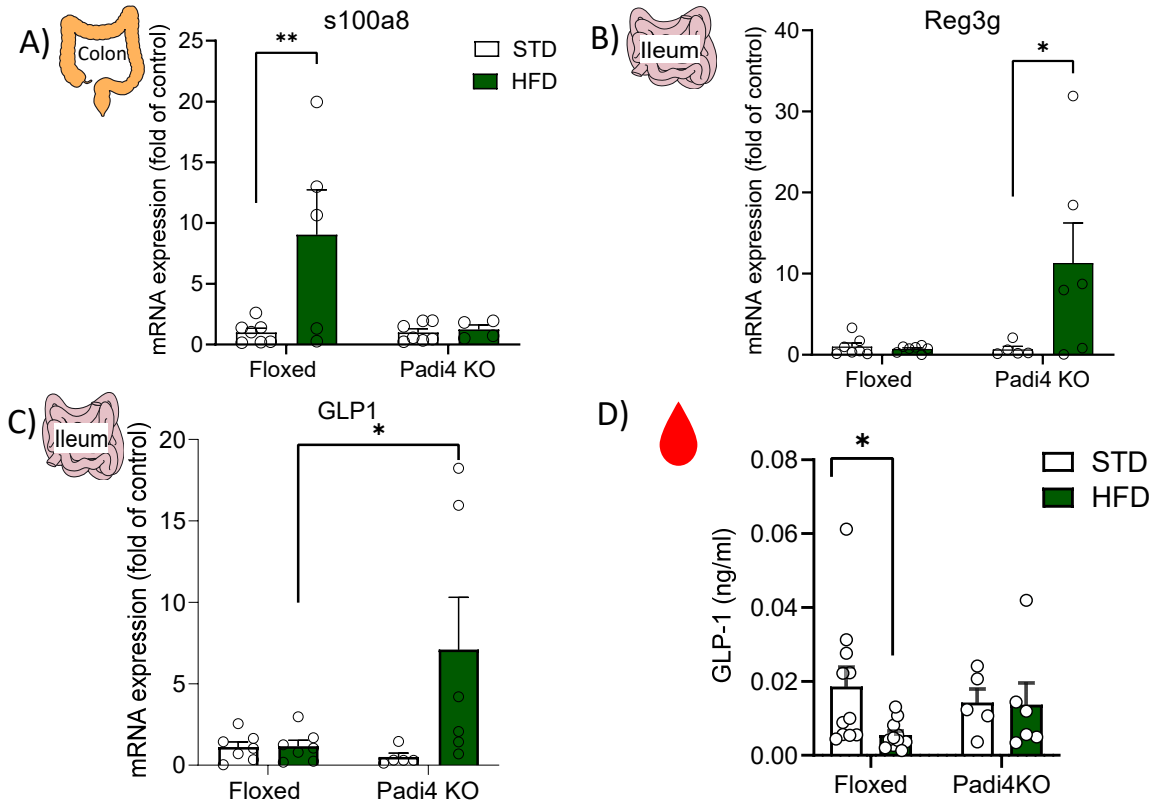

*Figure 2.29. A) Colon s100a8, B) ileum Reg3g and C) GLP-1after qPCR. Expression levels is represented as HFD normalized to STD. D) Plasma concentration of GLP-1 in Floxed and Padi4KO after STD and HFD. n=5-10. *, p<0.05. 2-way ANOVA with Bonferroni correction.*

Microbiota depletion with antibiotics reverted HFD-induced dysmetabolism and endotoxemia

It has been convincingly shown that that depletion of the microbiome in mice significantly improves dysmetabolism, gut permeability and inflammation[50], thereby providing evidence for an interplay among diet, microbiota and metabolism. At the end of HFD, we treated Floxed and Padi4KO mice with a cocktail of broad-spectrum antibiotic for 3 weeks to deplete their endogenous gut flora (Figure 2.30 A). Glucose intolerance (Figure 2.30 B) and insulin resistance (Figure 2.30 C) triggered by HFD were improved in Floxed mice after the antibiotic treatment. In Padi4KO mice, the effect of antibiotic treatment was significant, but less evident than Padi4KO mice, especially for ipGTT (Figure 2.30 D). Accordingly, HFD-induced increase of blood LPS level was completely reverted after antibiotic treatment in Floxed mice (Figure 2.30 E).

These results suggest that the detrimental effects of an obesogenic diet were largely abolished when deleting microbiome with antibiotic treatment in Floxed mice. Padi4KO mice already had a favourable metabolic profile, but the treatment with antibiotics resulted in a marginal metabolic improvement, probably due to the complete ablation of the microbiota.

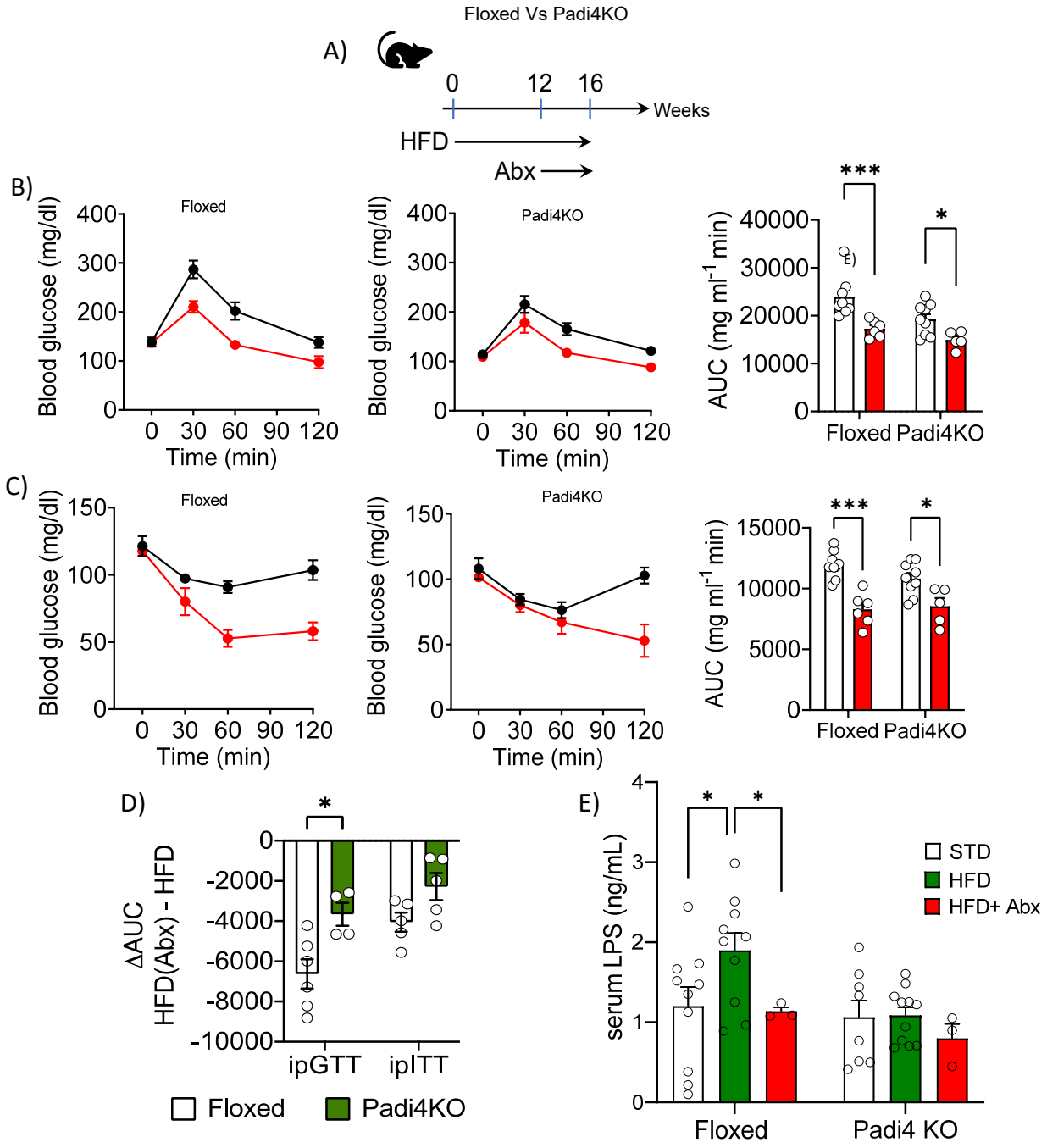

*Figure 2.30. A) Floxed and Padi4KO mice were treated for 3 weeks with antibiotic (abx) at the end of HFD. B) ipGTT and C) ipITT of Floxed and Padi4KO mice after HFD and after HFD+antibiotic treatment (abx). D) ΔAUC of ipGTT and ipITT was calculated as AUC (HFD+abx)-AUC(HFD) E) serum level of LPS in Floxed and Padi4KO after STD, HFD and HFD+Abx. n=3-10 ***p<0.001, *, p<0.05. 2-way ANOVA with Bonferroni correction.*

Padi4 deletion prevented the onset of dysmetabolism, endotoxemia and inflammation after transplantation with HFD-modified microbiota

The onset of dysbiosis in Padi4KO mice despite their favorable metabolic phenotype, led us to investigate the role of neutrophils as responders to dysbiosis and mediators in the development of dysmetabolism. We performed a fecal microbiota transplantation (FMT) experiment by ablating the endogenous microbiota of lean Floxed and Padi4KO mice (Figure 2.31 A), that was confirmed by quantifying 16s RNA abundance by qPCR, from stool cDNA extracted before and after antibiotic treatment (Figure 2.31 B). Next, mice were individually housed and received an oral gavage with fecal lysate from either STD or HFD-fed mice[123] and were allowed to achieve flora reconstitution. After 3 weeks we performed ipGTT, which showed that Floxed mice transplanted with an HFD-modified flora became glucose intolerance while Padi4KO were protected (Figure 2.31 C). Notably, Padi4KO mice were spared from the surge of serum LPS when transplanted with the HFD-modified flora (Figure 2.31 D). Moreover, when we assessed the circulating inflammatory fingerprint, we found that transplantation of the microbiota was sufficient to recapitulate the cytokine profile of HFD-fed mice, with an higher expression of several pro-inflammatory cytokines, such as IL-1A and TNF-α, in Floxed mice than in Padi4KO mice (Figure 2.31 E).

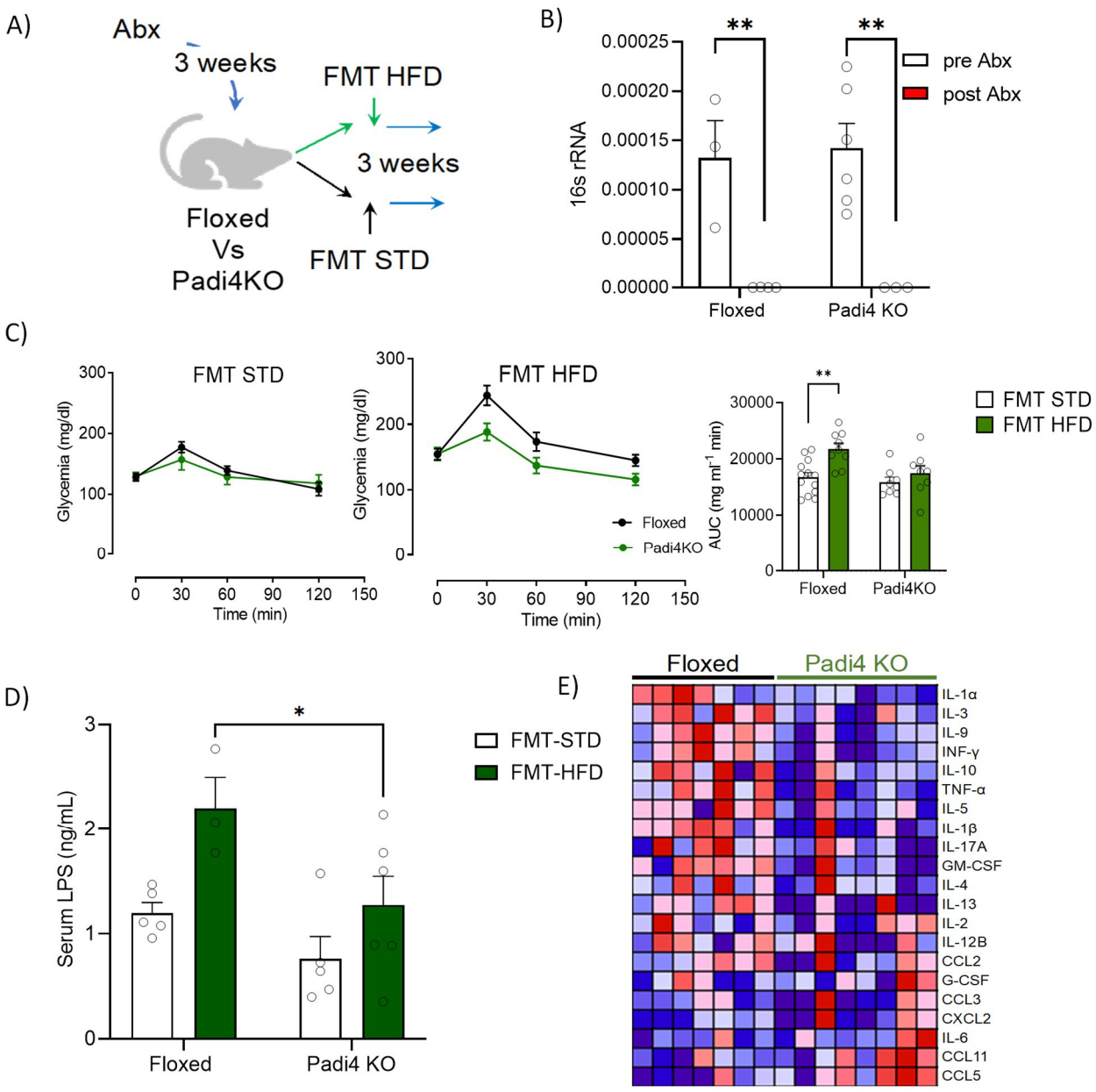

*Figure 2.31. A)Schematic rapresentation of Fecal Microbiota Transplantation (FMT). B) 16s RNA quantification after qPCR of DNA extracted from feces collected before and after antibiotic treatment (pre and post-abx). C) ipGTT D)ELISA assay of LPS concentration of lean Floxed and Padi4KO mice after FMT with STD and HFD-flora. E) Heatmap rapresentation after Multiplex cytokines analysis. FMT-HFD values are normalized to FMT-STD. GSEA software was used to analyze the arrays. n=10-12, **p<0,01, *p<0.05, 2-way ANOVA with Bonferroni correction.*

Treatment with a selective PAD4 inhibitor improved glucose tolerance and intestinal permeability after HFD

Cl-Amidine is a well-known irreversible pan-PAD inhibitor used to achieve pharmacological inhibition of PAD4 (Knuckley et al., 2010). However, novel PAD inhibitors have been developed,

such as GSK-484 which is a highly PAD4 selective, reversible inhibitor, which also has a more favorable pharmacokinetic profile (Lewis et al., 2015). As expected, 10μM GSK-484 was sufficient to dramatically reduce histone citrullination in neutrophils after stimulation with A23187 *in vitro* (Figure 2.32).

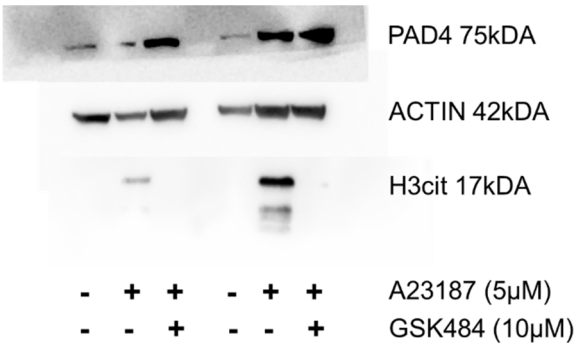

Figure 2.32. PAD4 and H3-cit expression in purified neutrophils in vitro. Western blot analysis from n=2 biological replicates.

Next, we tested if the pharmacological inhibition of PAD4 *in vivo* can be used as a long-term treatment to blunt dysmetabolism induced by HFD. To this end, we treated WT mice fed with HFD for 10 weeks with 8 mg/kg GSK-484 PAD4 inhibitor (i.p. injection every 2 days) (Figure 2.33 A). PAD4 inhibition was associated with a reduced weight gain (Figure 2.33 B) compared with vehicle-treated controls. Importantly, an improved glucose tolerance (Figure 2.33 C) was observed in HFD mice treated with the PAD4 inhibitor. In addition, GSK 484 treatment was effective in decreasing intestinal hyperpermeability in HFD-fed mice, as assessed with the 4 kDA FITC-dextran assay (Figure 2.33 D) along with a reduced abundance of dsDNA (Figure 2.33 E)

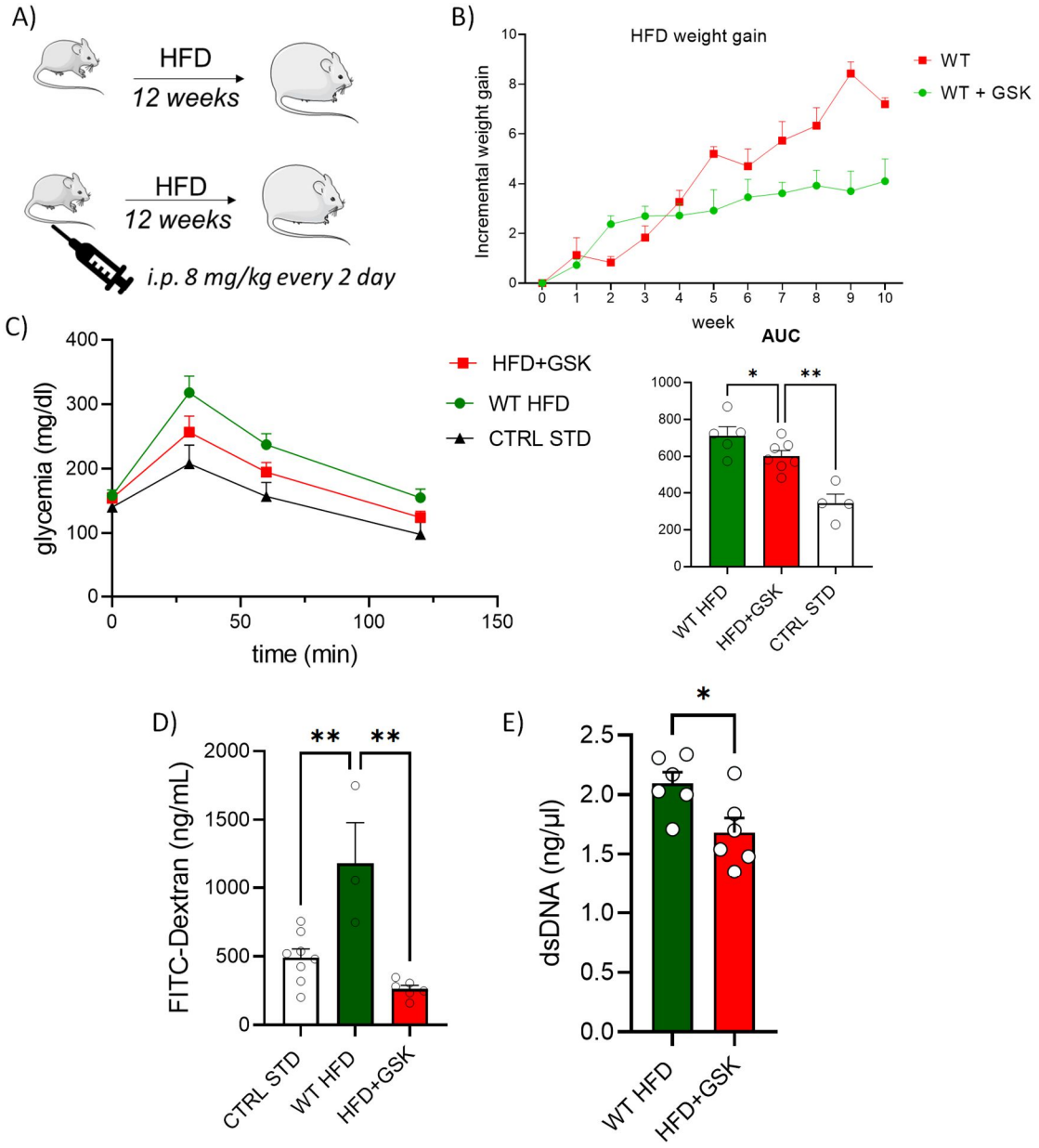

*Figure 2.33. A) Schematic representation of the pharmacological treatment with PAD4 inhibitor. B) Incremental weight gain over time, C) ipGTT, D) serum FITC-dextran and E) quantification of plasma dsDNA, of WT mice fed with HFD and treated with either vehicle or GSK-484. WT mice on STD (CTRL STD) were used as control. n=5-7 **p<0.01, 2-way ANOVA.*

NETting neutrophils and impaired intestinal barrier

To test whether NETs can directly impair barrier function, we used intestinal colonic organoids, which we co-cultured with neutrophils stimulated to release NETs. The incubation with 4 kDa FITC-dextran (Figure 2.34), showed that in the presence of unstimulated neutrophils, the organoid retained its integrity, preventing the influx of dextran inside the lumen. On the other hand, NETting neutrophils impaired the integrity of the epithelial layer, allowing for the translocation of fluorescent

dextran into the organoid, which can be quantified as the ratio of fluorescence outside and inside the organoid. Despite preliminary, this result suggests that NETs contribute to disrupt the intestinal barrier.

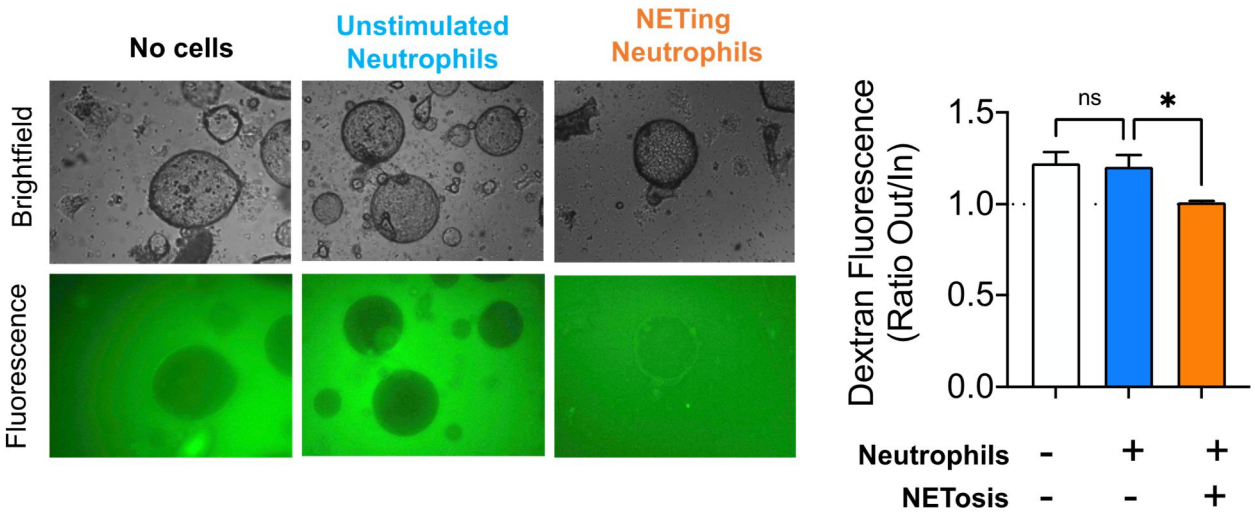

Figure 2.34. Rapresentative images of colonic organoids without cells, in the presence of unstimulated neutrophils and NETing neutrophils. Brightfield and green fluorescence. On the right quantification of Dextran-fluorescente signal.

DISCUSSION

Several works have shown that deregulation of NETosis in cardiometabolic diseases might favour thrombosis, impaired wound healing, and ultimately promote cardiovascular diseases [76]. Results of this study for the first time allow defining a pathophysiological role for NETosis in the metabolic deterioration in a model of HFD-induced obesity. Our work complements previous evidences showing that NETosis is dysregulated in obesity and type 2 diabetes and that $MPO^{-/-}$ and $NE^{-/-}$ mice, which lack enzyme granules embedded within NETs, are protected from the negative consequences of HFD-induced obesity and diabetes [124,125].

One of the earliest events of NETosis is mediated by PAD4, which catalyses histone citrullination, allowing for chromatin decondensation [81]. While this step is widely accepted as a key component in NETosis, the molecular machinery, however, is incompletely understood. For instance, *Candida albicans* triggers the release of NETs even in the absence of PAD4, thereby challenging the current view of NET induction follows an ineluctable series of events[126]. We characterized the effects of *Padi4* deletion on NET release and neutrophil physiology *in vivo* and *in vitro*. Monitoring the fluorescence ratio of Sytox green over Hoechst 33342 we defined the kinetics of chromatin release in the extracellular space. We confirmed that NADPH-independent NETosis, induced by ionomycin, occurs more rapidly than the NADPH-dependent pathway stimulated with PMA, as described by others [84]. As this technique cannot discriminate between NETosis and necrosis, more sophisticated imaging techniques, such as live two-photon confocal microscopy, are needed for a direct visualization of the cellular events taking place during NETosis, in order to obtain more thrustable results [116]. Thus, we performed live two-photon microscopy that confirmed that, upon PMA stimulation, neutrophils purified from Floxed mice undergo more cell death with the release of NETs compared to neutrophils isolated from Padi4KO mice. Another experiment supporting the upstream role of PAD4 in triggering NETosis is the luminol-based bioluminescence assay. MPO is a key component of the phagocytic activity of neutrophils because it reacts with ROS, and it is required for NET release [127]. PMA stimulation induced a higher peak of bioluminescence in neutrophils from Floxed mice in comparison to Padi4KO.

Western blot showed that stimulation of neutrophils with A23187 resulted in a robust and rapid histone citrullination in Floxed mice, that did not occur in response to PMA, as previously shown. [83]. In human neutrophils, however, PMA can trigger histone citrullination although conflicting results may arise from different experimental conditions such as the antibody used to detect citrullination [128]. Some authors suggest distinguishing between NETosis, triggered by PMA, fungi or bacterial which will not require histone citrullination, but ROS production, from leukotoxic hypercitrullination which

yields DNA release in response to massive influx of calcium and PAD activation [129] . Our experimental data partially agree with this concept, as we reported inhibition of DNA release in Padi4KO neutrophils in response either to PMA and calcium ionophores. Indeed, it has been shown that PAD4 activity and histone hypercitrullination, are important for NET formation under more naturally-occurring conditions, such as the exposure to bacteria *Shigella flexneri* [81]. These conflicting evidences arise from lack of a detailed biochemical definition of the diverse mechanisms that affect the release of NETs from neutrophil and that are particularly challenging to test *in vivo* due to the short lifespan of these cells.

Since Padi4KO neutrophils were defective in NET release in response to both PMA and calcium ionophores, we assumed that PAD4 is required for both NOX independent and NOX-dependent NETosis [60].

Next, we assessed whether *Padi4* deletion can impact the functions of neutrophils beyond DNA release and NETosis. It is well established that neutrophils change their gene expression profile after being released from the bone marrow into the circulation and when they are recruited at the sites of inflammation/infection [117]. Our data suggest that the deletion of *Padi4* did not affect activation of neutrophil during acute inflammation, which was also confirmed in wild type mice treated with PAD4 inhibitor Cl-Amidine [130]. These findings are consistent with the hypothesis that NETosis is a specific cell death subroutine that neutrophil experience under precise triggers. This important in view of the potential exploitation of NETosis as a target of therapy.

The metabolic improvements observed in Padi4KO mice conflict overtly with a small previous report which failed to show any metabolic effect when NETosis was supposedly inhibited with Cl-Amidine [106]. Despite the evident difference in the approach chosen to inhibit NETosis, such prior work has major experimental flaws, as the authors did not compare age-matched lean and obese mice, which exhibited only a modest dysmetabolic phenotype. Second, NETs were quantified in the adipose tissue with a dot blot for citrullinated histone that was not shown in the paper, making it extremely difficult to appreciate the outcomes of Cl-Amidine inhibition. The adipose tissue, along with the liver, were the obvious begin of our quest to understand the mechanism that might confer protection in Padi4KO mice.

Chronic inflammation in adipose tissue is considered a crucial risk factor for the development of dysmetabolism. The upregulation of MCP-1 and IL-6 was accompanied by a greater recruitment of macrophages and neutrophils within the VAT of Floxed mice in comparison to Padi4KO mice after HFD. The recruitment of neutrophils within the adipose tissue appeared to be an early event during the development of experimental obesity [13], but despite neutrophil progressive accumulation in the

adipose tissue and in liver, we did not find evidences of NETs in both tissues. This represent a limitation of our work. The challenges in the definition of NETosis *in vitro* are amplified when trying to detect NETs *in vivo*, as they can be undeniably identified only when highly abundant, usually upon acute stimuli [103] or microbial infection [131]. We speculate that in the contest of type 2 diabetes and obesity, the persistent, yet sterile and low-grade inflammatory state, might be insufficient to evoke the massive release of NETs as seen at sites of acute infection. However, HFD was associated with significantly increased levels of circulating cell-free double-strand (ds) DNA in Floxed mice, but not in Padi4 KO. Although the dsDNA assay lacks specificity, it has been used as a surrogate indicator of NETs as it is NETcomponent [132, 101].

Hepatic steatosis was less severe in Padi4KO mice, which agrees with the data about insulin resistance [133]. Nevertheless, hepatic gluconeogenesis, assessed through the pyruvate tolerance test, showed that blood glucose excursion was equally raised in Floxed and Padi4KO on HFD, which was also confirmed by *Pepck* gene expression.

A diet rich in fat has been reported to change the composition of the microbiota and compromise intestinal barrier integrity, triggering LPS translocation into the bloodstream [52]. Our results showed that, despite exhibiting a similar degree of dysbiosis, Padi4KO mice were protected against HFD-induced intestinal hyperpermeability and LPS dissemination. This allows us to speculate that the deletion of Padi4 protected from the metabolic consequences of dysbiosis, without a striking effect on microbiota composition. Intestinal inflammation has been often mentioned has an hallmark of T2D-related dysbiosis [17]. Here, we demonstrate that deletion of *Padi4* protected against intestinal inflammation and the recruitment of neutrophils within this tissue induced by HFD. The challenging in the detection of NETosis in the adipose and liver are extended to the intestine. The reason might be the same, since the chronic-low grade inflammation that characterizes obesity and T2D may not induce a release of NETs detectable with available methodologies. In a model of experimental colitis, NETs were previously detected in the inflamed intestine. The authors proposed that the web-like DNA filaments of NETs disrupted the integrity of the epithelial junctions [110].

A crosstalk between neutrophils and the intestinal environment has been described [69], as microbiota shapes neutrophil fingerprint in steady state, but also neutrophil activation [67]. It is reasonable to speculate that alterations in the microbiota composition would affect neutrophils, which are first-line defences against bacteria and pathogens, contributing to the tolerogenic environment of the gut [69]. We demonstrated that transplantation of an obesogenic intestinal flora in lean Floxed mice

recapitulated most of the features obtained in obese counterparts, while lean Padi4KO mice were protected from this dysmetabolic phenotypic switch.

Therefore, our study extended the complexity of the interaction between neutrophils and the microbiota. We hypothesized that the onset of NETosis, in response to dysbiosis, represents an important immuno-metabolic checkpoint, that leads to chronic inflammation and dysmetabolism, by sustaining barrier and enteroendocrine dysfunctions. However, the mechanism by which neutrophils work at the interface between the intestinal microenvironment and the metabolic system remains to be elucidated.

Preliminarily, we found that NETting neutrophils co-cultured with intestinal organoids, induced the passage of FITC-dextran into the lumen, suggesting that NETs affect the integrity of the epithelial barrier. Extracellular histones and DNA, the major components of NETs, may trigger intestinal injuries [134]. Moreover, other secreted factors, such as neutrophils granular proteins and enzymes released with NETs, may have detrimental effects on intestinal barrier.

Obesity-associated dysbiosis is accompanied by the release of microbial metabolites, such as SCFAs, TMAO or bile acids, that enter the systemic circulation and affect the metabolic outcomes on distant tissues [135]. For example, tryptophan-related compounds derange gut barrier integrity and impaired production of GLP-1 by enteroendrocrine L-cells of the ileum [49]. The impairments in barrier function induced by the decline in GLP-1 bioavailability results in increased drainage of dietary lipids, bacterial metabolites, and LPS to the liver through the portal system, ultimately activating hepatic immune cells, worsening inflammation, steatosis and insulin resistance [136].

Indeed, our data show that the decreased expression of GLP-1 in both ileum and peripheral circulation of Floxed mice may reflect impaired functions of intestinal L cells, contributing to defect in the gut barrier, thus worsening the metabolic phenotype. These findings highlight the possible role of bacterial metabolites at the interphase between the enteroendocrine system and metabolic alterations.

To this end, we are planning a metabolomic analysis of plasma from Floxed and Padi4KO mice after HFD to identify differentially released metabolites from the gut.

To explore the therapeutic potential of PAD4 we used the novel compound GSK-484, characterized by high selectivity to PAD4 in comparison to the pan-PAD irreversible inhibition exerted by Cl-Amidine.

In our work, pharmacological treatment with GSK-484 was effective in improving glucose tolerance and preservation of intestinal permeability after HFD. Surprisingly, mice treated with the inhibitor were leaner than their littermates treated with vehicle. This result was different from what we obtained

with Padi4KO mice. While we do not have a clear mechanistic explanation for this difference, it is reasonable to hypothesize that the germline deletion of *Padi4* might result in some compensatory mechanism that allows weight gain. In light of extending these findings to human, we should consider that NETosis is differentially regulated between mouse and human neutrophils, for example in the temporal dynamics. Several pharmacological attempts to inhibit PAD4 have shown to improve the progression of various NET-driven diseases , such as anti-inflammatory agents, anti-thrombosis or NADPH-inhibitors [137]. However, these compounds can have side effects on the immune system, leading to impairment in the normal immune response that may predispose patients to infections.

The links between gut microbiota and metabolic disorders make these interactions a promising therapeutic target. Previous works explored the strategies to prevent the onset of dysbiosis or modify the composition of the microbiome to counteract metabolic diseases[45]. This approach is intriguing but challenging, due to the complexity of the microbial ecosystem and the dynamic nature of the intestine. The use of probiotics, exercise, and caloric restrictions have health benefits, but their efficacy in treating obesity-related metabolic complications is still controversial. A drastic way to alter microbiota composition is FMT. However, this approach has limitations, regarding the short- and long-term engraftment of the donor microbiota in the recipient, and the lack of clinical validation in a larger population [138].

With our result, we propose a new exciting alternative strategy to cope with the consequences of the detrimental effects of the HFD on the microbiome, by taming the activation of neutrophils and blunting the metabolic sequelae. Manipulation of NETosis can result in the improvement of the metabolic consequences of obesity, providing a new integrated view of the interaction between the metabolism and the immune system.

In conclusion, our data drafted a new pathophysiological mechanism that promotes the neutrophil as a regulator of systemic metabolic health.

Mechanistically, we envisage that HFD-modified microbiota promotes the recruitment of neutrophils and triggers NETosis, which affect intestinal barrier function and lead to metabolic endotoxemia in turn resulting in glucose intolerance and insulin resistance (Figure 3). NETosis could be a novel therapeutic target to counter T2D.

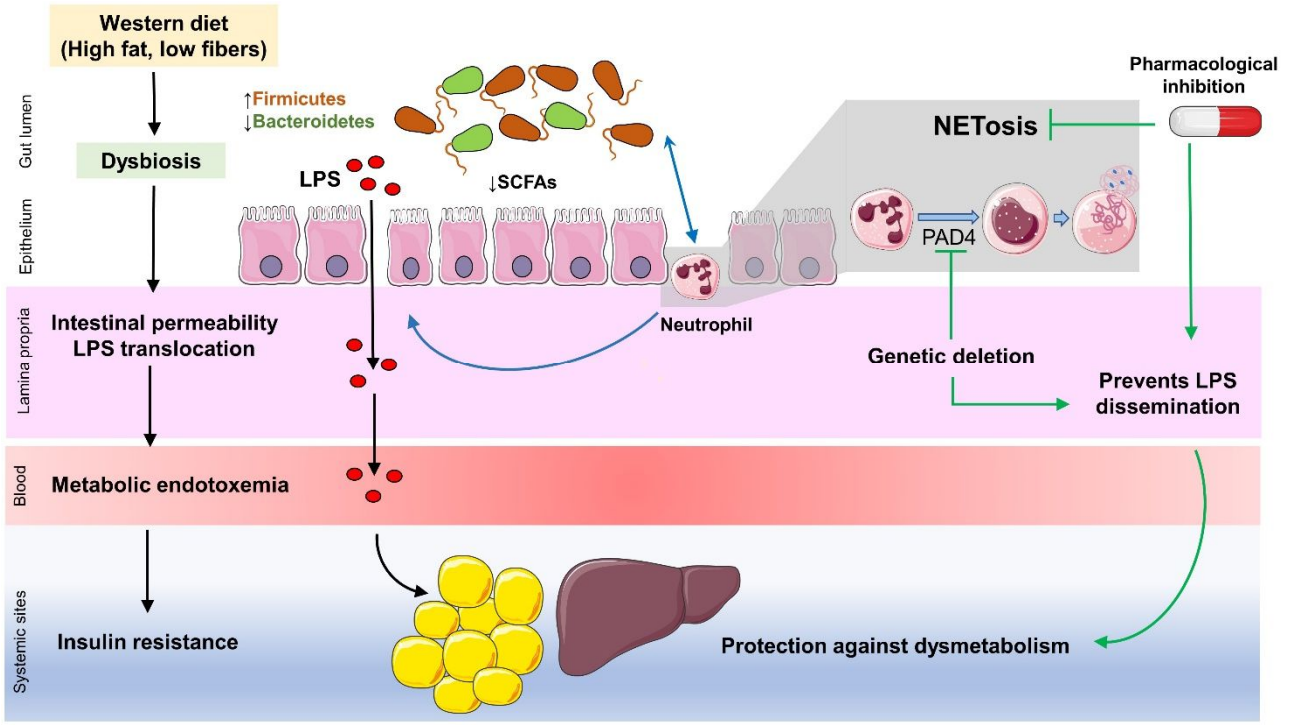

Figure 3. Proposed mechanism. A western diet, tipically defined as rich in fat and poor in fiber, alter the composition of the microbiota, leading to intestinal permeability and metabolic endotoxemia. All of these factors contribute to insulin resistance at the systemic sites. Neutrophils communicate with the microbiota and undergo NETosis. Both genetic deletion and pharmacological inhibition of Padi4 prevent LPS dissemination in the blood, thus protect against dysmetabolism. Therefore, neutrophils, through NETs release and NETosis, may regulate intestinal barrier integrity.

BIBLIOGRAPHY

1. Christ A, Latz E. The Western lifestyle has lasting effects on metaflammation. *Nat Rev Immunol*. 2019;19(5):267-268. doi:10.1038/s41577-019-0156-1
2. Rosales C. Inflammation and Pathological Complications. 2022;2019:9-11.
3. Zhou Y, Chi J, Lv W, Wang Y. Obesity and diabetes as high-risk factors for severe coronavirus disease 2019 (Covid-19). *Diabetes Metab Res Rev*. 2021;37(2). doi:10.1002/dmrr.3377
4. Lee YS, Olefsky J. Chronic tissue inflammation and metabolic disease. *Genes Dev*. 2021;35(5-6):307-328. doi:10.1101/GAD.346312.120
5. James DE, Stöckli J, Birnbaum MJ. The aetiology and molecular landscape of insulin resistance. *Nat Rev Mol Cell Biol*. 2021;22(11):751-771. doi:10.1038/s41580-021-00390-6
6. Robbins and Cotran. *Pathologic Basis of Disease*. ninth. (Elsevier Saunders, ed.).
7. Xavier AM, Kataryna A, Anunciato O, et al. Inflammation , stress , and diabetes. *Zhao, L, Zhang, F, Ding, X, Wu, G, Lam, Y Y, Wang, X, … Zeng, Y (2018) Gut Bact Sel Promot by Diet fibers alleviate type 2 diabetes Sci 1156(March), 1151–1156 https//doi.org/101126/science.aao5774 Leite, A Z, Rodrigues*. 2016;8(3):346-358. doi:10.1172/JCI200525102.The
8. Gregor MF, Hotamisligil GS. Inflammatory mechanisms in obesity. *Annu Rev Immunol*. 2011;29:415-445. doi:10.1146/annurev-immunol-031210-101322
9. Wang QA, Tao C, Gupta RK, Scherer PE. Tracking adipogenesis during white adipose tissue development, expansion and regeneration. *Nat Med*. 2013;19(10):1338-1344. doi:10.1038/nm.3324
10. Reilly SM, Saltiel AR. Adapting to obesity with adipose tissue inflammation. *Nat Rev Endocrinol*. 2017;13(11):633-643. doi:10.1038/nrendo.2017.90
11. Strissel K, Stancheva Z, et al. Adipocyte Death, Adipose Tissue Remodeling, and Obesity Complications. *Diabetes.* 2007; 56:2910-1918. doi: 10.2337/db07-0767
12. Bijnen M, Josefs T, Cuijpers I, et al. Adipose tissue macrophages induce hepatic neutrophil recruitment and macrophage accumulation in mice. *Gut*. 2018;67(7):1317-1327. doi:10.1136/gutjnl-2016-313654
13. Talukdar S, Oh DY, Bandyopadhyay G, et al. Neutrophils mediate insulin resistance in mice fed a high-fat diet through secreted elastase. *Nat Med*. 2012;18(9):1407-1412. doi:10.1038/nm.2885
14. Kwon H, Pessin JE. Adipokines mediate inflammation and insulin resistance. *Front Endocrinol (Lausanne)*. 2013;4(JUN):1-13. doi:10.3389/fendo.2013.00071

15. Kadowaki T, Yamauchi T, Kubota N, Hara K, Ueki K, Tobe K. Review series Adiponectin and adiponectin receptors in insulin resistance , diabetes , and the metabolic syndrome. *J Clin Invest*. 2006;116(7):1784-1792. doi:10.1172/JCI29126.1784
16. Strissel KJ, Stancheva Z, Miyoshi H, et al. Adipocyte death, adipose tissue remodeling, and obesity complications. *Diabetes*. 2007;56(12):2910-2918. doi:10.2337/db07-0767
17. Winer DA, Luck H, Tsai S, Winer S. The intestinal immune system in obesity and insulin resistance. *Cell Metab*. 2016;23(3):413-426. doi:10.1016/j.cmet.2016.01.003
18. Groschwitz KR, Hogan SP. Intestinal barrier function: Molecular regulation and disease pathogenesis. *J Allergy Clin Immunol*. 2009;124(1):3-20. doi:10.1016/j.jaci.2009.05.038
19. Johansson MEV, Hansson GC. Immunological aspects of intestinal mucus and mucins. *Nat Rev Immunol*. 2016;16(10):639-649. doi:10.1038/nri.2016.88
20. Schneeberger K, Roth S, Nieuwenhuis EES, Middendorp S. Intestinal epithelial cell polarity defects in disease: Lessons from microvillus inclusion disease. *DMM Dis Model Mech*. 2018;11(2). doi:10.1242/dmm.031088
21. Kurashima Y, Goto Y, Kiyono H. Mucosal innate immune cells regulate both gut homeostasis and intestinal inflammation. *Eur J Immunol*. 2013;43(12):3108-3115. doi:10.1002/eji.201343782
22. Thoo L, Noti M, Krebs P. Keep calm: the intestinal barrier at the interface of peace and war. *Cell Death Dis*. 2019;10(11). doi:10.1038/s41419-019-2086-z
23. Koch S, Nusrat A. Dynamic Regulation of Epithelial Cell Fate and Barrier Function by Intercellular Junctions. 2009;227:220-227. doi:10.1111/j.1749-6632.2009.04025.x
24. Barbara G, Barbaro MR, Fuschi D, et al. Inflammatory and Microbiota-Related Regulation of the Intestinal Epithelial Barrier. *Front Nutr*. 2021;8(September):1-24. doi:10.3389/fnut.2021.718356
25. Schoultz I, Keita Å V. The Intestinal Barrier and Current Techniques for the Assessment of Gut Permeability. *Cells*. 2020;9(8):1-30. doi:10.3390/cells9081909
26. Clarke TB, Davis KM, Lysenko ES, Zhou AY, Yu Y, Weiser JN. Recognition of peptidoglycan from the microbiota by Nod1 enhances systemic innate immunity. *Nat Med*. 2010;16(2):228-231. doi:10.1038/nm.2087
27. Mogensen TH. Pathogen recognition and inflammatory signaling in innate immune defenses. *Clin Microbiol Rev*. 2009;22(2):240-273. doi:10.1128/CMR.00046-08
28. Jandhyala SM, Talukdar R, Subramanyam C, Vuyyuru H, Sasikala M, Reddy DN. Role of the normal gut microbiota. *World J Gastroenterol*. 2015;21(29):8836-8847. doi:10.3748/wjg.v21.i29.8787

29. Hooper L V., MacPherson AJ. Immune adaptations that maintain homeostasis with the intestinal microbiota. *Nat Rev Immunol*. 2010;10(3):159-169. doi:10.1038/nri2710
30. Ursell LK, Haiser HJ, Van Treuren W, et al. The intestinal metabolome: An intersection between microbiota and host. *Gastroenterology*. 2014;146(6):1470-1476. doi:10.1053/j.gastro.2014.03.001
31. Nguyen TLA, Vieira-Silva S, Liston A, Raes J. How informative is the mouse for human gut microbiota research? *DMM Dis Model Mech*. 2015;8(1):1-16. doi:10.1242/dmm.017400
32. Kamada N, Chen GY, Inohara N, Núñez G. Control of pathogens and pathobionts by the gut microbiota. *Nat Immunol*. 2013;14(7):685-690. doi:10.1038/ni.2608
33. Belkaid Y, Hand TW. Role of the microbiota in immunity and inflammation. *Cell*. 2014;157(1):121-141. doi:10.1016/j.cell.2014.03.011
34. Belkaid Y, Harrison OJ. Homeostatic Immunity and the Microbiota. *Immunity*. 2017;46(4):562-576. doi:10.1016/j.immuni.2017.04.008
35. Kamada N, Seo SU, Chen GY, Núñez G. Role of the gut microbiota in immunity and inflammatory disease. *Nat Rev Immunol*. 2013;13(5):321-335. doi:10.1038/nri3430
36. Sansonetti PJ, Di Santo JP. Debugging how Bacteria Manipulate the Immune Response. *Immunity*. 2007;26(2):149-161. doi:10.1016/j.immuni.2007.02.004
37. Li X, Zhang S, Guo G, Han J, Yu J. Gut microbiome in modulating immune checkpoint inhibitors. *eBioMedicine*. 2022;82:104163. doi:10.1016/j.ebiom.2022.104163
38. Kelsen JR, Wu GD. The gut microbiota, environment and diseases of modern society. *Gut Microbes*. 2012;3(4). doi:10.4161/gmic.21333
39. Levy M, Kolodziejczyk AA, Thaiss CA, Elinav E. Dysbiosis and the immune system. *Nat Publ Gr*. 2017;17(4):219-232. doi:10.1038/nri.2017.7
40. Hartstra A V., Bouter KEC, Bäckhed F, Nieuwdorp M. Insights into the role of the microbiome in obesity and type 2 diabetes. *Diabetes Care*. 2015;38(1):159-165. doi:10.2337/dc14-0769
41. Mariat D, Firmesse O, Levenez F, et al. The firmicutes/bacteroidetes ratio of the human microbiota changes with age. *BMC Microbiol*. 2009;9:1-6. doi:10.1186/1471-2180-9-123
42. Le Chatelier E, Nielsen T, Qin J, et al. Richness of human gut microbiome correlates with metabolic markers. *Nature*. 2013;500(7464):541-546. doi:10.1038/nature12506
43. Wang J, Qin J, Li Y, et al. A metagenome-wide association study of gut microbiota in type 2 diabetes. *Nature*. 2012;490(7418):55-60. doi:10.1038/nature11450
44. Chambers ES, Preston T, Frost G, Morrison DJ. Role of Gut Microbiota-Generated Short-Chain Fatty Acids in Metabolic and Cardiovascular Health. *Curr Nutr Rep*. 2018;7(4):198-

206. doi:10.1007/s13668-018-0248-8

45. Scheithauer TPM, Rampanelli E, Nieuwdorp M, et al. Gut Microbiota as a Trigger for Metabolic Inflammation in Obesity and Type 2 Diabetes. *Front Immunol*. 2020;11(October):1-29. doi:10.3389/fimmu.2020.571731
46. Kimura I, Ichimura A, Ohue-Kitano R, Igarashi M. Free fatty acid receptors in health and disease. *Physiol Rev*. 2020;100(1):171-210. doi:10.1152/physrev.00041.2018
47. Wang Z, Roberts AB, Buffa JA, et al. Non-lethal Inhibition of Gut Microbial Trimethylamine Production for the Treatment of Atherosclerosis. *Cell*. 2015;163(7):1585-1595. doi:10.1016/j.cell.2015.11.055
48. Shapiro H, Kolodziejczyk AA, Halstuch D, Elinav E. Bile acids in glucose metabolism in health and disease. *J Exp Med*. 2018;215(2):383-396. doi:10.1084/jem.20171965
49. Natividad JM, Agus A, Planchais J, et al. Impaired Aryl Hydrocarbon Receptor Ligand Production by the Gut Microbiota Is a Key Factor in Metabolic Syndrome. *Cell Metab*. 2018;28(5):737-749.e4. doi:10.1016/j.cmet.2018.07.001
50. Manchester JK, Semenkovich CF, Gordon JI. Mechanisms underlying the resistance to diet-induced obesity in germ-free mice. 2007;104(3). doi:10.1073/pnas.0605374104
51. Turnbaugh PJ, Ley RE, Mahowald MA, Magrini V, Mardis ER, Gordon JI. An obesity-associated gut microbiome with increased capacity for energy harvest. *Nature*. 2006;444(7122):1027-1031. doi:10.1038/nature05414
52. Cani PD, Amar J, Iglesias MA, et al. Resistance. 2007;56(July):1761-1772. doi:10.2337/db06-1491.P.D.C.
53. Cani PD, Bibiloni R, Knauf C, Neyrinck AM, Delzenne NM. Changes in gut microbiota control metabolic diet–induced obesity and diabetes in mice. *Diabetes*. 2008;57(6):1470-1481. doi:10.2337/db07-1403.Additional
54. Hollander D, Kaunitz JD. The "Leaky Gut": Tight Junctions but Loose Associations? *Dig Dis Sci*. 2020;65(5):1277-1287. doi:10.1007/s10620-019-05777-2
55. Riedel S, Pheiffer C, Johnson R, Louw J, Muller CJF. Intestinal Barrier Function and Immune Homeostasis Are Missing Links in Obesity and Type 2 Diabetes Development. *Front Endocrinol (Lausanne)*. 2022;12(January):1-17. doi:10.3389/fendo.2021.833544
56. Boulangé CL, Neves AL, Chilloux J, Nicholson JK, Dumas ME. Impact of the gut microbiota on inflammation, obesity, and metabolic disease. *Genome Med*. 2016;8(1):1-12. doi:10.1186/s13073-016-0303-2
57. Tilg H, Zmora N, Adolph TE, Elinav E. The intestinal microbiota fuelling metabolic inflammation. *Nat Rev Immunol*. 2020;20(1):40-54. doi:10.1038/s41577-019-0198-4

58. Rohr MW, Narasimhulu CA, Rudeski-Rohr TA, Parthasarathy S. Negative Effects of a High-Fat Diet on Intestinal Permeability: A Review. *Adv Nutr*. 2020;11(1):77-91. doi:10.1093/advances/nmz061
59. Thaiss CA, Levy M, Grosheva I, et al. Hyperglycemia drives intestinal barrier dysfunction and risk for enteric infection. 2018;1383(March):1376-1383.
60. Sollberger G, Tilley DO, Zychlinsky A. Neutrophil Extracellular Traps: The Biology of Chromatin Externalization. *Dev Cell*. 2018;44(5):542-553. doi:10.1016/j.devcel.2018.01.019
61. Méndez-Ferrer S, Frenette PS. Hematopoietic stem cell trafficking: Regulated adhesion and attraction to bone marrow microenvironment. *Ann N Y Acad Sci*. 2007;1116:392-413. doi:10.1196/annals.1402.086
62. Soehnlein O, Steffens S, Hidalgo A, Weber C. Neutrophils as protagonists and targets in chronic inflammation. *Nat Rev Immunol*. 2017;17(4):248-261. doi:10.1038/nri.2017.10
63. Adrover JM, Nicolás-Ávila JA, Hidalgo A. Aging: A Temporal Dimension for Neutrophils. *Trends Immunol*. 2016;37(5):334-345. doi:10.1016/j.it.2016.03.005
64. Casanova-Acebes M1, Pitaval C, Weiss LA, Nombela-Arrieta C, Chèvre R, A-González N, Kunisaki Y, Zhang D, van Rooijen N, Silberstein LE, Weber C, Nagasawa T, Frenette PS, Castrillo A HA. Rhythmic Modulation of the Hematopoietic Niche through Neutrophil Clearance. *Cell*. 2013;157(5):1025-1035. doi:10.1016/j.cell.2013.04.040
65. Asada N, Takeishi S, Frenette PS. Complexity of bone marrow hematopoietic stem cell niche. *Int J Hematol*. 2017;106(1):45-54. doi:10.1007/s12185-017-2262-9
66. Frisch BJ, Porter RL, Calvi LM. Hematopoietic niche and bone meet. *Curr Opin Support Palliat Care*. 2008;2(3):211-217. doi:10.1097/SPC.0b013e32830d5c12
67. Zhang D, Chen G, Manwani D, et al. Neutrophil ageing is regulated by the microbiome. *Nature*. 2015;525(7570):528-532. doi:10.1038/nature15367
68. Adrover JM, Aroca-Crevillén A, Crainiciuc G, et al. Programmed 'disarming' of the neutrophil proteome reduces the magnitude of inflammation. *Nat Immunol*. 2020;21(2):135-144. doi:10.1038/s41590-019-0571-2
69. Zhang D, Frenette PS. Cross talk between neutrophils and the microbiota. *Blood*. 2019;133(20):2168-2177. doi:10.1182/blood-2018-11-844555
70. Hayashi F, Means TK, Luster AD. Toll-like receptors stimulate human neutrophil function. 2003;102(7):2660-2669.
71. Borregaard N. Neutrophils, from Marrow to Microbes. *Immunity*. 2010;33(5):657-670. doi:10.1016/j.immuni.2010.11.011
72. Sumimoto H, Miyano K, Takeya R. Molecular composition and regulation of the Nox family

NAD(P)H oxidases. *Biochem Biophys Res Commun*. 2005;338(1):677-686. doi:10.1016/j.bbrc.2005.08.210

73. Brinkmann V, Reichard U, Goosmann C, et al. Neutrophil Extracellular Traps Kill Bacteria Brinkmann Science 2004.pdf. *Science*. 2004;303(5663):1532-1535. doi:10.1126/science.1092385
74. Fuchs TA, Abed U, Goosmann C, et al. Novel cell death program leads to neutrophil extracellular traps. *J Cell Biol*. 2007;176(2):231-241. doi:10.1083/jcb.200606027
75. Thiama HR, Wong SL, Qiu R, et al. NETosis proceeds by cytoskeleton and endomembrane disassembly and PAD4-mediated chromatin decondensation and nuclear envelope rupture. *Proc Natl Acad Sci U S A*. 2020;117(13):7326-7337. doi:10.1073/pnas.1909546117
76. Fadini GP, Menegazzo L, Scattolini V, Gintoli M, Albiero M, Avogaro A. A perspective on NETosis in diabetes and cardiometabolic disorders. *Nutr Metab Cardiovasc Dis*. 2016;26(1):1-8. doi:10.1016/j.numecd.2015.11.008
77. Galluzzi L, Vitale I, Aaronson SA, et al. Molecular mechanisms of cell death: Recommendations of the Nomenclature Committee on Cell Death 2018. *Cell Death Differ*. 2018;25(3):486-541. doi:10.1038/s41418-017-0012-4
78. Remijsen Q, Kuijpers TW, Wirawan E, Lippens S, Vandenabeele P, Vanden Berghe T. Dying for a cause: NETosis, mechanisms behind an antimicrobial cell death modality. *Cell Death Differ*. 2011;18(4):581-588. doi:10.1038/cdd.2011.1
79. Uhlik MT, Abell AN, Johnson NL, et al. Rac-MEKK3-MKK3 scaffolding for p38 MAPK activation during hyperosmotic shock. *Nat Cell Biol*. 2003;5(12):1104-1110. doi:10.1038/ncb1071
80. Papayannopoulos V, Metzler KD, Hakkim A, Zychlinsky A. Neutrophil elastase and myeloperoxidase regulate the formation of neutrophil extracellular traps. *J Cell Biol*. 2010;191(3):677-691. doi:10.1083/jcb.201006052
81. Wang Y, Li M, Stadler S, et al. Histone hypercitrullination mediates chromatin decondensation and neutrophil extracellular trap formation. *J Cell Biol*. 2009;184(2):205-213. doi:10.1083/jcb.200806072
82. Bianchi M, Hakkim A, Brinkmann V, et al. Restoration of NET formation by gene therapy in CGD controls aspergillosis. *Blood*. 2009;114(13):2619-2622. doi:10.1182/blood-2009-05-221606
83. Elaine F Kenny, 1,* Alf Herzig, 1 Renate Krüger, 2, 3 Aaron Muth, 4 Santanu Mondal, 4 Paul R Thompson, 4 Volker Brinkmann, 5 Horst von Bernuth, 2, 3, 6 7 and Arturo Zychlinsky1. Diverse stimuli engage different neutrophil extracellular trap pathways. *Elife*.

2017;6(e24437). doi:[10.7554/eLife.24437]

84. Douda DN, Khan MA, Grasemann H, Palaniyar N. SK3 channel and mitochondrial ROS mediate NADPH oxidase-independent NETosis induced by calcium influx. *Proc Natl Acad Sci*. 2015;112(9):2817-2822. doi:10.1073/pnas.1414055112
85. Schoen J, Euler M, Schauer C, et al. Neutrophils' Extracellular Trap Mechanisms: From Physiology to Pathology. *Int J Mol Sci*. 2022;23(21):12855. doi:10.3390/ijms232112855
86. Pilsczek FH, Salina D, Poon KKH, et al. A Novel Mechanism of Rapid Nuclear Neutrophil Extracellular Trap Formation in Response to Staphylococcus aureus . *J Immunol*. 2010;185(12):7413-7425. doi:10.4049/jimmunol.1000675
87. Jorch SK, Kubes P. An emerging role for neutrophil extracellular traps in noninfectious disease. *Nat Med*. 2017;23(3):279-287. doi:10.1038/nm.4294
88. Yipp BG, Kubes P. NETosis: How vital is it? *Blood*. 2013;122(16):2784-2794. doi:10.1182/blood-2013-04-457671
89. Wang S, Wang Y. Peptidylarginine deiminases in citrullination, gene regulation, health and pathogenesis. *Biochim Biophys Acta - Gene Regul Mech*. 2013;1829(10):1126-1135. doi:10.1016/j.bbagrm.2013.07.003
90. Li P, Li M, Lindberg MR, Kennett MJ, Xiong N, Wang Y. PAD4 is essential for antibacterial innate immunity mediated by neutrophil extracellular traps. *J Exp Med*. 2010;207(9):1853-1862. doi:10.1084/jem.20100239
91. Fuchs TA, Brill A, Duerschmied D, et al. Extracellular DNA traps promote thrombosis. *Proc Natl Acad Sci*. 2010;107(36):15880-15885. doi:10.1073/pnas.1005743107
92. Martinod K, Demers M, Fuchs TA, Ling S, Brill A, Gallant M. Neutrophil histone modi fi cation by peptidylarginine deiminase 4 is critical for deep vein thrombosis in mice. *Pnas*. 2013;110(218674-8679). doi:10.1073/pnas.1301059110/-/DCSupplemental.www.pnas.org/cgi/doi/10.1073/pnas.1301059110
93. Martinod K, Fuchs TA, Zitomersky NL, et al. PAD4-deficiency does not affect bacteremia in polymicrobial sepsis and ameliorates endotoxemic shock. *Blood*. 2015;125(12):1948-1956. doi:10.1182/blood-2014-07-587709
94. Slade DJ, Subramanian V, Thompson PR. Pluripotency: Citrullination unravels stem cells. *Nat Chem Biol*. 2014;10(5):327-328. doi:10.1038/nchembio.1504
95. Hidalgo A, Libby P, Soehnlein O, Aramburu IV, Papayannopoulos V, Silvestre-Roig C. Neutrophil extracellular traps: from physiology to pathology. *Cardiovasc Res*. Published online 2021:2737-2753. doi:10.1093/cvr/cvab329
96. Semeraro F, Ammollo CT, Morrissey JH, et al. Extracellular histones promote thrombin

generation through platelet-dependent mechanisms: Involvement of platelet TLR2 and TLR4. *Blood*. 2011;118(7):1952-1961. doi:10.1182/blood-2011-03-343061

97. Pálmai-Pallag T, Bachrati CZ. Inflammation-induced DNA damage and damage-induced inflammation: A vicious cycle. *Microbes Infect*. 2014;16(10):822-832. doi:10.1016/j.micinf.2014.10.001
98. Middleton EA, He XY, Denorme F, et al. Neutrophil extracellular traps contribute to immunothrombosis in COVID-19 acute respiratory distress syndrome. *Blood*. 2020;136(10):1169-1179. doi:10.1182/blood.2020007008
99. Kessenbrock K, Krumbholz M, Schönermarck U, et al. Netting neutrophils in autoimmune small-vessel vasculitis. *Nat Med*. 2009;15(6):623-625. doi:10.1038/nm.1959
100. Schaper NC, Havekes B. Diabetes: Impaired damage control. *Diabetologia*. 2012;55(1):18-20. doi:10.1007/s00125-011-2368-1
101. Menegazzo L, Ciciliot S, Poncina N, et al. NETosis is induced by high glucose and associated with type 2 diabetes. *Acta Diabetol*. 2015;52(3):497-503. doi:10.1007/s00592-014-0676-x
102. Carestia A, Frechtel G, Cerrone G, et al. NETosis before and after hyperglycemic control in type 2 diabetes mellitus patients. *PLoS One*. 2016;11(12). doi:10.1371/journal.pone.0168647
103. Wong SL, Demers M, Martinod K, et al. Diabetes primes neutrophils to undergo NETosis, which impairs wound healing. *Nat Med*. 2015;21(7):815-819. doi:10.1038/nm.3887
104. Fadini GP, Menegazzo L, Rigato M, et al. NETosis delays diabetic wound healing in mice and humans. *Diabetes*. 2016;65(4):1061-1071. doi:10.2337/db15-0863
105. Talukdar S, Oh DY, Bandyopadhyay G, et al. Neutrophils mediate insulin resistance in mice fed a high-fat diet through secreted elastase. *Nat Med*. 2012;18(9):1407-1412. doi:10.1038/nm.2885
106. Braster Q, Roig CS, Hartwig H, et al. Inhibitionof NET release fails to reduce adipose tissue inflammationin mice. *PLoS One*. 2016;11(10):3-11. doi:10.1371/journal.pone.0163922
107. Chen K, Shao LH, Wang F, et al. Netting Gut Disease: Neutrophil Extracellular Trap in Intestinal Pathology. *Oxid Med Cell Longev*. 2021;2021. doi:10.1155/2021/5541222
108. Eng VV, Pearson JS. In vivo studies on Citrobacter rodentium and host cell death pathways. *Curr Opin Microbiol*. 2021;64:60-67. doi:10.1016/j.mib.2021.09.005
109. Ascher S, Wilms E, Pontarollo G, et al. Gut Microbiota Restricts NETosis in Acute Mesenteric Ischemia-Reperfusion Injury. *Arterioscler Thromb Vasc Biol*. 2020;(September):2279-2292. doi:10.1161/ATVBAHA.120.314491
110. Lin EYH, Lai HJ, Cheng YK, et al. Neutrophil extracellular traps impair intestinal barrier

function during experimental colitis. *Biomedicines*. 2020;8(8):1-21. doi:10.3390/BIOMEDICINES8080275

111. Swamydas M, Lionakis MS. Isolation, purification and labeling of mouse bone marrow neutrophils for functional studies and adoptive transfer experiments. *J Vis Exp*. 2013;(77):1-6. doi:10.3791/50586
112. Ciciliot S, Albiero M, Menegazzo L, et al. p66Shc deletion or deficiency protects from obesity but not metabolic dysfunction in mice and humans. *Diabetologia*. 2015;58(10):2352-2360. doi:10.1007/s00125-015-3667-8
113. Liu Z, Gu Y, Shin A, Zhang S, Ginhoux F. Analysis of Myeloid Cells in Mouse Tissues with Flow Cytometry. *STAR Protoc*. 2020;1(1):100029. doi:10.1016/j.xpro.2020.100029
114. Sanchez-Aguilera A, Lee YJ, Lo Celso C, et al. Guanine nucleotide exchange factor Vav1 regulates perivascular homing and bone marrow retention of hematopoietic stem and progenitor cells. *Proc Natl Acad Sci*. 2011;108(23):9607-9612. doi:10.1073/pnas.1102018108
115. Wang Y, Li M, Stadler S, et al. trap formation. 2009;184(2):205-213. doi:10.1083/jcb.200806072
116. Menegazzo L, Scattolini V, Cappellari R, et al. The antidiabetic drug metformin blunts NETosis in vitro and reduces circulating NETosis biomarkers in vivo. *Acta Diabetol*. 2018;55(6):593-601. doi:10.1016/S1957-2557(18)30035-X
117. Lakschevitz FS, Visser MB, Sun C, Glogauer M. Neutrophil transcriptional profile changes during transit from bone marrow to sites of inflammation. *Cell Mol Immunol*. 2015;12(1):53-65. doi:10.1038/cmi.2014.37
118. Calì B, Deygas M, Munari F, et al. Atypical CXCL12 signaling enhances neutrophil migration by modulating nuclear deformability. *Sci Signal*. 2022;15(761):eabk2552. doi:10.1126/scisignal.abk2552
119. Tschöp MH, Speakman JR, Arch JRS, et al. A guide to analysis of mouse energy metabolism. *Nat Methods*. 2012;9(1):57-63. doi:10.1038/nmeth.1806
120. Lihn AS1, Pedersen SB RB. Adiponectin: action, regulation and association to insulin sensitivity. *Obes Rev*. 2005;6(1):13-21. doi:10.1137/0731059
121. Xu H, Tartaglia LA, Chen H, et al. Chronic inflammation in fat plays a crucial role in the development of obesity-related insulin resistance Find the latest version : Chronic inflammation in fat plays a crucial role in the development of obesity-related insulin resistance. *J Clin Invest*. 2003;112(12):1821-1830. doi:10.1172/JCI200319451.Introduction
122. Shin JH, Bozadjieva-Kramer N, Shao Y, et al. The gut peptide Reg3g links the small

intestine microbiome to the regulation of energy balance, glucose levels, and gut function. *Cell Metab*. 2022;34(11):1765-1778.e6. doi:10.1016/j.cmet.2022.09.024

123. Bokoliya SC, Dorsett Y, Panier H, Zhou Y. Procedures for Fecal Microbiota Transplantation in Murine Microbiome Studies. *Front Cell Infect Microbiol*. 2021;11(September):1-14. doi:10.3389/fcimb.2021.711055
124. Mansuy-Aubert V, Zhou QL, Xie X, et al. Imbalance between neutrophil elastase and its inhibitor α1-antitrypsin in obesity alters insulin sensitivity, inflammation, and energy expenditure. *Cell Metab*. 2013;17(4):534-548. doi:10.1016/j.cmet.2013.03.005
125. Wang Q, Xie Z, Zhang W, et al. Myeloperoxidase deletion prevents high-fat diet-induced obesity and insulin resistance. *Diabetes*. 2014;63(12):4172-4185. doi:10.2337/db14-0026
126. Guiducci E, Lemberg C, Küng N, Schraner E, Theocharides APA, LeibundGut-Landmann S. Candida albicans-induced NETosis is independent of peptidylarginine deiminase 4. *Front Immunol*. 2018;9(JUL):1-15. doi:10.3389/fimmu.2018.01573
127. Gross S, Gammon ST, Moss BL, et al. Bioluminescence imaging of myeloperoxidase activity in vivo. *Nat Med*. 2009;15(4):455-461. doi:10.1038/nm.1886
128. Neeli I, Radic M. Current challenges and limitations in antibody-based detection of citrullinated histones. *Front Immunol*. 2016;7(NOV):1-5. doi:10.3389/fimmu.2016.00528
129. Konig MF, Andrade F. A critical reappraisal of neutrophil extracellular traps and NETosis mimics based on differential requirements for protein citrullination. *Front Immunol*. 2016;7(NOV). doi:10.3389/fimmu.2016.00461
130. Biron BM, Chung CS, O'Brien XM, Chen Y, Reichner JS, Ayala A. Cl-Amidine prevents histone 3 citrullination and neutrophil extracellular trap formation, and improves survival in a murine sepsis model. *J Innate Immun*. 2017;9(1):22-32. doi:10.1159/000448808
131. Ramos-Kichik V, Mondragón-Flores R, Mondragón-Castelán M, et al. Neutrophil extracellular traps are induced by Mycobacterium tuberculosis. *Tuberculosis*. 2009;89(1):29-37. doi:10.1016/j.tube.2008.09.009
132. Masuda S, Nakazawa D, Shida H, et al. NETosis markers: Quest for specific, objective, and quantitative markers. *Clin Chim Acta*. 2016;459:89-93. doi:10.1016/j.cca.2016.05.029
133. Chen Z, Yu R, Xiong Y, Du F, Zhu S. A vicious circle between insulin resistance and inflammation in nonalcoholic fatty liver disease. *Lipids Health Dis*. 2017;16(1):1-9. doi:10.1186/s12944-017-0572-9
134. Sun S, Duan Z, Wang X, et al. Neutrophil extracellular traps impair intestinal barrier functions in sepsis by regulating TLR9-mediated endoplasmic reticulum stress pathway. *Cell Death Dis*. 2021;12(6). doi:10.1038/s41419-021-03896-1

135. Agus A, Clément K, Sokol H. Gut microbiota-derived metabolites as central regulators in metabolic disorders. *Gut*. 2021;70(6):1174-1182. doi:10.1136/gutjnl-2020-323071
136. Khan S, Luck H, Winer S, Winer DA. Emerging concepts in intestinal immune control of obesity-related metabolic disease. *Nat Commun*. 2021;12(1):1-13. doi:10.1038/s41467-021-22727-7
137. Mutua V, Gershwin LJ. A Review of Neutrophil Extracellular Traps (NETs) in Disease: Potential Anti-NETs Therapeutics. *Clin Rev Allergy Immunol*. 2021;61(2):194-211. doi:10.1007/s12016-020-08804-7
138. De Groot P, Scheithauer T, Bakker GJ, et al. Donor metabolic characteristics drive effects of faecal microbiota transplantation on recipient insulin sensitivity, energy expenditure and intestinal transit time. *Gut*. Published online 2019:502-512. doi:10.1136/gutjnl-2019-318320